BIOLOGICAL ELECTRON TRANSFER IN COPPER PROTEINS

Thesis by

Cynthia N. Kiser

In Partial Fulfillment of the Requirements for the
Degree of Doctor of Philosophy

California Institute of Technology
Pasadena, California

1998

(Submitted January 8, 1998)

Acknowledgments

First my advisors. Thanks to my thesis advisor, Jack Richards. Your patience and support, financial and otherwise, were something I could always count on while I fought my battles with research and learned to find my own path in science. I would also like to thank Harry Gray for his enthusiasm for electron transfer and for leading the band of rogues I have infiltrated in the last couple of years. And Howard Lipshitz, the advisor who almost was. Though I never joined your lab, Howard, your mentoring at a pivotal time was vital to my eventual success in hunting the elusive title, Ph. D. Thank you.

And the rogues gallery. My last few years in grad school have been immeasurably enriched by contact with the motley crew known as the Gray Group. The social and especially scientific camaraderie you have provided rekindled my joy in science as a group effort. Special thanks go to Ralf Langen, for starting the azurin ET project and for teaching me labeling and lasers; to Angelo Di Bilio, for advice, critical reading of this manuscript, and new labeling technologies that opened the door to several projects still in progress; to Kevin Hoke for taking over where I left off; to Jay Winkler and Torbjörn Pascher for their laser system and their help with data acquisition and analysis; and to Jon Wilker, for all the grief he has given me about getting out of here. All right, I'm out, OK?

Most particular thanks go to Claire Slutter, my partner in crime in the Richards lab. In addition to teaching me molecular biology, you taught me to really grapple with a scientific problem. In addition, you willed to me the most interesting project I have ever worked on. I can never thank you enough for your scientific and personal mentoring and your continuing friendship.

To Parandeh Kia and Helen Hasenfeld, working with you on the TA training committee has been great fun - and the best 'Organizational Behavior' seminar one could hope for. I think it will serve me well wherever I go.

I would also like to thank the friends who made this long haul called graduate school, not only passable, but pleasant: Tim Conrow, Suzanne Elsasser, Alycia Weinberger, Beth Wedeman, Sonja Opstrup, John Marohn, Patty Sipman, Laura Mizoue, Kathleen Spellman, Daniel Hurley, Brenda Roder, Brian Primeau. The Williams gang: Anne Lewinson, Becky Barr, Jen Mach, Sheila Dacey, Chris and Martita Fleming. I would also like to thank Rob Rossi for his support and encouragement during my thesis writing hibernation.

Lastly, I would like to thank my family, my parents, Paul and Jeanne Kiser, and my sister, HB Kiser. You may not have always understood why I was holed up in Pasadena fighting recalcitrant experiments but I never doubted that if that was what I wanted to do with my life, I could count on your continual support and encouragement.

Abstract

Nature has used a variety of protein systems to mediate electron transfer. In this thesis I examine aspects of the control of biological electron transfer by two copper proteins that act as natural electron carriers.

In the first study, I have made a mutation to one of the ligand residues in the azurin blue copper center, methionine 121 changed to a glutamic acid. Studies of intramolecular electron transfer rates from that mutated center to covalently attached ruthenium complexes indicate that the weak axial methionine ligand is important not only for tuning the reduction potential of the blue copper site but also for maintaining the low reorganization energy that is important for fast electron transfer at long distances.

In the second study, I begin to examine the reorganization energy of the purple copper center in the CuA domain of subunit II of cytochrome *c* oxidase. In this copper center, the unpaired electron is delocalized over the entire binuclear site. Because long-range electron transfer into and out of this center occurs over long distances with very small driving forces, the reorganization energy of the CuA center has been predicted to be extremely low. I describe a strategy for measuring this reorganization energy starting with the construction of a series of mutations introducing surface histidines. These histidines can then be labeled with a series of ruthenium compounds that differ primarily in their reduction potentials. The electron transfer rates to these ruthenium compounds can then be used to determine the reorganization energy of the CuA site.

Table of Contents

Acknowledgments iii
Abstract iv
List of Figures vii
Abbreviations ix

Chapter 1: Electron Transfer in Proteins
Marcus theory in biological electron transfer 2
Protein control of electronic coupling 4
Donor-bridge coupling 7

Chapter 2: Electron Transfer in M121E Azurin
Measuring electron transfer rates in proteins 36
Photoinduced electron transfer 36
Flash/quench methodology 37
Experimental design 38
Materials and methods 38
General 38
Inorganic reagents 38
Mutant construction 39
Protein production 39
Protein purification 40
Ruthenation and purification - M121E/K122H/H83Q azurin 41
Ruthenation and purification - M121E(H83) azurin 42
Laser sample preparation 42
Results and discussion 44
Oxygen lability of reduced M121E azurin 44
Electron transfer rates 45

Chapter 3: Functional Changes in the M121E Mutant of Azurin
Marcus-type analysis of ET rates 75
Driving force 75
Electronic coupling 78
Reorganization energy 80
Conclusions 83

Chapter 4: Probing the CuA Center by Intramolecular Electron Transfer
Introduction 94
Experimental design 96

Table of Contents Continued

Materials and methods 97
General 97
Mutant construction 98
Protein expression and purification 100
Metal modifications 102

Results and discussion 103
Design of surface accessible histidines for labeling 103
Metal modifications 104
Preliminary ET data 105

Appendix A:
Site-saturation Mutagenesis of M121 of *Pseudomonas aeruginosa* Azurin
Chang et al. (1991) 129
Selected M121 mutants in the pET9a expression system 134

Appendix B: Map and Gene Sequence of pET/ASA
..... 138

Appendix C: Map and Gene Sequence of pET/T9CuA
..... 143

List of Figures

Figures for Chapter 1: Electron Transfer in Proteins
1.1 Photoinduced and thermal electron transfer 13
1.2 The effect of ΔG° on ΔG^* 15
1.3 The 'Marcus inverted region' 17
1.4 Uniform barrier model of electronic coupling 19
1.5 Comparison of distance and σ-tunneling distance 21
1.6 Wild type azurin Cu^{2+} site 23
1.7 Hydrogen bonds between the C112 and M121 strands of azurin 25
1.8 pH dependence of the UV/Vis spectrum of M121E azurin 27
1.9 Cu-ligand bond distances 29

Figures for Chapter 2: Electron Transfer Rates in M121E Azurin
2.1 Photoinduced ET Scheme 47
2.2 Difference spectra of Ru^{2+*} - Ru^{2+} and Ru^{3+} - Ru^{2+} 49
2.3 Flash/Quench ET Scheme 51
2.4 FPLC purification of ruthenated M121E/K122H azurin 53
2.5 FPLC purification of ruthenated M121E (H83) azurin 56
2.6 Reoxidation of M121E/K122H$Ru(bpy)_2Im$ azurin 59
2.7 Transient absorption laser data 61
2.8 Overlap of UV/Vis spectra: Ru label and M121E azurin 68
2.9 Rates of luminescence decay and electron transfer 70

Figures for Chapter 3: Functional Changes in the M121E mutant of Azurin
3.1 Potentials of Ru^{2+*}, Ru^{2+}, and Ru^{3+} species 84
3.2 Predicted ET rates if only ΔG° changes 86
3.3 M121E azurin Cu^{2+} site 88

Figures for Chapter 4: Probing the CuA Center By Intramolecular ET
4.1 The binuclear CuA site 106
4.2 PCR scheme for mutating CuA 108
4.3 Oligonucleotides for CuA mutagenesis 112
4.4 Spectra of CuA and Ru(tpy)(bpy)Im 114
4.5 Spectra of IMACS CuA fractions 116
4.6 Alignment of protein sequences with CuA domains 118
4.7 Locations of the surface histidines made for this study 120
4.8 Preliminary CuA rate data 122

Appendix A: Site-saturation Mutagenesis of M121 of *P. aeruginosa* azurin
A.1 Primers used for PCR mutagenesis of M121 136

List of Figures Continued

Appendix B: Azurin sequences and plasmid maps
B.1 Annotated sequence of the synthetic azurin gene 139
B.2 Map of the pET9a/ASA plasmid 141

Appendix C: CuA sequences and gene maps
C.1 Annotated sequence of 'T9' CuA 144
C.2 Map of the pET9a/CuA plasmid 146

Abbreviations

Az	azurin
bpy	bipyridine
CCO	cytochrome *c* oxidase
cyt *c*	cytochrome *c*
DA	donor and acceptor
EDTA	Ethylenediamine tetraacetic acid
ES-MS	Electrospray mass spectrometry
ET	electron transfer
EXAFS	extended X-ray absorption fine structure
HEPES	N-[2-hydroxyethyl]piperazine-N'[2-ethanesulfonic acid]
HOMO	highest occupied molecular orbital
Im	imidazole
IMAC	Immobilized metal ion adsorption chromatography
IPTG	Isopropyl-B-D-thiogalactoside
LB	Luria-Bertini Broth
LUMO	lowest unoccupied molecular orbital
LMCT	ligand-to-metal charge transfer
MALDI-TOF MS	matrix assisted, laser desorption ionization time-of-flight mass spectrometry
M. W.	molecular weight
SCF Xα	Self consistent field Xα calculations
tpy	2,2':6',2''-terpyridine
Tris	tris(hydroxymethyl)aminomethane
UV-Vis	ultraviolet and visible absorption spectroscopy
WT	wild type

Chapter 1

Electron Transfer in Proteins

Marcus theory in biological electron transfer

Electron transfer (ET) is central to biological organisms' ability to manage energy. For example, the respiratory chains of many different types of bacteria consist of a series of electron transfer steps. The initial event in photosynthesis is the transformation of light energy into a charge separation across a membrane. And, in oxidative phosphorylation in mitochondria, electron transfer events are coupled to proton transfers that build up the chemiosmotic gradient which drives ATP synthesis. The way the amino acids and cofactors of these protein complexes control electron flow has been the subject of much theoretical and experimental work (Marcus and Sutin 1985; Beratan et al. 1991; Moser et al. 1992; Winkler and Gray 1992; Evenson and Karplus 1993; Farid et al. 1993; Friesner 1994; Stuchebrukhov 1996).

The most generally useful theoretical framework for thinking about electron transfer is Marcus theory (Franzen et al. 1993). Marcus's essential insight (Marcus 1993) is that the equilibrium positions of the nuclei around the donor and acceptor atoms are different before and after electron transfer and that, according to the Franck-Condon principle, nuclear rearrangements occur on much longer time scales than electronic changes. So, in order to conserve the total energy of the system, electron transfer must proceed either by pre-equilibration to a nuclear configuration whose energy is the same for the DA and D^+A^- electronic configurations (thermal ET reactions) or by addition of light energy to make the energy of the DA complex equal to that of a D^+A^- complex with the DA equilibrium nuclear configuration (photoinduced ET reactions). The energy that must be supplied to overcome the lack of prior rearrangement of the nuclei is the reorganization energy, λ, defined as the charge transfer energy for a system where the $\Delta G°$ for the reaction is zero (self-exchange reactions). (See figure 1.)

The $\Delta G°$ for an ET reaction is the difference in the reduction potentials of the donor and acceptor. According to semiclassical Marcus theory, the energies of the products and reactants can be plotted as a function of an abstract reaction coordinate which takes into account the positions of all nuclei relevant to the system (the donor and acceptor plus a solvation sphere). The energies for the products and reactants, plotted as a function of the reaction coordinate, form two parabolas. The point at which they cross gives the activation energy, ΔG^*, which is a function of the driving force for the reaction, $-\Delta G°$, and λ, the nuclear

reorganization barrier to the reaction: $\Delta G^* = (\Delta G^\circ + \lambda)^2/4\lambda$. Taking a semiclassical approach, one can describe the rate of electron transfer by the following equation:

$$k_{ET} = \sqrt[2]{\frac{4\pi^3}{h^2 \lambda k_B T}} (H_{AB})^2 \exp - \frac{(\Delta G^\circ + \lambda)^2}{4\lambda k_B T}$$

where $(H_{AB})^2$ is the electronic coupling, and the exponential term is the Franck-Condon or nuclear energy term.

An unusual prediction of the Marcus equation, the so-called inverted effect, comes from the form of the exponential term in the nuclear (Franck-Condon) factor, $\exp-(\Delta G^\circ+\lambda)^2/4\lambda k_B T$. This indicates that as the driving force for the reaction increases (ΔG° becomes more negative), the activation barrier, ΔG^*, decreases until, at $-\Delta G^\circ = \lambda$, it reaches zero. (See figure 2.) Then as the driving force increases further (ΔG° becomes even more negative), the activation energy increases again so that k_{ET} decreases with increasing driving force. (See figure 3.) The presence of this inverted region indicates that biological systems must modulate $-\Delta G^\circ$ and λ simultaneously to achieve fast electron transfer. Interestingly, there has been some suggestion that this inverted effect might be put to use in a situation where one wants a reaction to be inefficient. The inverted effect may help limit the rate of the non-productive charge recombination in the photosynthetic reaction center (Moser et al. 1992).

Proteins modulate ΔG° and λ in various ways. In order to conserve energy during ET, the driving force should be as small as possible so little chemical potential energy is lost in the transfer. In biological systems such as cytochrome c oxidase that mediate a series of ET reactions, the reduction potentials of successive electron acceptors are often only slightly higher than the potential of the upstream donor. To get high ET rates, $-\Delta G^\circ$ should be almost equal to λ. These two factors dictate that, to achieve high ET rates, the reorganization energy, λ, should be small too.

It is often useful to partition λ into inner sphere and outer sphere components and examine each of these separately. The inner sphere contributions to λ are generally changes in equilibrium bond lengths and bond angles around the donor and acceptor. In systems such as plastocyanin and azurin, crystal structures of the oxidized and reduced proteins indicate the λ_{inner} is small because the positions of the metal ligands change only slightly (Guss and

Freeman 1983; Guss et al. 1986; Baker 1988; Shepard et al. 1990). In most cases, the largest contribution to λ_{outer} is the reorientation of solvent dipoles to align with the new electric fields around D and A. Many ET proteins minimize λ_{outer} by burying the electron transfer centers under a layer of low dielectric protein matrix.[1]

For a series of reactions differing only in the driving force of the reaction, $-\Delta G°$, as the driving force increases (becomes more negative) and approaches λ, the activation energy, ΔG^*, drops to zero. As the ET reaction becomes activationless, it is controlled only by factors which determine the frequency of electron transfer once the nuclei have reached the required intermediate configuration. In the adiabatic limit, this transmission coefficient is 1; electrons are transferred every time the nuclear configuration is correct. In nonadiabatic situations, such as long-range ET in biological systems, the transmission coefficient is determined by the electronic coupling between the donor and acceptor, $(H_{AB})^2$. This electronic coupling, the overlap between the donor and acceptor wavefunctions, is determined by the match in energies of these wavefunctions and the way they attenuate over the distance between the two sites. The way in which the protein medium affects the electronic coupling between donor and acceptor has been the subject of much theoretical and experimental work (Winkler and Gray 1992; Farid et al. 1993; Franzen et al. 1993; Bjerrum et al. 1995; Stuchebrukhov 1996).

Protein control of electronic coupling

A compilation by Dutton and coworkers (Moser et al. 1992) of intramolecular protein ET rates at a variety of driving forces in natural and model systems suggests that many of the observed ET rates are near their predicted limit ($k_{ET} \approx k_{max}$, $-\Delta G° = \lambda$). This would indicate that many biological ET reactions are controlled not by the nuclear/energetic factors but by the

---

[1]Small changes in bond angles with changes in oxidation state may not be enough to give small reorganization energies and thus fast rates of electron transfer. In a study of model complexes, Flanangan (Flanagan et al. 1993) demonstrated that a small Cu complex with ligand rearrangements on the order of those seen for blue copper proteins did not give fast electron transfer rates. Conversely, another model complex that goes from square pyramidal, pentacoordinate in the +2 state to pseudotetraheral, tetracoordinate in the +1 state, has much faster electron self-exchange rates - almost as fast as the self-exchange rates measured for azurin. They speculate that this may be due to the flexibility of the complex since they saw a correlation between flexibility of a complex and its ET rate.

electronic coupling between the donor and acceptor $(H_{AB})^2$. For the reactions included in his analysis (mainly ET rates for various components of the photosynthetic reaction center and a few ruthenium-labeled heme proteins) Dutton asserts that distance is the primary controlling factor in biological ET and that the system is well modeled by a simple exponential decay of the orbital overlaps with increasing distance, $k_{ET} = k_{ET}^{\circ} \exp(-\beta(r-r^{\circ}))$, where k_{ET}° is the ET rate at close contact distance ($\sim 10^{13}$ s^{-1}) and $\beta \approx 1.4$ $Å^{-1}$. (See figure 1.4.) This value of β is similar to that measured for ET reactions in a frozen organic glass of methyltetrahydrafuran, $\beta=1.2$ $Å^{-1}$, intermediate between the β predicted for ET through a vacuum, 2.8 $Å^{-1}$, and that measured from a series of covalently coupled small molecule DA pairs, 0.7 $Å^{-1}$.

Dutton's data span 12 Å and eight orders of magnitude in ET rates[2] and would seem to offer a broad range of conditions to observe long-range ET within ordered, biological systems. However, when the data set is expanded to include charge recombination rates at even longer distances within the photosynthetic reaction complex, the simple distance dependence model breaks down (Franzen et al. 1993). Using Dutton's distance decay parameter ($\beta = 1.4$ $Å^{-1}$), one would predict that, with a separation distance of 43 Å, the charge recombination rate between the first heme of the bound cytochrome subunit and the menaquinone (C_{H1}^{+} Q_A^{-}) would be unobservably slow (10^{-6} s^{-1}) but the measured rate is 2 s^{-1}. Boxer and coworkers showed that the observed rate could be explained by including the ion pairs for the forward ET reactions as mediating states in a superexchange formalism describing the charge recombination reaction. Thus, even within the photosynthetic reaction center, ET rates appear to have a complex distance dependence that is sensitive to the details of the intervening medium.

Inconsistencies in the dependence of k_{ET} on distance have led to a search for alternative representations of the electronic coupling factors controlling biological ET. In the Beratan-Onuchic pathways model, the transferring electron is conceptualized as localized in the series of one electron molecular orbitals linking the donor and acceptor (Beratan et al. 1987; Onuchic and Beratan 1990). The tunneling matrix element, T_{DA} (analogous to the electronic coupling element

---

[2]Including only rates where the k_{max} is known from driving force studies and excluding those reactions where k_{max} is inferred from k_{obs} using very limited data.

H_{AB}), is the sum of the individual pathway tunneling elements, t_{DA}, for all physical pathways between the donor and acceptor in the protein. Each individual tunneling element is the product of the bonded and nonbonded interactions along the pathway (t_{DA} = prefactor $\Pi\varepsilon_C\Pi\varepsilon_H\Pi\varepsilon_S$). Covalent bonds provide the strongest coupling between atoms in the pathway (ε_C = 0.6). Hydrogen bonds are thought to provide reasonable, perhaps somewhat weaker, coupling between the atoms involved. The original formulation weighted hydrogen bonds as two covalent bonds with an adjustment in the coupling if the hydrogen bond were significantly longer or shorter than average. However, measurements of ET across a hydrogen-bonded interface in a porphyrin model system suggest the coupling is better than for the same distance bridged by covalent bonds (ε_H = 0.51 rather then 0.6^2) (de Rege et al. 1995). Recent measurement of ET rates in the β-barrel protein azurin confirm that, in proteins, the electronic coupling through a hydrogen bond may be similar to that through covalent bonds (Regan et al. 1995; Langen et al. 1996).

Sometimes the through bond (covalent and hydrogen bonds) path between a donor and acceptor in a protein is excessively long, even though the two might be relatively close when the direct, through-space distance between them is measured. In this situation, even though ET through a vacuum is much slower than ET mediated by bridging molecular orbitals, it is sometimes better to include a disadvantageous through-space jump in a proposed ET pathway to 'straighten out' the meandering of the protein structure. Through-space jumps are usually included as a penalty parameter times the difference in length of the jump and the length of a normal covalent bond ($\varepsilon_S = 0.6\exp(-1.7(r-1.4))$).

Onuchic, Beratan, and coworkers have developed algorithms to find the best - most strongly electronically coupled - ET pathways in proteins (Betts et al. 1992). One of the early successes of the pathways model of biological ET was to explain the very similar ET rates within cytochrome *c* 's with ruthenium labels appended at different distances from the porphyrin (Wuttke et al. 1992). (See figure 5.) It has also been used to map sites in cytochrome *c* and azurin that are predicted to be more poorly coupled to the metal center than would be expected from the straight-line distance. In the most recent of the pathways programs, collections of closely-related (largely redundant) pathways have been consolidated and dealt with as 'tubes' of pathways that exhibit positive and negative interferences (Regan et al. 1993; Regan et al. 1995). This was done, in

part, to deal explicitly with the situations such as is found in myoglobin where there is not one clearly best path; several paths give similar total couplings (Casimiro et al. 1993; Langen et al. 1996). However, the existence of multiple pathways brings up the question of whether those pathways provide alternative routes for ET (constructive interference) or are dissipating dead-ends (destructive interference). Since this interference is a quantum phenomenon, examining this requires a more detailed description of the propagation of the donor wave function by the bridge than is provided by the simple product of couplings. The use of Green's functions allows examination of these interferences without requiring a full description of system (Regan et al. 1993); Skourtis, 1994 #91.

Recent advances in computing power and numerical methods have enabled some researchers to attempt more detailed calculations of the electronic coupling within proteins. Marcus and Siddarth (Siddarth and Marcus 1993) developed an artificial intelligence method which allowed them to identify the amino acids that contribute to electronic coupling between a donor and acceptor in a protein system. This simplification of the system allowed them to use a superexchange method to calculate the coupling between donor and acceptor through these amino acids. One of the advantages of the more detailed superexchange methodology is that it allows one to calculate absolute rates and electronic couplings. In the Beratan-Onuchic model, the initial coupling of the donor (or acceptor) into the bridge is not treated explicitly so one may only compare electron transfer rates within systems of related proteins. In comparing observed and calculated ET rates for a series of cytochrome *c* and myoglobin mutants, Siddarth and Marcus obtained very smooth correlations between their calculated absolute rates and experimentally determined ET rates; however, for reasons that were unclear, the slopes of their plots of calculated vs. observed rates differ from each other and from the desired slope of 1.

Donor-bridge coupling

In the Beratan-Onuchic model, as stated above, the initial coupling of the donor (or acceptor) into the bridge is not treated explicitly and is usually assumed to be the same for the proteins and pathways that are being compared. The reason for this lies more in the utility of the simplification than a true conviction of its validity. In the heme proteins, cytochrome *c* and myoglobin, treating all links equally ignores the anisotropic nature of the porphyrin ring and

the possibility of very real differences in coupling to the iron via an axial ligand rather than through the more delocalized orbitals of the conjugated porphyrin ring system. A recent paper calculating electronic coupling using a superexchange methodology explicitly addressed how big an effect one might expect to see in electron transfer reactions coupled through different Fe orbitals in the heme protein cyt *c* (Stuchebrukhov and Marcus 1995). Stuchebrukhov and Marcus found that the symmetry of the donor and acceptor metal ions imposed selection rules on the tunneling pathways that can be used. They predict the coupling from the Fe t_{2g} to the porphyrin ligand orbitals will be of π symmetry; the correlation of experimental coupling with matrix elements calculated using an s orbital as the donor and acceptor states was much worse than any of the calculations using the Fe t_{2g} orbitals. In addition, while all three t_{2g} orbitals of the Ru label contributed approximately equally to all of the predicted ET routes, the contribution of each Fe t_{2g} to a particular ET matrix element was highly dependent on its orientation relative to the Ru label (variations between 2 and 20 fold in individual contributions to the matrix elements were calculated).

While the anisotropy of the coupling into the cytochrome heme iron is intuitively satisfying, the anisotropic nature of couplings of β-strands to the copper center in azurin is less apparent from casual inspection of the X-ray structure. (See figure 6.) But a combination of spectroscopic evidence and self consistent field Xα (SCF-Xα) calculations (modeling the analogous blue copper center in plastocyanin) indicate that the coupling of the copper ion to its ligands is very unequal (Gerwith and Solomon 1988; Lowery and Solomon 1992). The UV-Vis absorption spectrum of type I (blue) copper centers is dominated by the unusually strong interaction of the cysteine 112 sulfur with the copper ion. The extinction coefficient (indicative of the oscillator strength of the interaction) of this 625 nm ligand to metal charge transfer (LMCT) band is ~6,000 $M^{-1}cm^{-1}$ (compared to an ε of ~50 $M^{-1}cm^{-1}$ in small molecule copper complexes) (Solomon et al. 1980). The CysS-Cu^{2+} bond is unusually short (2.25 Å in WT azurin (Nar et al. 1991)) and is thought to be highly covalent in character. By contrast, the histidine ligands, which are both respectable metal ligands with bond distances of 2.03 Å and 2.11 Å, contribute only a small amount (~4 %) to the ground state wave function (Gerwith and Solomon 1988). The difference in metal-ligand coupling between the Cys and His ligands was invoked to explain the rates of electron transfer to two different sites on plastocyanin. The hydrophobic patch

on the surface centered near His37 mediates electron transfer to neutral and anionic complexes; ET to cationic complexes, on the other hand, mainly proceeds after their association with the acid patch centered around Tyr83. The rates of ET to complexes bound at these two sites are remarkably similar (~10^4-10^5 $M^{-1}s^{-1}$) despite the difference in the Cu to surface distances (6 Å for the hydrophobic patch vs. 13 Å for the acid patch). Using Newton's relationship between ligand covalency and the electronic coupling through that ligand (Newton 1988), Lowery *et al.* calculated that the difference in coupling through the strong Cys84 ligand would balance the rate enhancement expected for ET to the closer site (Lowery et al. 1993).

The fourth conserved ligand in most type I copper sites is a methionine. This methionine ligand is somewhat puzzling. Though it is found in most type I sites, the length of the Cu-Met bond (2.8 Å in plastocyanin (Guss et al. 1992), 3.1 Å in azurin (Nar et al. 1991)) and the fact that in plastocyanin its interaction with the Cu ion cannot be seen by EXAFS[3] (Scott et al. 1982), called into question its role as a copper ligand. SCF-Xα calculations by Solomon and coworkers demonstrate that, while a weaker interaction, the methionine sulfur does interact with the Cu^{2+} ion in blue copper sites; they estimate the Cu-Met bond to be about 30% of a normal ligand-metal bond (Lowery and Solomon 1992). Site saturation mutagenesis has shown that methionine is not needed in order to form a blue copper site (Chang 1991), though the observation that most mutant sites are not fully occupied by Cu^{2+} suggest the methionine may contribute to the stability of the site (Karlsson et al. 1991).

In an attempt to directly probe the relative abilities of the Cys and Met ligands to mediate electron transfer, Langen introduced histidines at several sites on the β-strands leading from Cys112 and Met121 in *P. aeruginosa* azurin (Langen et al. 1995; Langen et al. 1996). Electron transfer rates to $Ru(bpy)_2Im$ labels at these sites have been analyzed by several different methods. Regan *et al.* modified their Green's function pathways method to explicitly include a term describing the initial coupling from the Cu into the bridge (Regan et al. 1995). Comparing the case in which all the Cu-ligand couplings are weighted equally with one in which the relative couplings match the estimates from Solomon's

---

[3]One can see a S interaction at a distance of 3.04 Å in the azurin EXAFS (Murphy et al. 1993) which has been attributed to M121 (X-ray Cu-S(Met) distance: 3.15 Å).

SCF-Xα calculations of the Cu^{2+} HOMO (Cys = 1.0: Met =0.3: His = 0.1: His = 0.1), he showed that both give physically reasonable estimates for the DA coupling.

The ET rate to the label at 126, at the far end of the Met β-strand, does not attenuate as sharply as one might expect given its distance and the expected weak coupling of the all covalent bond path through the Met ligand. This is readily explained if one considers the effects of multiple constructively interfering paths. An electron leaving the Cu^{1+} center could either leave through the weakly coupled Met ligand and follow an entirely covalent pathway to the Ru^{3+} acceptor or it could leave by the strongly coupled Cys sulfur, travel through part of the Cys β-strand and then cross via one of several interstrand hydrogen bonds to reach the acceptor. (See figure 7.) The number of possible interstrand crossings increases down the strand so the existence of alternative pathways would affect the ET rates to labels at the far ends of the strands more strongly to the nearby His122 label.

Stuchebrukhov and colleagues have used several different computational methods at the extended Hückel level of approximation to model electron transfer in azurin (Stuchebrukhov 1996; Diazadeh et al. 1997). In each case, to limit the computational expense they first 'prune' the protein to select the most important subset of amino acids on which to perform more rigorous calculations. In a direct comparison, they show that exact diagonalization of the Hamiltonian, perturbation theory, and their tunneling currents method all are in excellent agreement (Diazadeh et al. 1997). Because their tunneling currents method gives the flux of current between two atoms, one can estimate not just the net result of the coupling, but can see the effects of interfering currents. This enables one to determine the contribution of individual bonds to the electron transfer process and to address questions such as the importance of hydrogen bonds.

In their examination of ET in labeled azurins, they used a donor wavefunction for the blue copper center that contained a strong contribution from the Cys-S and weaker contributions from the other ligands (in accordance with Solomon's studies of the blue copper site). At both the acceptor and donor sites they saw strong circular currents. For electron transfer to a $Ru(bpy)_2Im$ label at His122 they saw the majority of the tunneling current flow from the Cu, through the Met ligand, down the peptide backbone through His122, and into a Ru t_{2g} orbital. This is what one might intuitively expect and is substantially the same as is predicted by a pathway model. The more interesting result is for the

tunneling currents to His126. For this residue, the pathways model shows paths through both the Met and Cys strands with the possibility of crossing between them via the series of backbone hydrogen bonds; the relative contributions of these pathways depends on the parameterization for hydrogen vs. covalent bonds and the choice of donor-bridge coupling through the two very different sulfur ligands. The tunneling currents model shows substantial current flux through both strands; each β-strand is a strongly coupling backbone linked strongly to the metal at one end and weakly to the metal at the other. But the Met strand, despite its weak ligation to the Cu^{1+} donor, carries three times as much current as the Cys strand. Most interestingly, the flux is in opposite directions along the two strands, toward the Ru acceptor along the Met strand and away from it via the Cys strand. This is an example of destructive interference in which the existence of the coupling through the Cys strand decreases the overall rate of electron transfer. In contrast with the pathways model, the hydrogen bonds between the two strands carry no flux. At least in this system with parallel covalent ET routes, hydrogen bonds are not major contributors to electron transfer.

If destructive interference between the two ligand containing strands in azurin explains the slower rates of electron transfer down the Met strand, would changing the nature of the Met ligand so it could compete more effectively for flux out of the Cu^{1+} center increase overall rate of electron transfer? Site-saturation mutagenesis has replaced the M121 ligand with all 19 other natural amino acids (Chang et al. 1991; Karlsson et al. 1991). Not only are all of these substitutions possible, but they make remarkably little difference in the properties of the type I center. The UV-Vis spectra of most of the M121X mutants of the *Pseudomonas aeruginosa* azurin remain remarkably similar to that of wild type azurin with the major difference being increases in a peak near 420 nm. This peak is not seen in the WT azurin but has been observed in the spectra of other blue copper proteins and has been discussed as a possible indication of distortion in a type I site (Lu et al. 1993). The spectra of two of the mutants, M121E and M121K, show an interesting pH dependence in the relative heights of these two peaks. The absorption spectra of the M121E mutant at low and high pH are shown in figure 8. At low pH, the normal absorbance around 600 nm dominates, but at high pH, when the ligand would be presumed to be deprotonated, this peak diminishes in intensity and shifts to the blue (λ_{max} = 570 nm) while the

420 nm peak increases in intensity. Interpretation of this spectroscopic change as the addition of an axial ligand is supported by EXAFS studies of the M121E mutant which show an additional oxygen at 1.9 Å at pH 8.0 (Strange et al. 1996). (For comparison, at pH 4.0, there is not fifth ligand in the M121E coordination sphere; the WT center shows a sulfur at 3.04 Å.) (See figure 9.)

This thesis sets out to examine how the changes in the azurin blue copper center evidenced by these spectroscopic changes affect the functional properties of the M121E azurin mutant. As described in the next chapter, ruthenium labels ($Ru^{(II)}(bpy)_2(Im)$) were placed either at the naturally occurring H83 or at an introduced histidine at position 122 and ET rates to these labels were measured at high and low pH using photoinduced and flash/quench laser techniques. Chapter 3 discusses the rates obtained and their interpretation within the context of the spectroscopy and function of blue copper centers. Chapter 4 discusses a related project, initial attempts to characterize the electron transfer dynamics of the CuA center from cytochrome *c* oxidase using similar ruthenium labeling and transient-absorbance laser spectroscopy techniques to obtain intramolecular electron transfer rates.

Figure 1.1 Energy diagram for a self-exchange electron transfer reaction. The horizontal axis is an abstract reaction coordinate that represents the changes in position of the nuclei in the system during the course of the electron transfer. The vertical axis is the free energy of the system. The parabola on the left represents the energy of the reactants ($D\text{-}A^+$), the parabola on the right, the energy of the products ($D^+\text{-}A$). The reorganization energy, λ, is the energy required for an instantaneous electron transfer to give $D^+\text{-}A$ product but with the bond distances and bond angles that are the equilibrium configuration for the reactants.

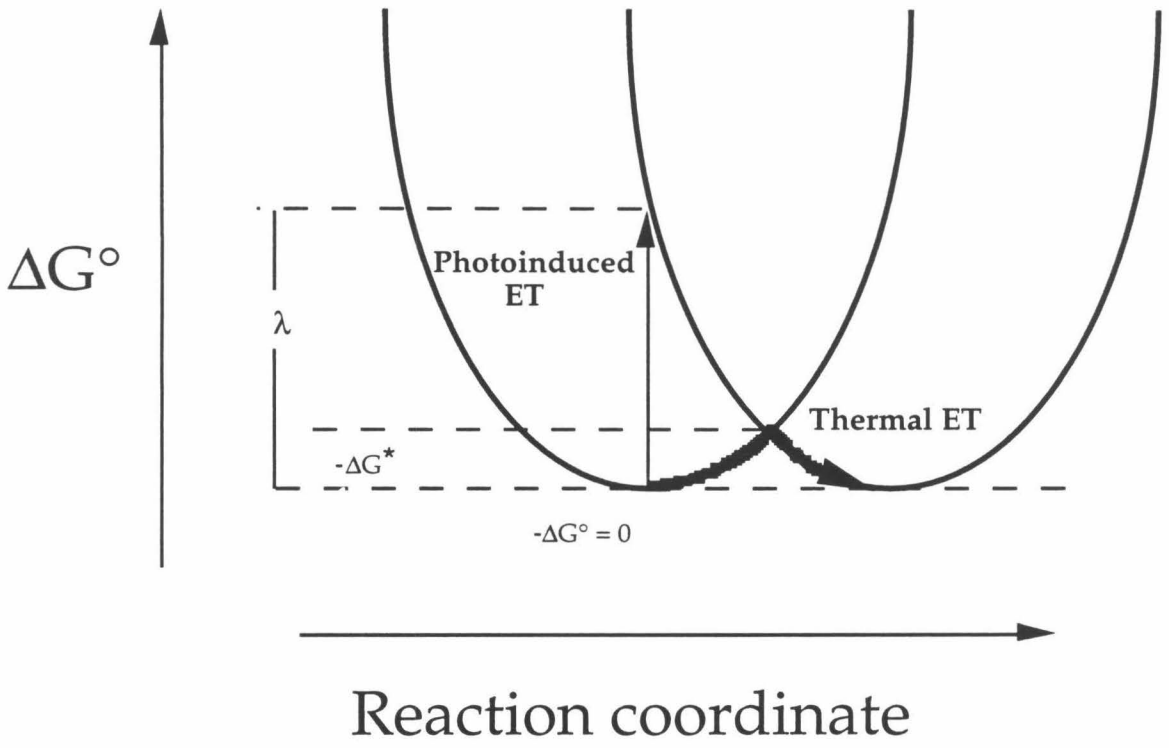
ΔG°
Photoinduced
ET
λ
Thermal ET
-ΔG*
-ΔG° = 0
Reaction coordinate

Figure 1.2 As in Figure 1, the energy is depicted on the vertical axis, while the horizontal axis represents the abstract reaction coordinate. In the three diagrams, the increasing driving force for the reaction is shown by the product curve shifting downward.

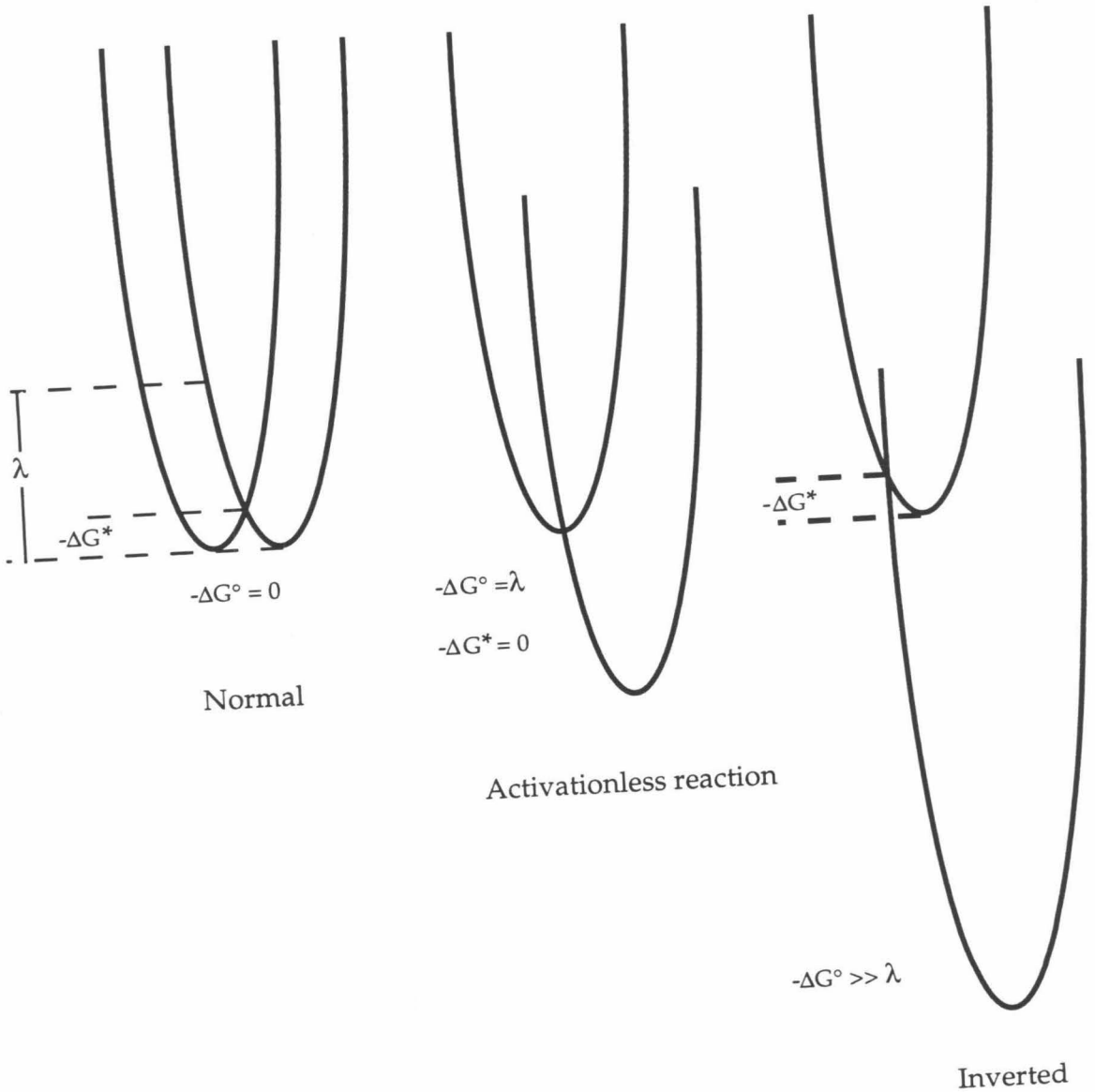
λ
-ΔG*
-ΔG° = 0
Normal
-ΔG° =λ
-ΔG* = 0
Activationless reaction
-ΔG*
-ΔG° >> λ
Inverted

Figure 1.3 Marcus parabola showing the relationship between driving force ($-\Delta G°$) and the log of the electron transfer rate.

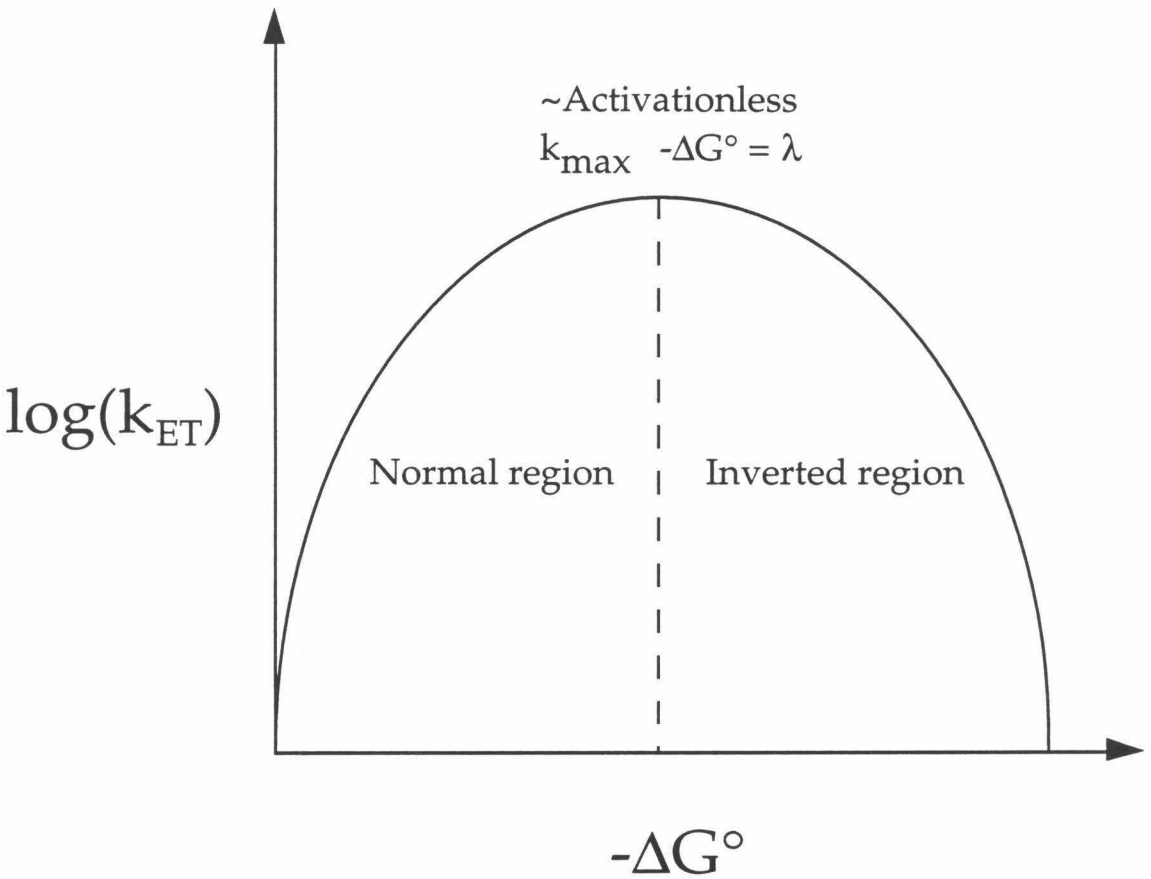
~Activationless
k_{max} $-\Delta G° = \lambda$
$\log(k_{ET})$
Normal region
Inverted region
$-\Delta G°$

Figure 1.4 Plot of the maximal rate of electron transfer vs. the edge to edge distance between donor and acceptor for electron transfer reactions within the photosynthetic reaction center (open circles) and in select protein model systems (filled triangles). The solid line is the expected rate of electron transfer for a system with a close-contact electron transfer rate of 10^{13} s^{-1} and a uniform rate decay, β=1.4 $Å^{-1}$. Data from (Moser et al. 1992).

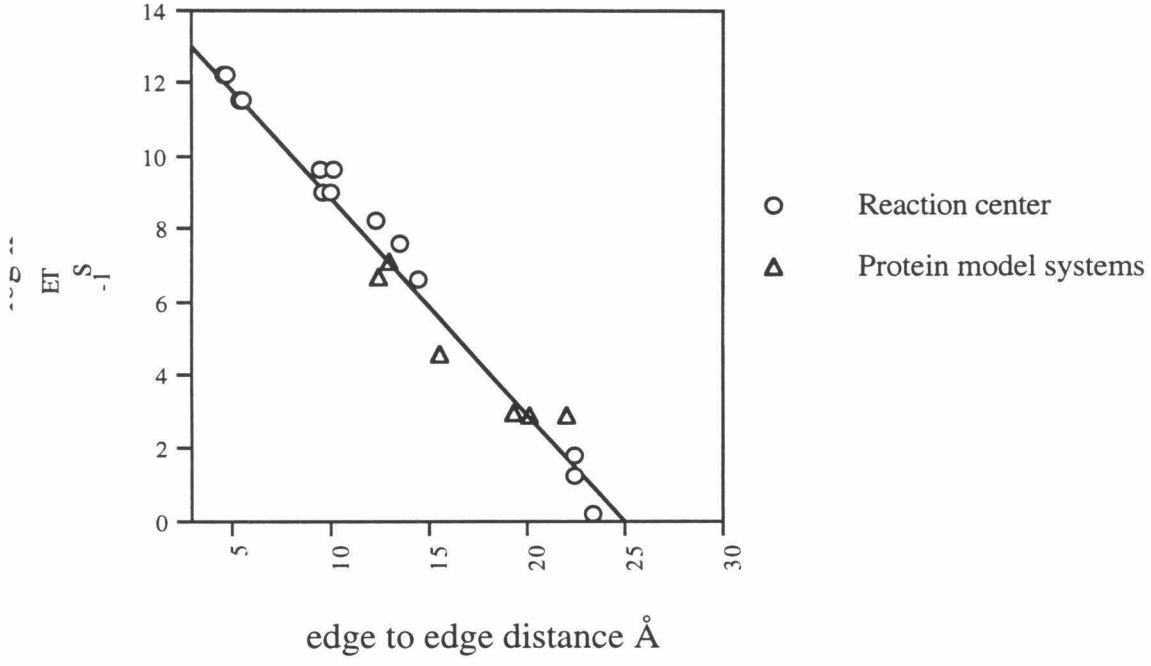
14
12
10
8
6
4
2
0
5
10
15
20
25
30
Reaction center
Protein model systems
edge to edge distance Å

Figure 1.5 The maximal rates of electron transfer for a series of ruthenium-modified cytochrome *c* proteins are plotted against (a) the edge-to-edge distance between the metal centers and (b) the σ-tunneling lengths predicted by the Beratan-Onuchic pathways model (Wuttke et al. 1992).

In (a) the solid line denotes the best fit to the data, which gives β=0.66 $Å^{-1}$ and a close contact ET rate of 1.6 x 10^8 s^{-1}. The dotted line is the expected change in rate with distance if the cytochromes behaved like the steroid compounds of Closs and Miller (Closs and Miller 1988), β=1.0 $Å^{-1}$ and a close contact ET rate of 3 x 10^{12} s^{-1} at 3 Å separation. The dashed line is the distance dependence found by Dutton and coworkers for other protein ET systems (Moser et al. 1992), β=1.4 $Å^{-1}$ and a close contact ET rate of 1 x 10^{13} s^{-1} at 3 Å separation.

In (b) the log of the ET rate is plotted vs. the tunneling length as predicted by the Beratan/Onuchic model; the through bond coupling was converted to Å using an average bond length of 1.4 Å. The solid line represents the best fit to the data (including the estimate of a close contact ET rate of 3 x 10^{12} s^{-1} at 3 Å separation). The k_{max} falls off at a rate of 0.71 $Å^{-1}$.

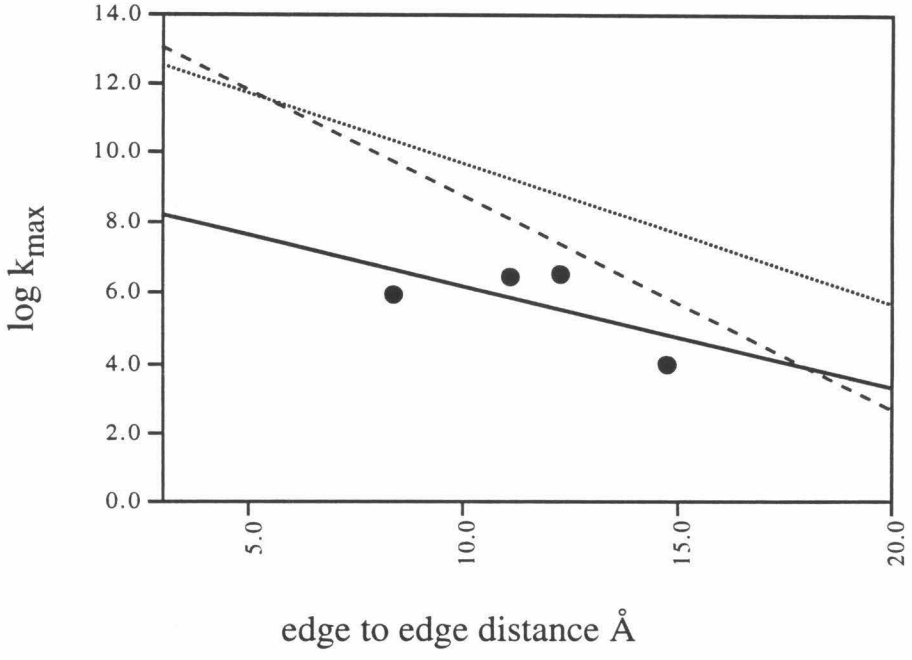
14.0
12.0
10.0
8.0
6.0
4.0
2.0
0.0
log k_{max}
5.0
10.0
15.0
20.0
edge to edge distance Å

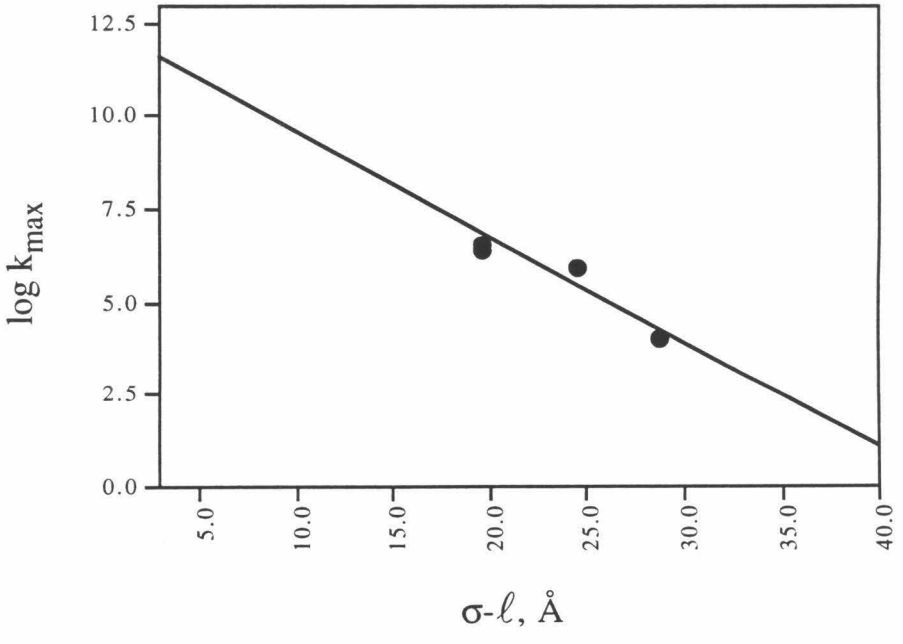
12.5
10.0
7.5
5.0
2.5
0.0
log k_{max}
5.0
10.0
15.0
20.0
25.0
30.0
35.0
40.0
σ-ℓ, Å

Figure 1.6 The type I copper center of *Pseudomonas aeruginosa* azurin (Nar et al. 1991). The copper ion is ligated by a trio of in-plane ligands, C112 (to the left and behind the Cu ion in this view), H117 (left front), and H46 (right). M121 (above) and the carbonyl oxygen of G45 (below and to the right) provide weaker axial interactions. The Cu ion is dark blue; the rest of the heavy atoms are colored according to the standard CPK scheme: carbon: gray, nitrogen: blue, oxygen: red, sulfur: yellow.

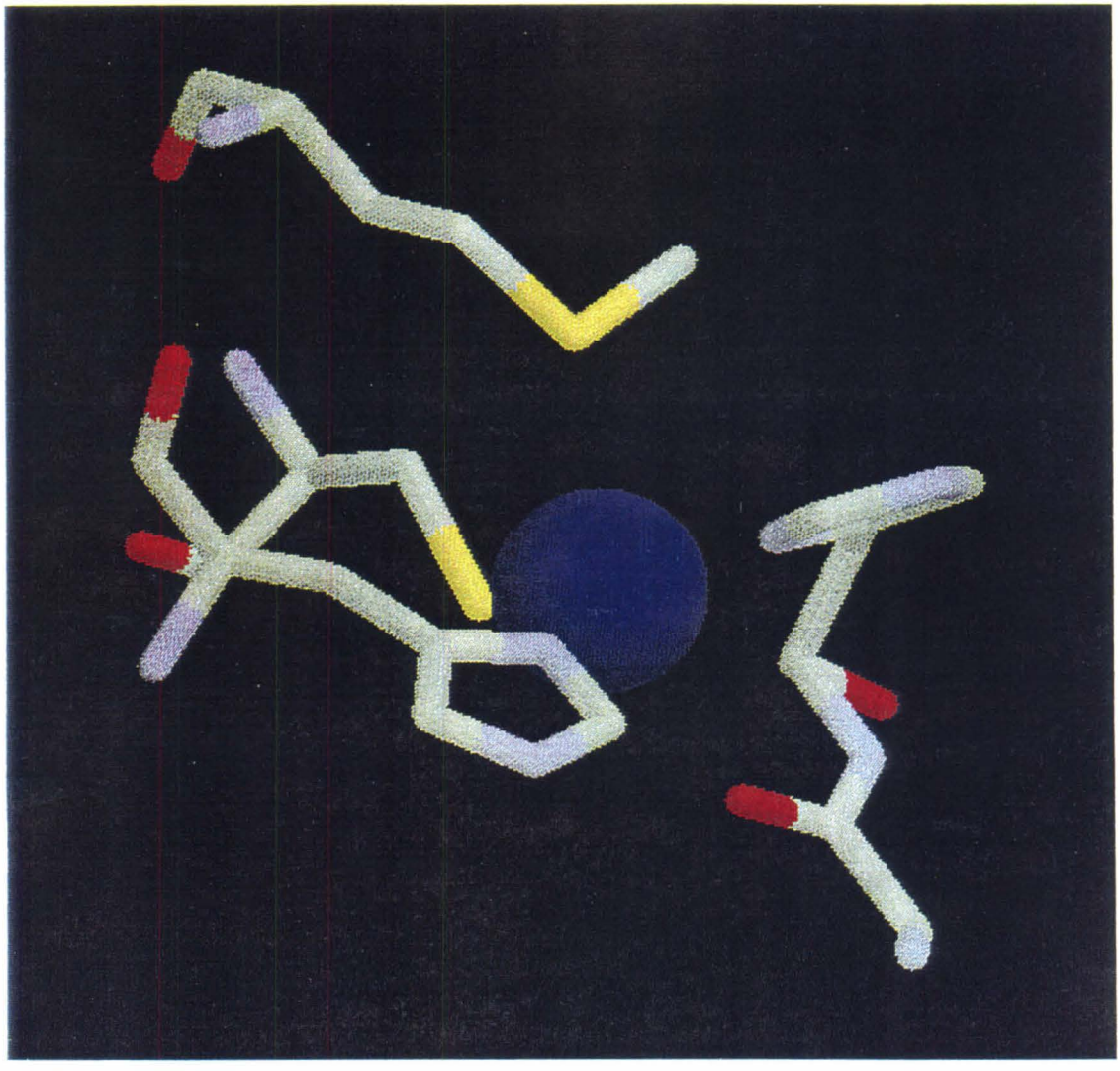

Figure 1.7 The β-strands leading away from the azurin copper center via the Cys112 and Met121 ligands are shown as their peptide backbone; the 121-126 strand is on the left, the 112-107 strand on the right. The 5 hydrogen bonds linking the two strands are shown in white.

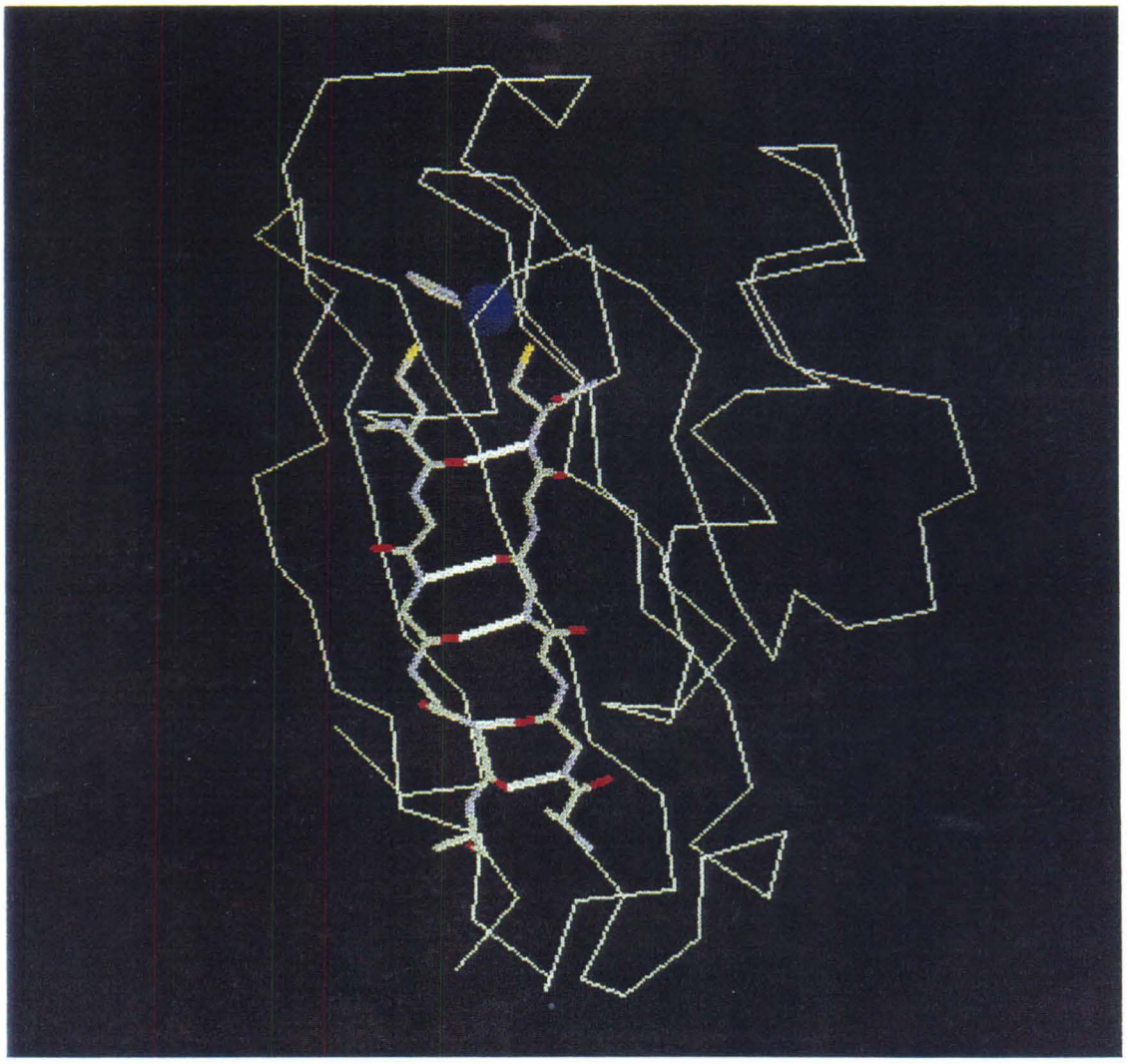

Figure 1.8 UV-Vis spectra of M121E at pH 4.5 and pH 8.0.

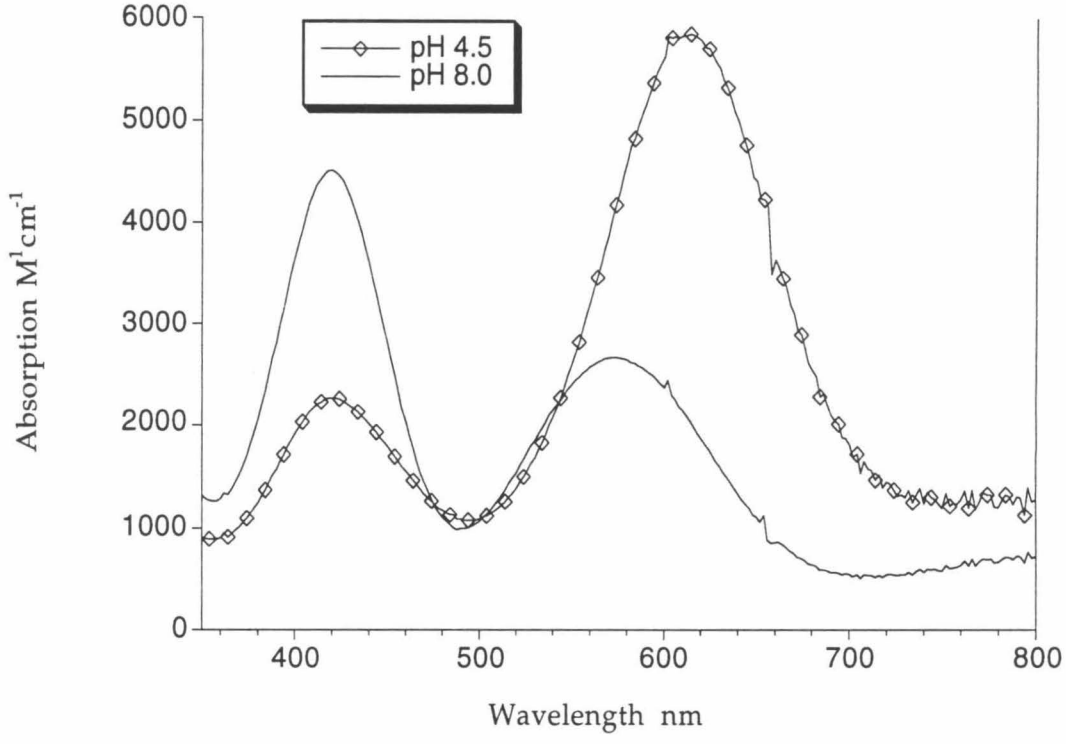
pH 4.5
pH 8.0
Absorption M^{1}cm^{-1}
Wavelength nm
0
1000
2000
3000
4000
5000
6000
400
500
600
700
800

Figure 1.9 Comparison of Cu-ligand distances for WT and M121E *Pseudomonas aeruginosa* azurin obtained by EXAFS and X-ray crystallography (Nar et al. 1991; Murphy et al. 1993; Strange et al. 1996; Karlsson et al. 1997).

	EXAFS			X-ray		
	WT	M121E		WT		M121E
	8.0	4.0	8.0	5.5	9.0	6.0
Residue						
Cys 112 S	2.12	2.15	2.21	2.25	2.26	2.11
His 117 N	1.93	1.93	2.00	2.03	2.04	2.02
His 46 N	1.93	1.93	2.00	2.11	2.09	2.02
Gly 45 C=O	2.79	2.86	2.86	2.97	2.95	3.42
Met 121 S	3.04	-	1.90	3.15	3.12	
or Glu 121 O						2.21

References

Baker, E. N. (1988). "Structure of azurin from *Alcaligenes denitrificans*. Refinement at 1.8 Å resolution and comparison of the two crystalographically independent molecules." J. Mol. Biol. **203**: 1071-1095.

Beratan, D. N., Betts, J. N. and Onuchic, J. N. (1991). "Protein electron transfer rates set by the bridging secondary and tertiary structure." Science **252**: 1285-1288.

Beratan, D. N., Onuchic, J. N. and Hopfield, J. J. (1987). "Electron tunneling through covalent and noncovalent pathways in proteins." J. Chem. Phys. **86**(8): 4488-4498.

Betts, J. N., Beratan, D. N. and Onuchic, J. N. (1992). "Mapping electron-tunneling pathways - an algorithm that finds the minimum length maximum coupling pathway between electron-donors and acceptors in proteins." J. Am. Chem. Soc. **114**: 4043-4046.

Bjerrum, M. J., Casimiro, D. R., Chang, I.-J., Di Bilio, A., Gray, H. B., Hill, M. G., Langen, R., Mines, G. A., Skov, L. K., Winkler, J. R. and Wuttke, D. S. (1995). "Electron transfer in ruthenium-modified proteins." J. Bioenerg. Biomemb. **27**(3): 295-302.

Casimiro, D. R., Wong, L. L., Colon, J. L., Zewert, T. E., Richards, J. H., Chang, I. J., Winkler, J. R. and Gray, H. B. (1993). "Electron transfer in ruthenium zinc porphyrin derivatives of recombinant human myoglobins - analysis of tunneling pathways in myoglobin and cytochrome *c*." J. Am. Chem. Soc. **115**: 1485-1489.

Chang, T. K., Iverson, S. A., Rodrigues, C. G., Kiser, C. N., Lew, A. Y. C., Germanas, J. P. and Richards, J. H. (1991). "Gene synthesis, expression, and mutagenesis of the blue copper proteins azurin and plastocyanin." Proc. Natl. Acad. Sci. USA **88**: 1325-1329.

Chang, T. K.-Y. (1991). Gene Synthesis, Expression, and Mutagenesis of Azurin. California Institute of Technology.

Closs, G. L. and Miller, J. R. (1988). "Intramolecular long-distance electron transfer in organic molecules." Science **240**: 440-446.

de Rege, P. J. F., Williams, S. A. and Therien, M. J. (1995). "Direct evaluation of electronic coupling mediated by hydrogen bonds: implications for biological electron transfer." Science **269**: 1409-1413.

Diazadeh, I., Gehlen, J. N. and Stuchebrukhov, A. A. (1997). "Calculation of electronic tunneling matrix element in proteins: comparison of exact and

approximate methods for Ru-modified azurin." J. Chem. Phys. **106**(13): 5658-5666.

Evenson, J. W. and Karplus, M. (1993). "Effective coupling in biological electron transfer: exponential or complex distance dependence?" Science **262**: 1247-1249.

Farid, R. S., Moser, C. C. and Dutton, P. L. (1993). "Electron transfer in proteins." Curr. Biol. **3**: 225-233.

Franzen, S., Glodstein, R. F. and Boxer, S. G. (1993). "Distance dependence of electron-transfer reactions in organized systems: the role of superexchange and non-Condon effects in photosynthetic reaction centers." J. Phys. Chem. **97**: 3040-3053.

Friesner, R. A. (1994). "Comparison of theory and experiment for electron transfers in proteins: where's the beef?" Curr. Biol. **4**: 339-343.

Gerwith, A. A. and Solomon, E. I. (1988). "Electronic structure of plastocyanin: excited state spectral features." J. Am. Chem. Soc. **110**: 3811-3819.

Guss, J. M., Bartunik, H. D. and Freeman, H. C. (1992). "Accuracy and precision in protein structure analysis: restrained least-squares refinement of the structure of poplar plastocyanin at 1.33 Å resolution." Acta. Cryst. **B48**: 790-811.

Guss, J. M. and Freeman, H. C. (1983). "Structure of oxidized poplar plastocyanin at 1.6 Å resolution." J. Mol. Biol. **169**: 521.

Guss, J. M., Harrowell, P. R., Murata, M., Norris, V. A. and Freeman, H. C. (1986). "Crystal structure analysis of reduced poplar plastocyanin at six pH values." J. Mol. Biol. **192**: 361.

Karlsson, B. G., Nordling, M., Pascher, T., Tsai, L.-C., Sjölin, L. and Lundberg, L. G. (1991). "Cassette mutagenesis of Met121 in azurin from *Pseudomonas aeruginosa*." Protien Eng. **4**(3): 343-349.

Karlsson, B. G., Tsai, L.-C., Nar, H., Sanders-Loehr, J., Bonander, N., Langer, V. and Sjölin, L. (1997). "X-ray structure determination and characterization of the *Pseudomonas aeruginosa* azurin mutant Met121Glu." Biochem. **36**: 4089-4095.

Langen, R., Chang, I.-J., Germanas, J. P., Richards, J. H., Winkler, J. R. and Gray, H. B. (1995). "Electron tunneling in proteins: coupling through a β-strand." Science **268**: 1733-1735.

Langen, R., Colon, J. L., Casimiro, D. R., Karpishin, T. B., Winkler, J. R. and Gray, H. B. (1996). "Electronic tunneling in proteins: role of the intervening medium." JBIC **1**: 221-225.

Lowery, M. D., Guckert, J. A., Gebhard, M. S. and Solomon, E. I. (1993). "Active-site electronic structure contributions to electron-transfer pathways in rubredoxin and plastocyanin: direct vs. superexchange." J. Am. Chem. Soc. **115**: 3012-3013.

Lowery, M. D. and Solomon, E. I. (1992). "Axial ligand bonding in blue copper proteins." Inorg. Chim. Acta **198-200**: 233-243.

Lu, Y., Roe, J. A., Gralla, E. B. and Valentine, J. S. (1993). Metalloprotein ligand redesign: characterization of copper-cysteinate proteins derived from yeast copper-zinc superoxide dismutase. Bioinorganic Chemistry of Copper. New York, Chapman & Hall. 64-77.

Marcus, R. A. (1993). "Electron transfer reactions in chemistry: theory and experiment (Nobel lecture)." Angew. Chem. Int. Ed. Engl. **32**: 1111-1121.

Marcus, R. A. and Sutin, N. (1985). "Electron transfers in chemistry and biology." Biochim. Biophys. Acta **811**: 265-322.

Moser, C. C., Keske, J. M., Warncke, K., Farid, R. S. and Dutton, P. L. (1992). "Nature of biological electron transfer." Nature **355**: 796-802.

Murphy, L. M., Strange, R. W., Karlsson, B. G., Lundberg, L. G., Pascher, T., Reinhammer, B. and Hasnian, S. S. (1993). "Structural characterization of azurin from *Pseudomonas aeruginosa* and some of its methionine-121 mutants." Biochem. **32**: 1965-1975.

Nar, H., Messerschmidt, A., Huber, R., van de Kamp, M. and Canters, G. W. (1991). "Crystal structure analysis of oxidized *Pseudomonas aeruginosa* azurin at pH 5.5 and pH 9.0. A pH-induced conformational transition involves a peptide bond flip." J. Mol. Biol. **221**: 765-772.

Newton, M. D. (1988). "Electronic-structure analysis of electron-transfer matrix-elements for transition-metal redox pairs." J. Phys. Chem. **92**: 3049-3056.

Onuchic, J. N. and Beratan, D. N. (1990). "A predictive theoretical-model for electron-tunneling pathways in proteins." J. Chem. Phys. **92**: 722-733.

Regan, J. J., Di Bilio, A. J., Langen, R., Skov, L. K., Winkler, J. R., Gray, H. B. and Onuchic, J. N. (1995). "Electron tunneling in azurin: the coupling across a β-sheet." Chem. & Biol. **2**: 489-496.

Regan, J. J., Risser, S. M., Beratan, D. N. and Onuchic, J. N. (1993). "Protein electron-transport - single versus multiple pathways." J. Phys. Chem. **97**(50): 13083-13088.

Scott, R. A., Hahn, J. E., Doniach, S., Freeman, H. C. and Hodgson, K. O. (1982). "Polarized X-ray absorption spectra of oriented plastocyanin single crystals. Investigation of methionine-copper coordination." J. Am. Chem. Soc. **104**: 5364-5369.

Shepard, W. E. B., Anderson, B. F., Lewandoski, D. A., Norris, G. E. and Baker, E. N. (1990). "Copper coordination geometry in azurin undergoes minimal change on reduction of copper(II) to copper (I)." J. Am. Chem. Soc. **112**: 7817-7819.

Siddarth, P. and Marcus, R. A. (1993). "Correlation between theory and experiment in electron-transfer reactions in proteins: electronic couplings in modified cytochrome *c* and myoglobin derivatives." J. Phys. Chem. **97**: 13078-13082.

Solomon, E. I., Hare, J. W., Dooley, D. M., Dawson, J. H., Stephens, P. J. and Gray, H. B. (1980). "Spectroscopic studies of stellacyanin, plastocyanin, and azurin. Electronic structure of the blue copper sites." J. Am. Chem. Soc. **102**: 168-178.

Strange, R. W., Murphy, L. M., Karlsson, B. G., Reinhammar, B. and Hasnian, S. S. (1996). "Effect of pH and ligand binding on the structure of the Cu site of the Met121Glu mutant of azurin from *Pseudomonas aeruginosa*." Biochem. **35**: 16391-16398.

Stuchebrukhov, A. A. (1996). "Tunneling currents in electron transfer reaction in proteins. II. Calculation of electronic superexchange matrix element and tunneling currents using nonorthoganal basis sets." J. Chem. Phys. **105**(24): 10819-10829.

Stuchebrukhov, A. A. and Marcus, R. A. (1995). "Theoretical study of electron transfer in ferrocytochromes." J. Phys. Chem. **99**: 7581-7590.

Winkler, J. R. and Gray, H. B. (1992). "Electron transfer in ruthenium-modified proteins." Chem. Rev. **92**: 369-379.

Wuttke, D. S., Bjerrum, M. J., Winkler, J. R. and Gray, H. B. (1992). "Electron-tunneling pathways in cytochrome-*c*." Science **256**: 1007-1009.

Chapter 2

Electron Transfer in M121E Azurin

Measuring electron transfer rates in proteins

Several methods have been used to obtain electron transfer rates within protein media. One may study the natural systems plants and animals use to obtain energy, for example the oxidase systems of the mitochondria or the photosynthetic reaction center. Studying most oxidase systems is complicated by the fact that electron transfer is coupled to proton transfer, adding another layer of complexity. Several bacterial photosynthetic reaction centers have been widely studied. They are large but well defined; X-ray structures are available for *Rhodopseudomonas viridis* (Allen et al. 1987; Yeates et al. 1987) and *Rhodobacter sphaeroides* (Deisenhofer et al. 1984). Electron transfers between various of the multiple chromophores can be followed spectroscopically and yield rates for ET over various distances and with different driving forces (Boxer 1990).

However, one is limited in these natural systems to the distances, driving forces, and intervening media provided by the particular reaction center. The Gray group, among others, have chosen to study electron transfer reactions in model systems consisting of a metalloprotein that has been covalently modified to add a second metal center at various places on the protein surface (Winkler and Gray 1992). The metal modification used in this study is a ruthenium bisbipyridyl imidazole ($Ru(bpy)_2Im$-) bound to surface histidines introduced on the surface of azurin through site-directed mutagenesis. Excitation with 480 nm laser light creates a long-lived $Ru(bpy)_2ImHis$ excited state (66 ns for the $Ru(bpy)_2Im_2$ model compound (Wuttke 1994), 100 ns for $Ru(bpy)_2Im$-labeled azurin (Di Bilio et al. 1997; Kiser 1997)) which is a good reductant. The reducing potential of the $Ru(bpy)_2Im$ label has been exploited for the direct reduction of the Cu^{2+} center of azurin, in the photoinduced ET scheme, and, for the indirect oxidation of a Cu^{1+} center after the reduction of an exogenous quencher in the flash/quench scheme.

Photoinduced electron transfer

In the photoinduced electron transfer scheme (see figure 1), the $Ru(bpy)_2ImHis$ label is excited at 480 nm, creating an excited electron on one of the bipyridyl ligands. This can decay by phosphorescence (emitting in a broad band around 670 nm), energy transfer, and non-radiative decay (collectively k_d), and by electron transfer (k_{ET}). When the Ru label is attached at points on the surface of azurin close to the copper center, the excited electron may be

transferred to the half filled Cu^{2+} HOMO. This reduction causes a bleach in the characteristic azurin ~600 nm LMCT band. The concomitant creation of the Ru^{3+} center can most easily be monitored as a bleach in the Ru^{2+}/Ru^{3+} couple at 430 nm, the isobestic point for the $Ru(bpy)_2Im_2^{2+/2+*}$. (See figure 2 (Sigfridsson et al. 1996).) The Cu^{1+}/Ru^{3+} couple that is created is thermodynamically unstable and returns to the Cu^{2+}/Ru^{2+} ground state through a second electron transfer reaction (k_{BET}). Since we are mainly interested in metal to metal, ground state electron transfers, this back electron transfer is the reaction of interest. This is fortunate, since the forward, excited state electron transfer reaction is on time scales too fast to be resolved from the 25 ns laser pulse used to create the initial Ru^{2+} excited state. Additional strong absorbance changes in the Ru^{2+}/Ru^{3+} difference spectrum occur at 310 and 500 nm. At these wavelengths, there are also strong absorbance changes due to the Ru^{2+*} excited state. Rates for both the excited state decay and the back electron transfer can be identified using biexponential fits of the data because they occur on sufficiently different time scales as to be distinguishable.

Flash/quench methodology

The photoinduced electron transfer scheme only works in systems where the initial electron transfer from the Ru label competes favorably with the other processes by which the excited state electron may relax. In general, this requires an acceptor with a fairly high reduction potential located close to the point of attachment of the label. To study electron transfer at slower rates (longer distances), the flash/quench scheme was developed (Chang et al. 1991). (See figure 3.) With this methodology, one starts with reduced azurin. The excited state of the Ru^{2+} label is rapidly quenched using an exogenously added $[Ru(NH_3)_6]^{3+}$ quencher.[1] The Ru^{3+} label can then be reduced intramolecularly by electron transfer from a reduced Cu^{1+} center in protein. Again this ground state electron transfer can be monitored at wavelengths characteristic of the $Cu^{2+/1+}$ and $Ru^{3+/2+}$ couples (600, 430, 310, and 500 nm). On longer time scales (0.5 ms), the reduced $[Ru(NH_3)_6]^{2+}$ quencher rereduces the azurin Cu center. Because both the photoinduced reaction and the flash/quench reaction using $[Ru(NH_3)_6]^{3+}$ are reversible, the sample can be excited repeatedly and the resulting absorption transients averaged to increase the signal-to-noise ratio.

---

[1]The second order rate constant for $Ru(NH_3)_6^{3+}$ quenching of $Ru(bpy)_2(Im)(His33)Fe^{2+}$-cyt *c* is $4.9 \times 10^8\ M^{-1}s^{-1}$ (Chang et al. 1991).

Experimental design

In this project I have attempted to alter the electron transfer properties of the blue copper protein, azurin, by altering one of its ligand residues. Using site-directed mutagenesis, M121E mutants of azurin containing a single surface-exposed histidine at either position 83 or 122 were constructed. They were labeled with $Ru(bpy)_2Im$ and, using the photoinduced and flash/quench schemes described above, ET rates from Cu^{1+} to Ru^{3+} were measured at pH 4.3 and 8.1. These rates were compared to rates of ET to labels at the same places on the wild-type protein (Langen 1995). In chapter 3 the observed alterations in ET rates are discussed within the framework of semiclassical Marcus theory and attempts are made to correlate changes in the ET function of the M121E mutant to other spectroscopic and structural changes at the Cu site.

Material and methods

General

Unless otherwise stated, all chemicals were reagent grade. Restriction enzymes and T4 DNA ligase were purchased from a variety of suppliers (New England Biolabs, Beverly MA; Boehringer Mannheim, Indianapolis, IN) and used according to the manufacturer's instructions. PD10 columns, disposable columns prepacked with Sephadex G25, were purchased from Pharmacia Biotech (Uppsala, Sweden) and used for most buffer exchanges. Protein concentration was done by ultrafiltration using either an Amicon YM10 membrane or a Centricon10 spin concentrator (Amicon, Beverly, MA). Oligonucleotide synthesis was done at the Caltech polymer synthesis facility. Sequencing was originally done manually using a Sequenase Version 2.0 kit from US Biochemical and, later in the project, by the Caltech DNA sequencing facility. Protein purifications used a Pharmacia FPLC with a MonoQ 10/10 column and protein elution was monitored by absorption at 280 nm. Absorption spectra were taken using a Hewlett Packard 8452A diode array UV/Vis spectrophotometer. The pET expression system (vectors and the *E. coli* expression strain BL21(DE3)) were purchased from Novagen (Madison, WI).

Inorganic reagents

Ruthenium(II) bis-bipyridine carbonate was prepared according to the method of Johnson and coworkers (Johnson et al. 1978). 1.01grams of dichloro bis(2, 2' bipyridine)ruthenium(II) dihydrate (Strem Chemicals, Inc., Newburyport, MA) was refluxed for 25 minutes in 100 ml water under a stream

of nitrogen gas. To this hot solution was added 3.3 g sodium carbonate (Na_2CO_3); the solution turned a purple/red almost immediately. This solution was refluxed for a further two hours, still flushing the flask with nitrogen gas. The solution was allowed to cool, then filtered through Whatman No. 5 filter paper to collect the crystals. UV/Vis absorption spectra show the expected bis(2, 2' bipyridine)ruthenium(II)carbonate product.

Hexamine ruthenium(III) trichloride, used as an oxidative quencher in laser experiments, was purchased from Strem Chemicals, Inc. Before use, it was recrystalized by first dissolving 1 g in 15 ml water, then precipitating it by addition of excess acetone (75 ml). The solid filtered out of this water/acetone mixture was then redissolved in 20-25 ml 1 M HCl, filtered, and the solvent and acid were removed by rotary evaporation. The spectrum of the purified hexamine ruthenium(III) trichloride shows a strong absorbance at 276 nm and a greatly reduced shoulder at 322 nm.

Mutant construction

Our expression system for wild type azurin is the synthetic gene for *Pseudomonas aeruginosa* azurin constructed by Dr. Thomas K.-Y. Chang (Chang et al. 1991) cloned into a T7 promoter expression vector (pET, Novagen, Madison, WI) (Germanas et al. 1993). The construct I currently use is cloned into pET9a and is a gift from Dr. Jy-Ye Luo. The M121E mutant was constructed using the Kunkel method (Kunkel et al. 1991) of mutagenesis (Muta-gene kit from Bio-Rad) on a single stranded pTZ18U/azurin template with subsequent subcloning of the mutants into the pET9a expression vector; M121E azurin in pET9a was a gift from Dr. T. Jack Mizogouchi. The M121E/K122H/H83Q mutant was constructed using the Kunkel mutagenesis method (bottom strand mutagenic oligo: 5' CAG AGT CAG GGT ACC GTG CTC CAG TGC GGA GTG on a single-stranded template, pTZ18U/azurin containing the H83Q mutation, a kind gift from Dr. Ralf Langen) and was sub-cloned into pET9a. The M121E/T124H/H83Q gene was prepared by ligating a BamHI/KpnI fragment containing the M121E mutation into a pET3a construct containing the H83Q/T124H azurin described by Dr. Ralf Langen (Langen 1995). See appendix B for maps and sequences of these constructs.

Protein production

The expression vector is transformed into chemically competent BL21(DE3) *E. coli* (Novagen). Single colonies are used to inoculate starter cultures of LB (1% tryptone, 0.5% yeast extract, 0.5% NaCl) supplemented with

the appropriate antibiotic (50 μg/ml ampicillin for pET3a constructs or 50 μg/ml kanamycin for pET9a constructs). These are grown overnight shaking at 37°C and used to inoculate three 3 liter flasks of LB containing antibiotic. Cultures are grown to an OD_{600} of 0.6-1.0. Protein production is initiated by addition of IPTG to a final concentration of 0.4 mM. After 4-8 hours at 37°C, the cells are harvested by centrifugation for 10 minutes, 4,000 x g. The cell paste is resuspended in 1/10th volume of a high osmolarity solution (20% sucrose, 30 mM Tris pH 8.0, 1 mM EDTA) and shaken for 10-30 minutes. The cells were repelleted (20 minutes, 8,000 x g) then resuspended in 1/10th volume distilled water and left shaking at 4°C for 4-12 hours. The cells are then pelleted (20 minutes, 8,000 x g) and the periplasmic extrudate is decanted from the cell debris, taking care to minimize the amount of lysed cell material carried into the next step. The protein solution is made acidic by the addition of sodium acetate to 20-100 mM and the pH adjusted to 4.5; this precipitates most of the other periplasmic proteins as well as the DNA from lysed cells, leaving mainly azurin in solution. After sitting at room temperature for an hour or more, the precipitate is removed by centrifugation (30 minutes 8,000 x g). The solution is brought to 10 mM $CuSO_4$ and left at room temperature for up to a week to allow the protein to incorporate Cu. Then the protein solution is concentrated by ultrafiltration with an Amicon YM10 membrane. The protein is generally stored at 4°C in sodium acetate buffer, pH 4.3-4.5, with 5-10 mM $CuSO_4$. Upon storage at concentrations of 1-6 mg/ml, protein, mainly azurin, tends to precipitate.

Protein purification

For the labeling reactions, the proteins were used without further purification. For studies requiring pure holo-azurin, this crude protein preparation is purified by FPLC on a MonoQ anion exchange column using 20 mM diethanolamine, pH 8.8, and eluting with a salt gradient of 0-30 mM NaCl; holo-azurin elutes at ~20 mM NaCl. The apo-azurin can be made by exhaustive washing (concentration and dilution using a Centricon10) with buffer consisting of 100 mM thiourea, 10 mM EDTA, 100 mM NaOAc pH 4.5. The apo-protein is purified on a MonoS cation exchange column, loading with 25 mM NaOAc, pH 4.5, 1 mM EDTA and eluting with a gradient of 300 mM NaOAc, pH 4.5, 1 mM EDTA; apoM121EAz elutes at 8-9% B. Apo-azurin may also be purified with a MonoQ anion exchange column, loading with 20 mM diethanolamine, pH 8.8, and eluting in the same buffer containing 200 mM NaCl; apo-azurin elutes at ~17% B.

Ruthenation and purification - M121E/K122H/H83Q azurin

Approximately 100 mg of crude azurin (quantitated using an ε=3000 M^{-1} cm^{-1} for the 610 nm band) is washed by repeated concentration and dilution to remove the excess $CuSO_4$ in which the protein is usually stored. Then, again by repeated concentration and dilution, the protein is exchanged into fresh 300 mM $NaHCO_3$, pH 7.3. $Ru(bpy)_2CO_3 \cdot 4H_2O$ is added to a final azurin:Ru ratio of 20mg:1mg (3:4 azurin:Ru molar ratio). The total volume of the reaction is adjusted to give final protein concentration of approximately 3 mg/ml and the reaction is left at room temp in the dark overnight (generally 12-16 hours). To check extent of the reaction, a small amount is exchanged into 25 mM NaOAc pH 4.5, using a PD10 column; the ruthenated azurin migrates as a forest green band, while the excess inorganic Ru migrates as a slower-moving red band. Initially there is a broad symmetric absorption near 465 nm which gradually shifts toward 486 nm, becoming sharper and less symmetric, leaning toward the red. The reaction is stopped when the inorganic Ru is consumed or when the Ru absorption band has shifted to 486 nm. The ratio of the extinction coefficients of the Ru^{2+} 486 nm band and M121E azurin Cu^{2+} band near 600 nm is $\approx$ 3.

The 'mono-aquo' species azurinHis122$Ru(bpy)_2(H_2O)$ is concentrated and exchanged into 300 mM imidazole, pH 8.0. The imidazole reaction is again monitored by exchanging small aliquots into 25 mM NaOAc pH 4.5 using a PD10 column. Again one generally sees a trailing band of inorganic Ru on the PD10 column, indicating that some non-specifically bound Ru dissociates from the protein. As the reaction progresses the visible spectrum shows a shoulder growing in near 440 nm. One also generally sees an increase in the Ru:Az 486/600 ratio, perhaps indicating Cu^{2+} loss due to imidazole chelation. After 3-6 days, there are generally no further changes in the spectrum.

The ruthenium modified azurin is purified by two successive FPLC separations using a Mono Q 10/10 column. The protein is loaded with 20 mM ethanolamine, pH 9.2, and eluted with 20 mM ethanolamine, pH 9.2, containing 200 mM NaCl. The first separation uses a linear gradient from 0-30% buffer B. The constellation of peaks eluting between 0 and 10% B are thought to be multiply ruthenated azurins because the ratios of their 486 to 600 nm bands are greater than 3. The next fraction, the largest of the peaks (at ~14% B), is $Ru(bpy)_2$ImHis122Az. This is followed by the unmodified azurin (which still contains Cu^{2+}) and then another peak with a spectrum nearly identical to the main peak (as yet unidentified). The pooled main peak is re-chromatographed

using the same column and buffers but with a much shallower gradient, 10-12% B. Typical elution profiles are shown in figure 4. Pooled main peak fractions are stored at 4°C in 25 mM NaOAc, pH 4.5, with or without addition of excess $CuSO_4$ (~5 mM). Typical yields of $Ru(bpy)_2ImHis122Az$ are around 60%.

Ruthenation and purification - M121E(H83) azurin

The protein is exchanged into 300 mM $NaHCO_3$ buffer, pH 7.40, using a Centricon10. The extinction coefficient of a stock solution of $Ru(bpy)_2CO_3 \cdot 4H_2O$ in 300 mM $NaHCO_3$ (ε_{510} = 9,200 $M^{-1}cm^{-1}$) is used to calculate the amount needed to achieve a 1:1 or 1:2 molar ratio of azurin:Ru. The final protein concentration is adjusted to 3 mg/ml and the reaction is allowed to proceed for 12 hours at room temperature in the dark. The protein is exchanged into 300 mM imidazole, pH 8.0, and left at room temperature in the dark for 1-3 days.

Two rounds of FPLC purification are performed using a MonoQ 10/10 column, loading in a buffer of 20 mM ethanolamine, pH 9.4, and eluting with a buffer containing 20 mM ethanolamine, pH 9.4, and 200 mM NaCl (see figure 5). For the initial purification, a gradient of 0-20% buffer B was used. $M121EH83Ru(bpy)_2Im$ elutes as the main peak at ~5% B. For the second round of purification, the sample is again loaded onto the column in 20 mM ethanolamine, pH 9.4, and washed with buffer A for 1/2 column volume before initiating a gradient of 0-10% buffer B. Sodium borate buffers (20 mM, pH 9.6) have also been used to purify $M121EH83Ru(bpy)_2Im$. At this pH, the protein interacts more strongly with the column and elutes with ~30 mM NaCl.

Laser sample preparation

For photoinduced electron transfer experiments, purified protein was exchanged into either 100 mM sodium phosphate, pH 8.1, or 25 mM sodium acetate, pH 4.3, using a PD10 column. 1-2 ml samples with protein concentrations ranging between 30 and 115 μM were placed in a 1 cm path-length laser cuvette and degassed by repeated cycles of vacuum pumping and flushing with N_2 gas. Luminescence and absorption transients were taken using the Beckman Institute Laser Research Center (BILRC) nanosecond dye laser, exciting with 25 nanosecond, 1.5 mJ pulses of 480 nm light. Luminescence decay was monitored at 670 nm. Transient species were monitored at 600 ($Cu^{1+/2+}$), 430 ($Ru^{3+/2+}$), 500 and 310 ($Ru^{2+/3+}$ and $Ru^{2+*/2+}$) nm. The BILRC laser and transient absorption detection apparatus have been described previously (Wuttke 1994).

For flash/quench laser experiments, initial data were taken using a scheme allowing *in situ* reduction of oxidized azurin. Laser samples were

prepared using the photoinduced methodology above except that during the sample preparation, 1/10th volume of 60 mM $[Ru(NH_3)_6]^{3+}$ in the appropriate buffer was placed in the other side of a two chambered laser cuvette - along with enough sodium ascorbate to be in 1-3 fold molar excess over the protein when the contents of the two chambers were mixed together. The sample was degassed and photoinduced laser data was taken. A UV/Vis spectrum of the sample verified that the photoinduced laser experiment did not degrade the labeled protein sample. The ascorbate and quencher were then mixed into the protein sample and reduction of the Cu center was verified by UV/Vis spectroscopy. Luminescence decay and transient absorption data were then taken in the same manner as the photoinduced data was taken. In samples containing only a 1:1 molar ratio of ascorbate to protein (which is a 2 fold excess of electrons), the spectra indicated that the initial protein reduction was not complete. In the electron transfer data taken on *in situ* reduced samples, absorption transients did not return to baseline, even on time scales 10 times longer that than those required for the decay of the initial signal. In addition, the rate of the slower reoxidation of Ru^{2+} depended on the ascorbate concentration - higher ascorbate leading to faster bimolecular reoxidation.

To remove the effects of ascorbate, in later experiments purified protein was reduced with a large excess of sodium dithionite then immediately loaded on a PD10 column. The column served both to remove the excess dithionite and to exchange the protein into the desired phosphate or acetate buffer. Sample was loaded into the cuvette side of a 2 chambered laser cuvette. One volume of 12 mM $[Ru(NH_3)_6]^{3+}$ in the appropriate buffer (or 1/10th volume of 60 mM $[Ru(NH_3)_6]^{3+}$) was placed in the other side and the sample degassed. Luminescence decay measurements were taken on the reduced sample alone then the quencher was mixed in and luminescence decay and transient absorption data were taken. Initially samples were prepared on the lab bench and degassed with normal N_2 gas. The M121E Cu^{1+} center appears to be very susceptible to reoxidation (see below) so in the final experiments for this thesis, flash/quench samples were prepared in a glove box under a nitrogen atmosphere and degassed using repeated cycles of vacuum pumping and flushing with N_2 gas passed over a manganese-based oxygen-scrubbing catalyst to remove any residual impurities.

Results and discussion

Oxygen lability of reduced M121E azurin

In flash/quench experiments using samples prepared on the lab bench, absorption signals did not return to baseline, even on time scales 10x the rate of the initial decay (see figure 7f). This was believed to indicate heterogeneity in the sample, either lack of copper occupancy (with possible Zn contamination of the sample (Nar et al. 1992)) or reoxidation of the Cu center, which prevents electron transfer to the quenched ruthenium label. At the concentrations used, the $[Ru(NH_3)_6]^{3+}$ quencher will oxidize less than 1% of the reduced protein. Experiments described below indicated that the M121E mutant copper site was far more susceptible to reoxidation in air than the wild type center.

UV/Vis spectra taken after shooting WT azurin did not show signs of steady-state reoxidation of the copper center during the course of flash/quench laser experiments. However, spectra taken after flash/quench experiments with the M121E mutant showed some signs of reoxidation of the Cu site. The 600 nm Cu^{2+} absorption seen at low pH increased with time even after shooting ceased. This raised the possibility that the absorption transients not returning to baseline was due to reoxidation of the Cu^{1+} center but in amounts that were hard to detect by steady state spectroscopy. The extinction coefficient of the 610 nm Cu^{2+} band[2] is about 3000 $M^{-1}cm^{-1}$, while the 486 Ru^{2+} band, which has a considerable tail to lower wavelengths, has an extinction coefficient of 9,200 $M^{-1}cm^{-1}$ (Regan et al. 1995). In high pH experiments, no immediate information is available on the reoxidation of the sample because at pH 8.1 the copper peaks at 413 and 570 nm are obscured by the tails of the much larger $Ru(bpy)_2$ImHis absorption.

Steady state reoxidation rates were studied using unlabeled WT and labeled and unlabeled M121E azurin. Samples were prepared by reduction with excess dithionite which was then removed using a PD10 column. When the experiment was done on the lab bench, extensive reoxidation, up to 61% of the M121E sample, was seen on the time that it takes to run the PD10 column, transfer the sample to the laser cuvette, and degas (10-15 minutes). Minimal reoxidation of the WT protein (14%) was seen on this time scale. Once degassed, the M121E does not reoxidize further; data for an experiment using M121E/H83Q/K122H Ru(bpy)2(Im) is shown in figure 2.6. The reoxidation of the M121E Cu^{1+} center while on the PD10 column indicates that, while the

---

[2]CNK unpublished observations. From the integration of the EPR signal, Karlsson and coworkers report ε = 4,500 M^{-1}cm-1 at 614 nm, pH 3.5 (Karlsson et al. 1997).

reduction potential of the M121E mutant at pH 4 is substantially the same as that of the WT protein (0.37 vs. 0.35 mV (Pascher et al. 1993)), the center is far more kinetically labile and so is susceptible to attack by atmospheric O_2. Preparation of laser samples in a glove box with a N_2 atmosphere solved the problem of long-lived $Ru^{2+}(bpy)_2ImHis$ signals and the O_2 lability of the M121E Cu^{2+} center was not explored further.

Electron transfer rates

The first step in the photoinduced electron transfer scheme is injection of the excited electron from the $Ru^{2+*}(bpy)_2Im$ label into the oxidized blue copper site. The estimated driving force for this reaction is -1.39 eV at pH 4.0 (see chapter 3). With this relatively strong driving force, electron transfer is able to compete effectively with other relaxation processes when the electron acceptor is close to the label. Thus for labels placed at position 122 (metal to metal distance of 15.9Å) and at the native His83 (metal to metal distance of 16.9Å (Faham et al. 1998)), considerable photoinduced electron injection occurs. The initial injection rate in these experiments was not measured but it could be determined from the change in emission lifetime between the Zn^{2+} and Cu^{2+} proteins if the quantum yield for the reaction were measured. The absorbance transients that can be monitored on the time scale of our instrument are for the second step of the photoinduced electron transfer - the back electron transfer from the transiently reduced Cu center to the Ru^{3+} label.

Photoinduced electron transfer experiments performed at low pH (25 mM NaOAc, pH 4.3) show good absorbance transients when the label was placed at position 122 and 83. At high pH (pH 8.1), no rate associated with electron transfer can be seen in photoinduced experiments with either of the labeled proteins. Absorption transients at all observed wavelengths for both the H83 and H122 samples decay with the same rate, $2 \times 10^7\ s^{-1}$. The driving force for electron injection is lower at high pH but it is still considerably exothermic, -1.20 eV. The major difference between the high and low pH experiments is the major CT absorption band is considerably blue shifted at high pH. This has a major impact on the ability of energy transfer to compete with electron transfer and fluorescence as a means of relaxing the Ru^{2+} excited state. Energy transfer is promoted by close contact and good spectral overlap between the donor and acceptor states. In the oxidized protein at low pH, the absorption spectra of the Cu center and $Ru(bpy)_2Im$ label overlap somewhat (see figure 8). At high pH,

this overlap is further enhanced by the shift of the azurin LMCT band from 610 to 570 nm.

While we do not have enough information to calculate the individual contributions of energy transfer, forward electron transfer, radiative and non-radiative decay, some idea of the magnitude of the energy transfer reaction can be obtained by comparing the emission rates of the Ru^{2+*} in different experiments. The observed emissions rate is the sum of all processes that lead to the decay of the $Ru(bpy)_2ImHis$ excited state (Connors 1990). When the photoinduced experiment is done using the reduced Cu^{1+} azurin, the protein's metal center is d^{10} so there is no acceptor state for the excited electron. In addition the site is colorless so there is no spectral overlap to facilitate energy transfer. The decay of the Ru^{2+} excited state (τ = 111(7) or 105(9) ns at positions 83 and 122 respectively) is thus only due to fluorescence and non-radiative relaxation processes. The excited-state lifetimes of the oxidized proteins are all much shorter than this. At high pH, where no photoinduced electron transfer could be seen, the Ru^{2+*} lifetimes are 76(6) and 50(7) ns for positions 83 and 122 respectively. At low pH, where the Ru^{2+*} excited state is quenched by both energy and electron transfer, the lifetimes are shorter still, τ = 65(10) and 37(11) ns for positions 83 and 122.

Electron transfer rates for each protein at high and low pH are given in the table in figure 9. Confirmatory photoinduced rates are included where available. All of the electron transfer rates from the M121E Cu center are much slower than their WT counterparts. In addition, contrary to expectations we do not see a consistent increase in rate with increasing pH; ET to position 83 is faster at high pH but the 122 rate decreases with increasing pH. The interpretation of these rates will be taken up in chapter 3. In all cases, the rates observed were independent of protein concentration.

Figure 2.1 Photoinduced electron transfer scheme.

Photoinduced Electron Transfer Scheme

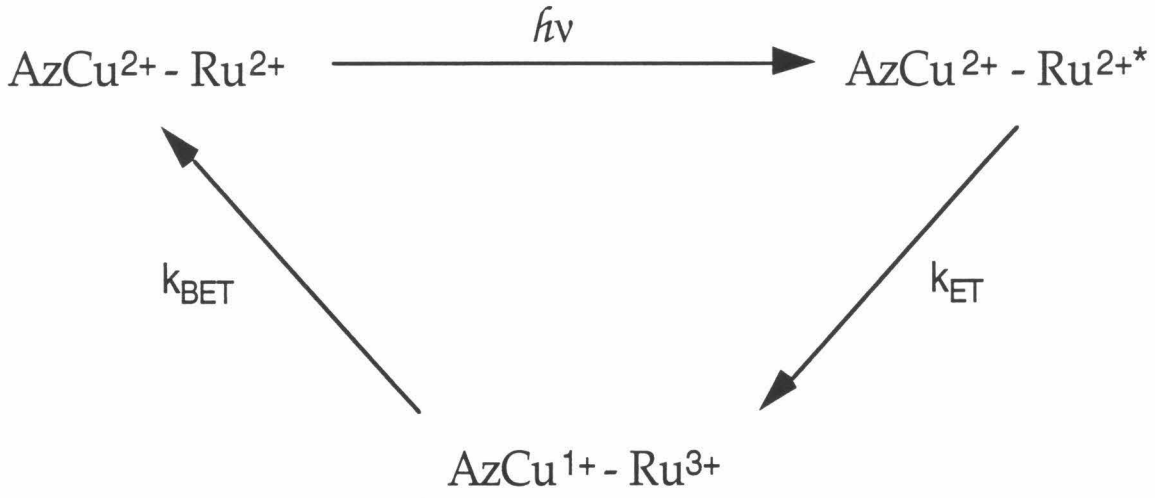

Figure 2.2 Difference spectra for the Ru^{2+*}-Ru^{2+} excited state and the Ru^{3+}-Ru^{2+} ground state couples of the model complex $Ru(bpy)_2Im_2$. The difference spectra were taken by Morten Bjerrum and described in (Sigfridsson et al. 1996).

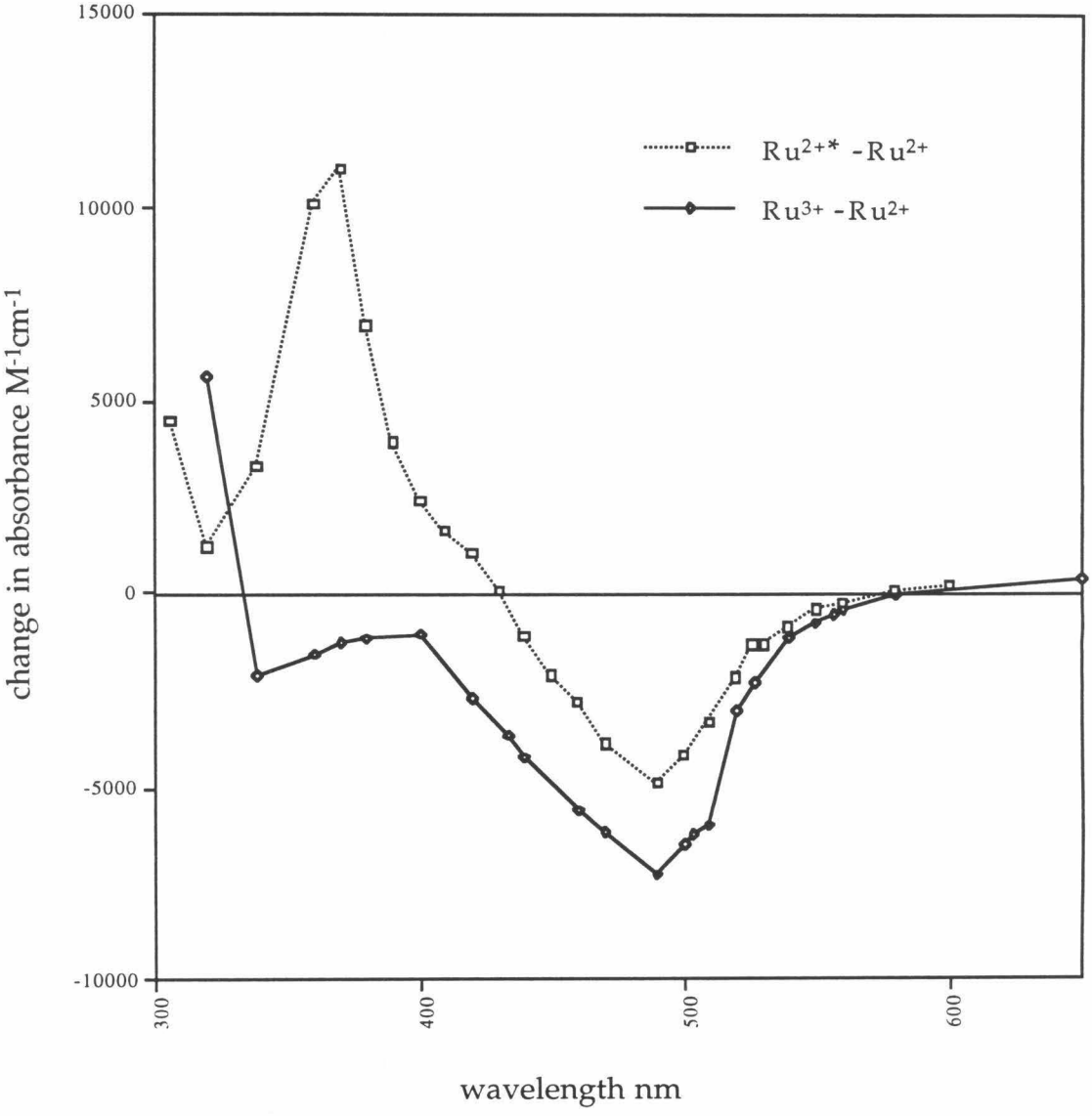
15000
10000
5000
0
-5000
-10000
300
400
500
600
change in absorbance M-1cm-1
wavelength nm
Ru2+* -Ru2+
Ru3+ -Ru2+

Figure 2.3 Flash/quench electron transfer scheme.

Flash/QuenchElectron Transfer Scheme

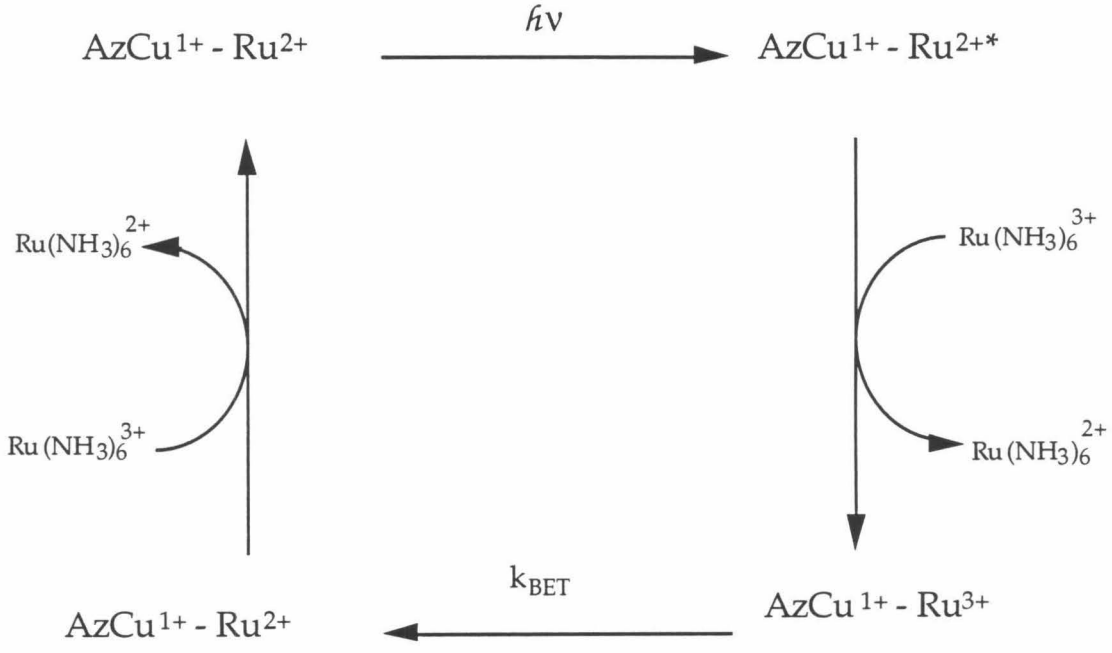

Figure 2.4 FPLC purification of M121E/K122H Ru(bpy)$_2$Im azurin.Mono Q 10/10 Buffer A: 20 mM ethanolamine, pH 9.2 Buffer B: 20 mM ethanolamine, pH 9.2 with 200 mM NaCl. (a) Early peaks are multiply ruthenated protein. The main peak, eluting at 14% B, is the desired M121E/K122H Ru(bpy)$_2$Im azurin. The peak at 20% B is ruthenated but lacks the type I Cu center. And the peak at 23% B is unmodified azurin. (b) The main peak from (a) rerun with a shallower gradient.

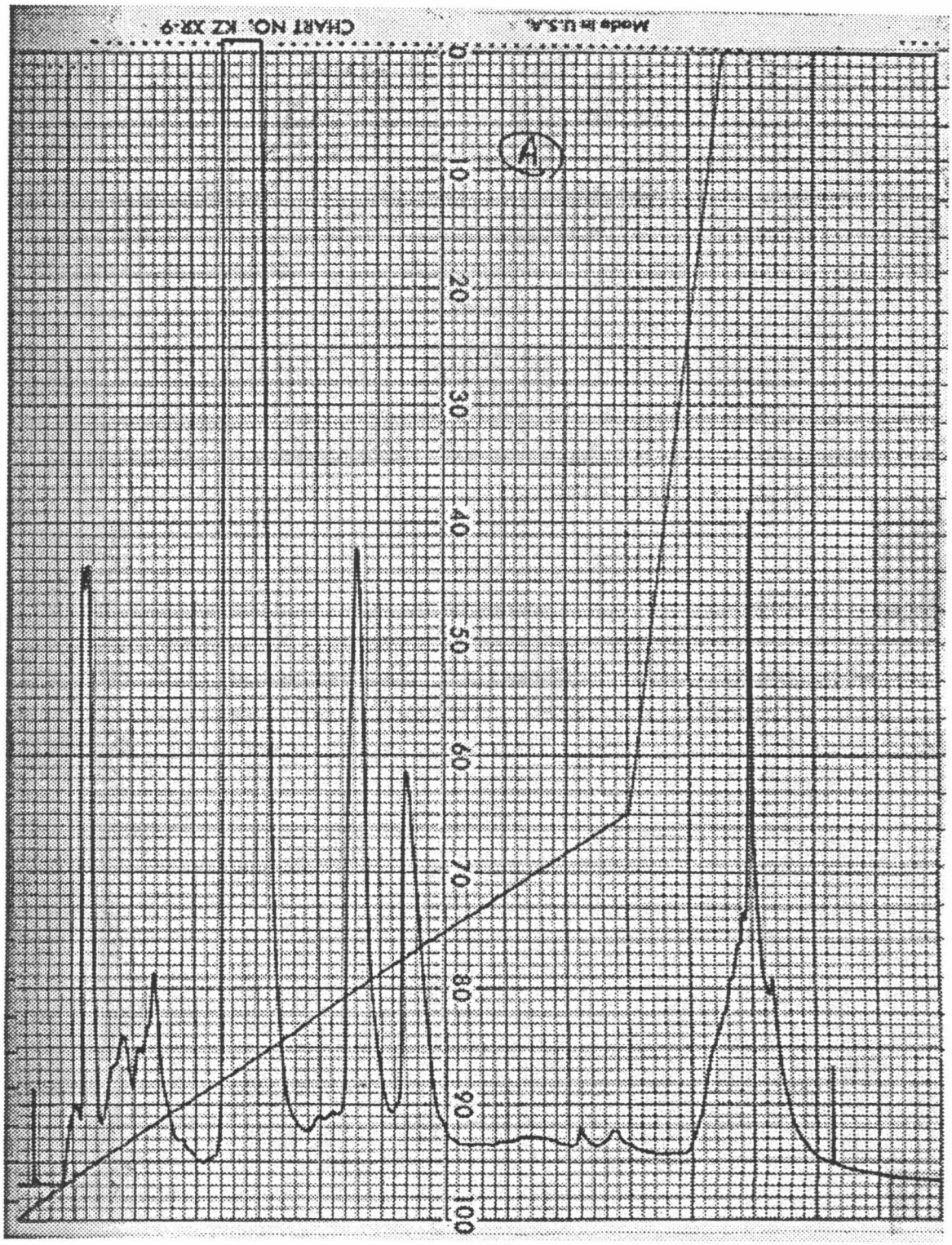
CHART NO. KZ XR-9
Made in U.S.A.
A
0
10
20
30
40
50
60
70
80
90
100

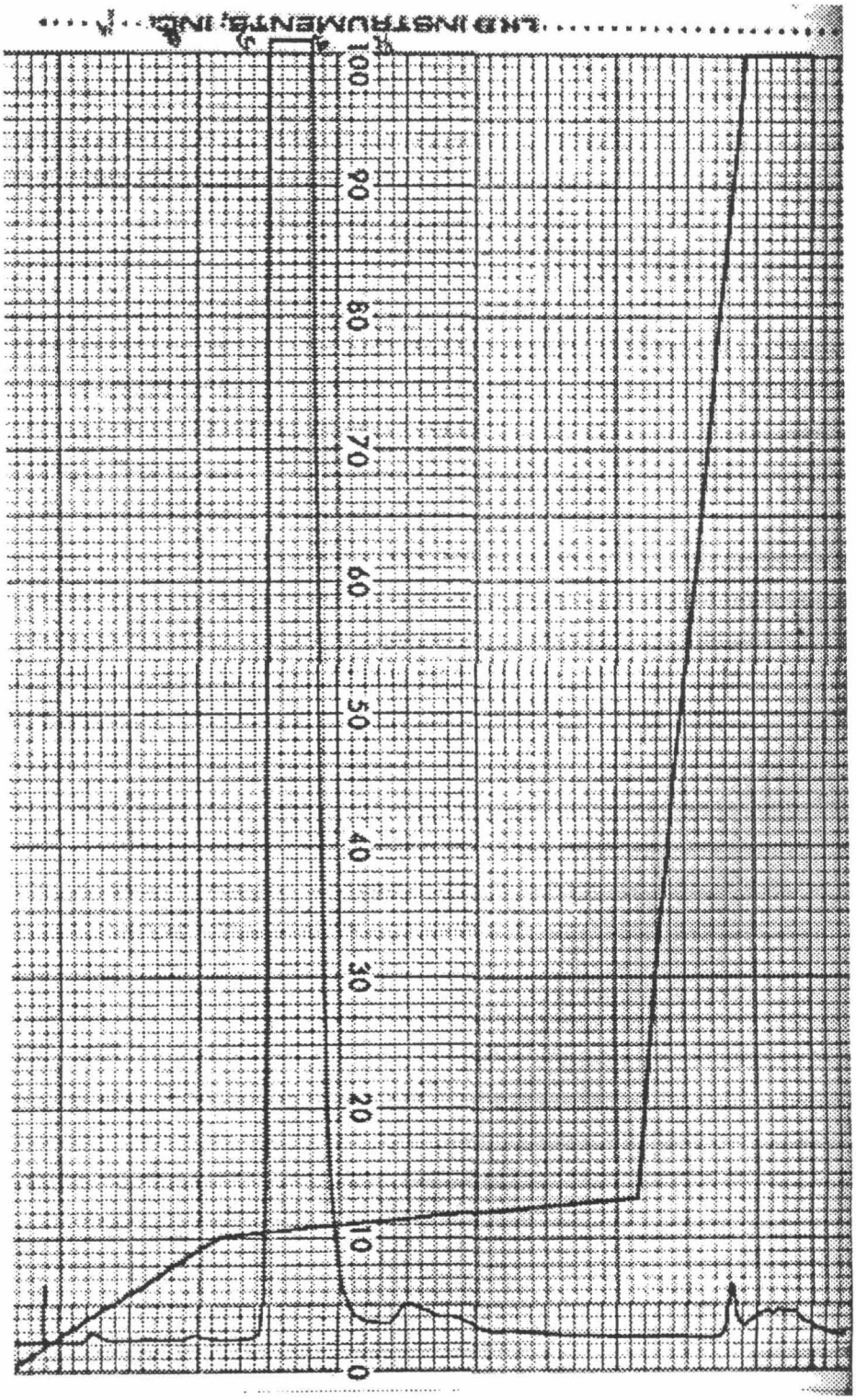
LKB INSTRUMENTS, INC.
100
90
80
70
60
50
40
30
20
10
0

Figure 2.5 FPLC purification of M121E/H83 $Ru(bpy)_2Im$ azurin.Mono Q 10/10 Buffer A: 20 mM ethanolamine, pH 9.4 Buffer B: 20 mM ethanolamine, pH 9.4 with 200 mM NaCl. (a) The early peak is multiply ruthenated protein. The main peak, eluting at 6% B, is the desired M121E/H83 $Ru(bpy)_2Im$ azurin. (b) The main peak from (a) rerun with a shallower gradient; multiply ruthenated protein elutes early, at 0% B.

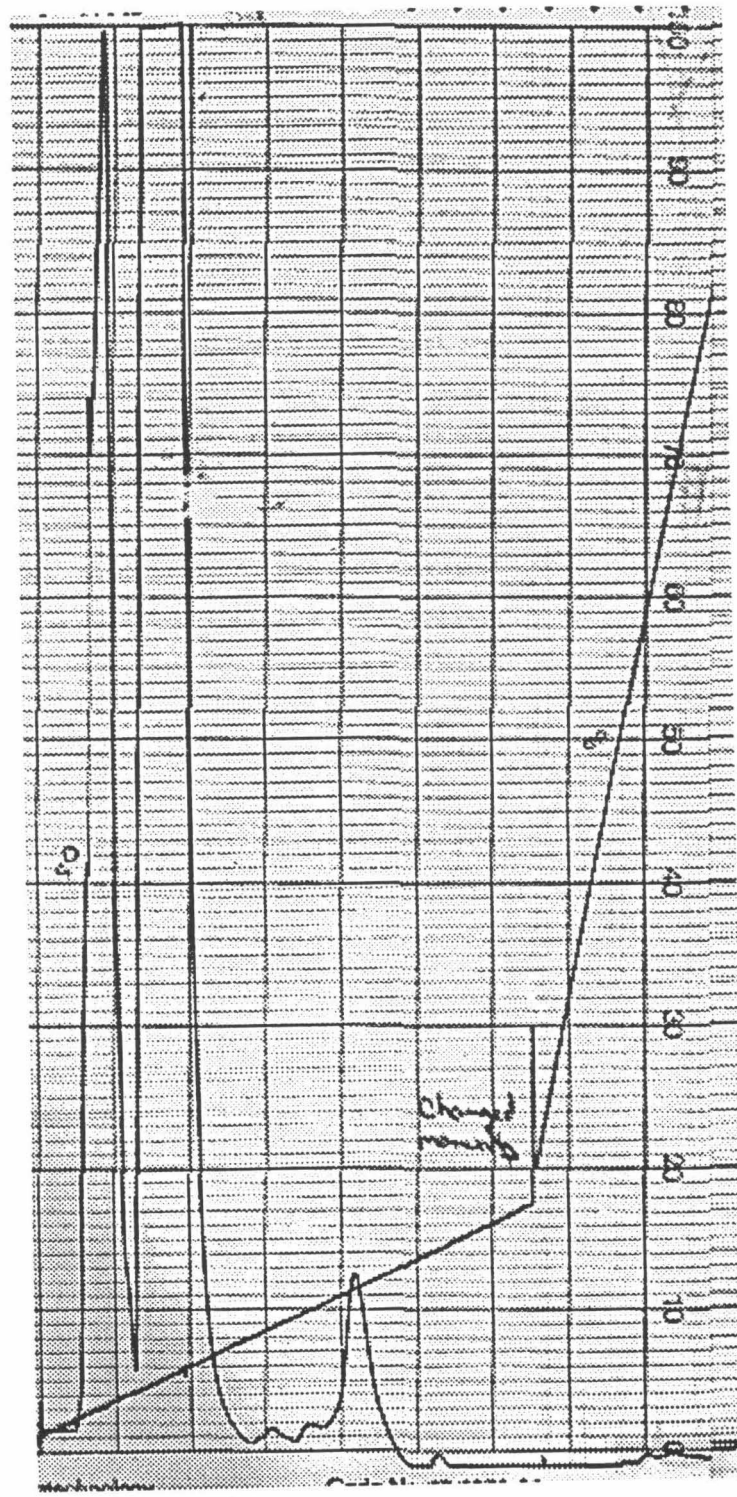

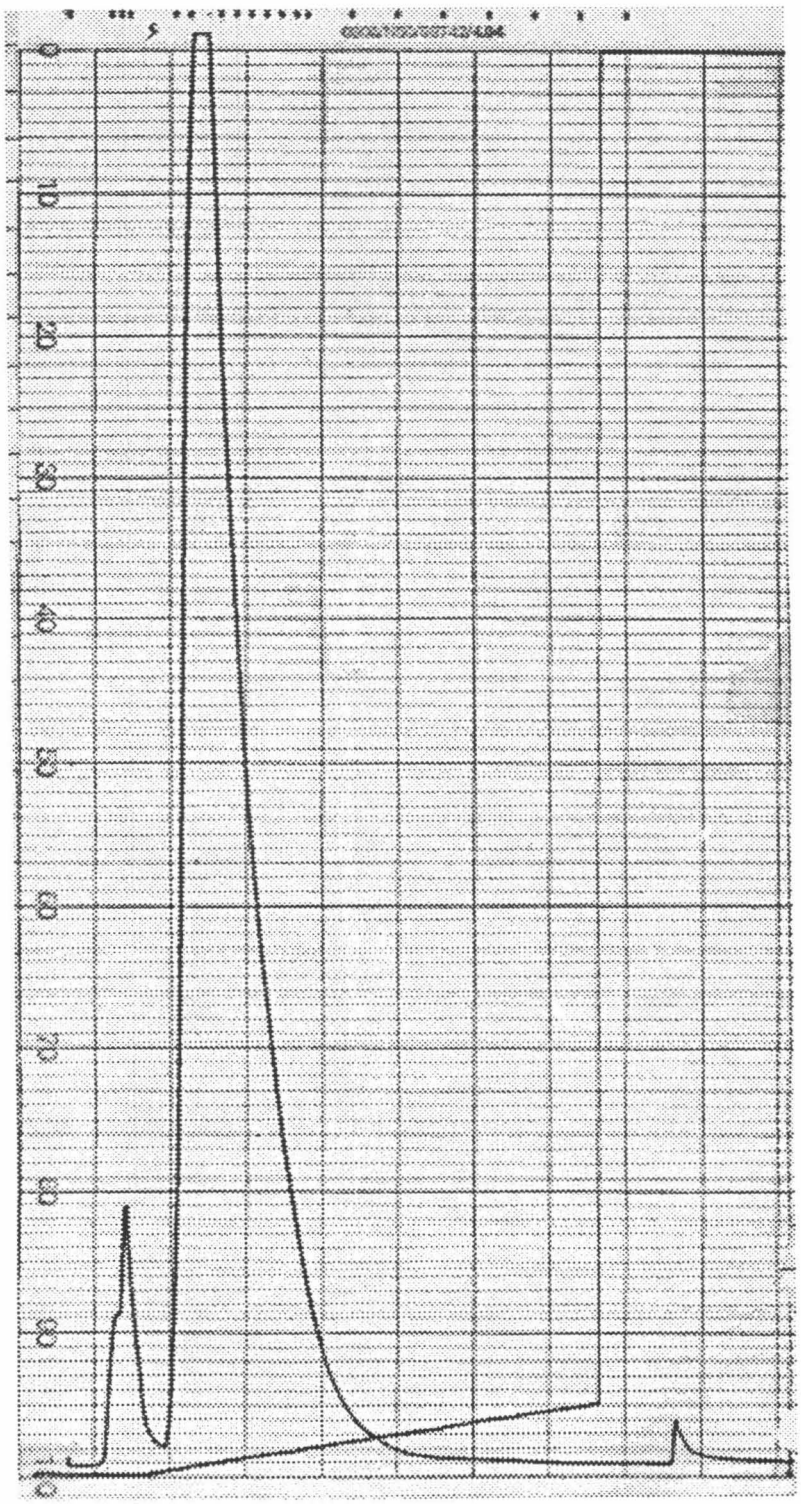

Figure 2.6 Reoxidation experiment using with Ru(bpy)$_2$Im-labeled H83Q/M121E/K122H azurin. The first data point gives the A486/A600 ratio of the protein sample before reduction. Time zero is the reduced sample before it is introduced into the laser cuvette. The first time point for the sample with quencher (6 mM [$Ru(NH_3)_6$]) is immediately after degassing and mixing with the quencher. The final data point on each curve is the sample after removal from the laser cuvette and reoxidation using excess $K_3Fe(CN)_6$.

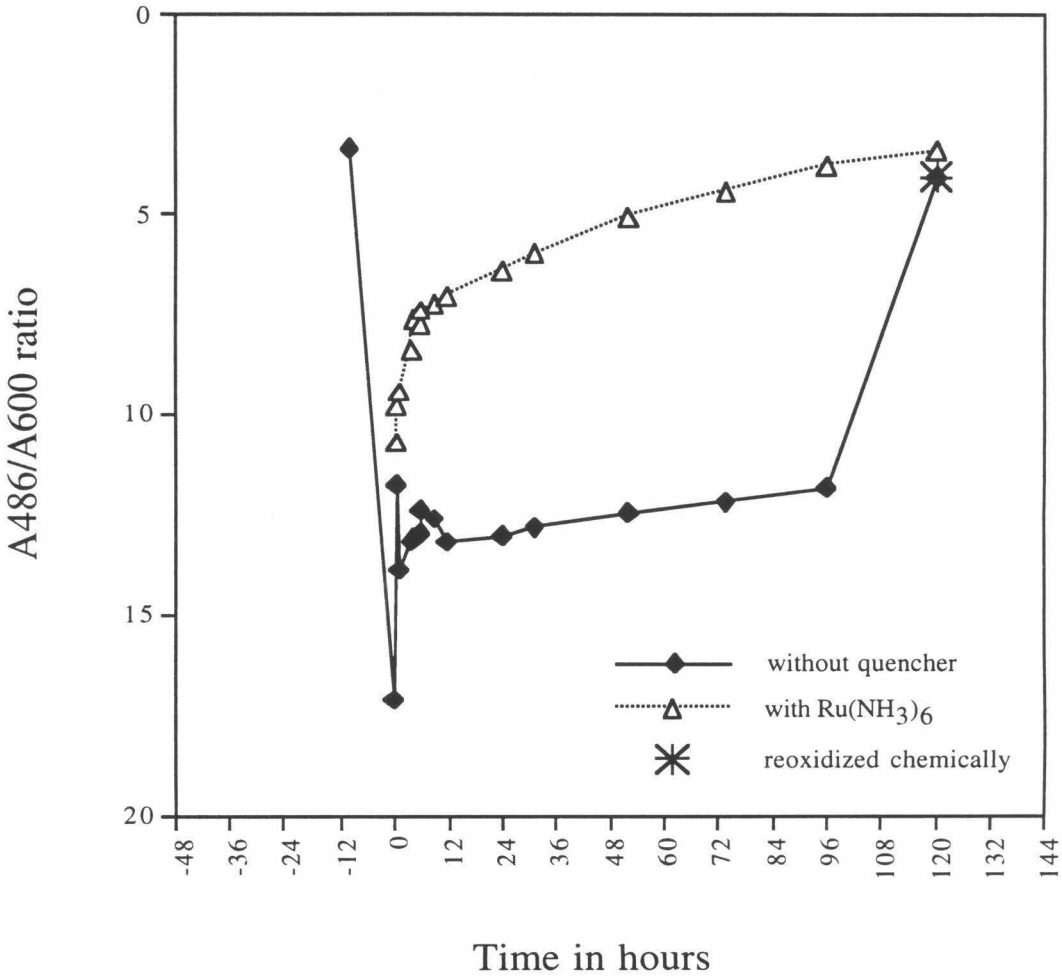
A486/A600 ratio
0
5
10
15
20
-48
-36
-24
-12
0
12
24
36
48
60
72
84
96
108
120
132
144
Time in hours
without quencher
with Ru(NH3)6
reoxidized chemically

Figure 2.7 Laser data: (a-c) Photoinduced ET monitored at 430 nm. At pH 4.3, we can see the Ru^{3+} signal disappear as the electron is transferred back out of the transiently reduced Cu center ((a) M121E/H83Ru(bpy)$_2$Im (c) M121E/H83Q/K122HRu(bpy)$_2$Im. At pH 8.0, although plenty of Ru^{2+*} excited state is seen at other wavelengths, no Ru^{3+} is made ((b) M121E/H83Ru(bpy)$_2$Im).

(d-f) ET measured using the flash/quench technique with 6 mM [$Ru(NH_3)_6$] quencher. Data taken at pH 4.3 with reduced M121E/H83Ru(bpy)$_2$Im show that monitoring at characteristic Cu (590 nm (d)) and Ru wavelengths (430 nm (e)) give the same rate. (f) Data taken with samples prepared on the bench top show evidence of reoxidation. Data taken at high pH on reduced M121E/H83Q/K122HRu(bpy)$_2$Im show rapid electron transfer but only about 1/3 of the sample is still reduced and so able to undergo intramolecular ET to the Ru^{3+} label.

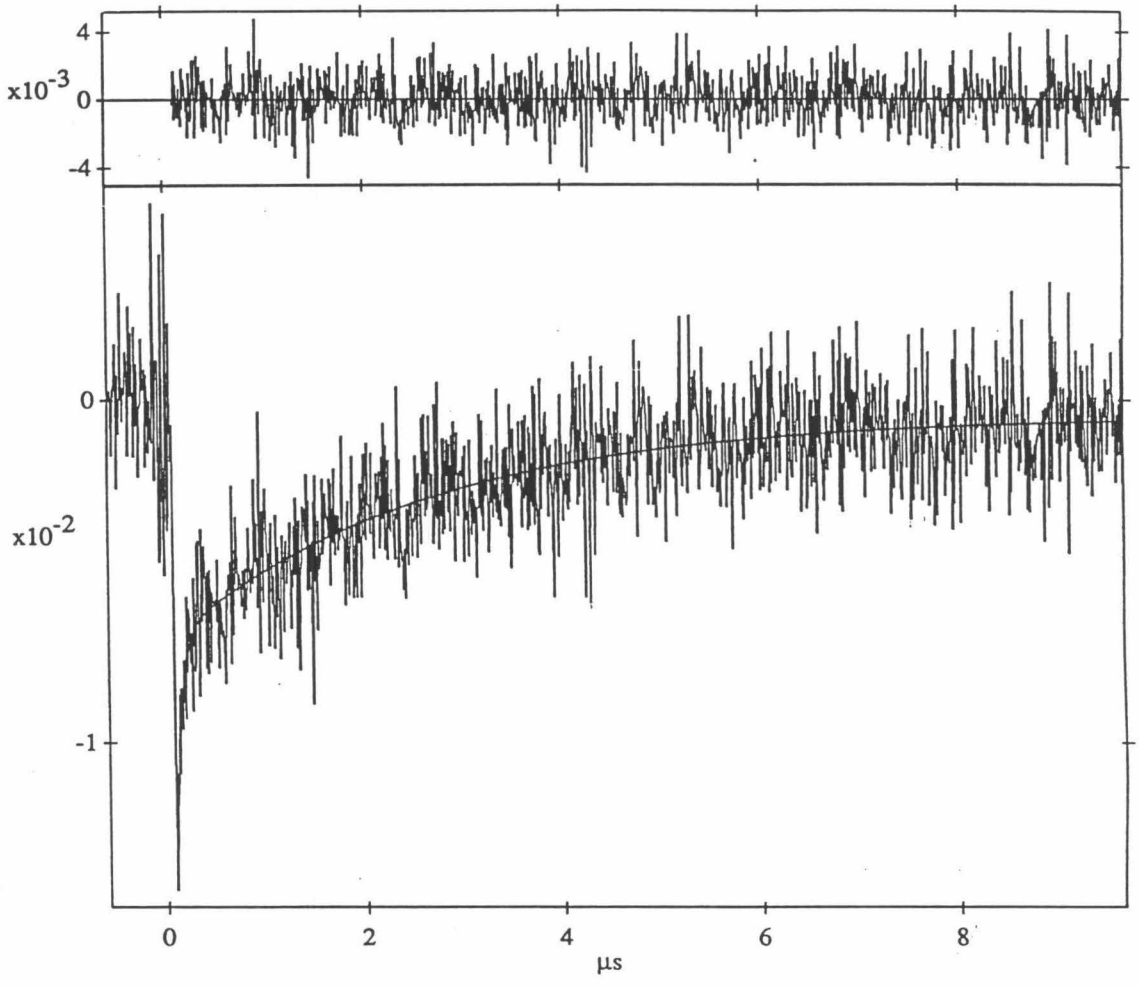
4
x10-3 0
-4
0
x10-2
-1
0
2
4
6
8
μs

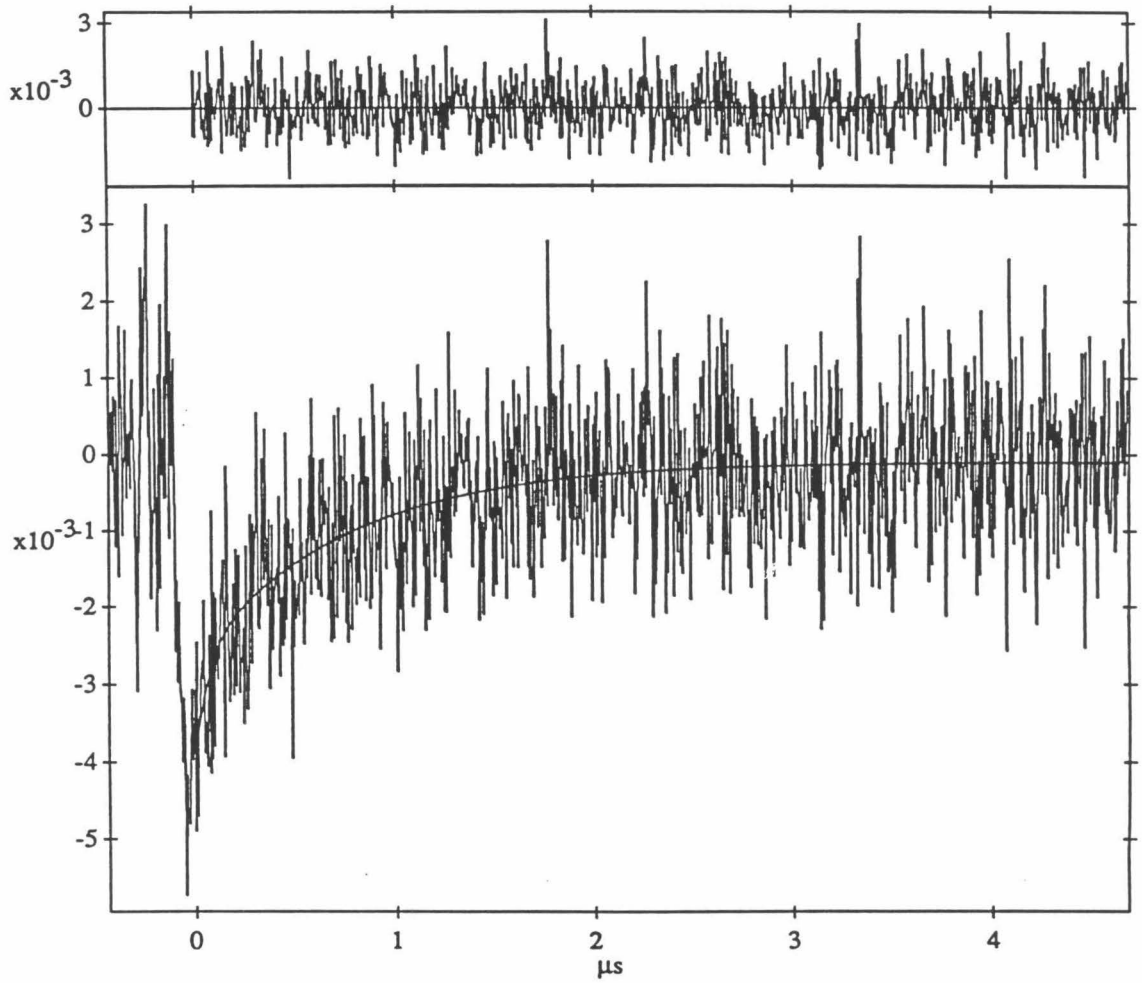
x10-3
3
0
3
2
1
0
x10-3
-1
-2
-3
-4
-5
0
1
2
3
4
μs

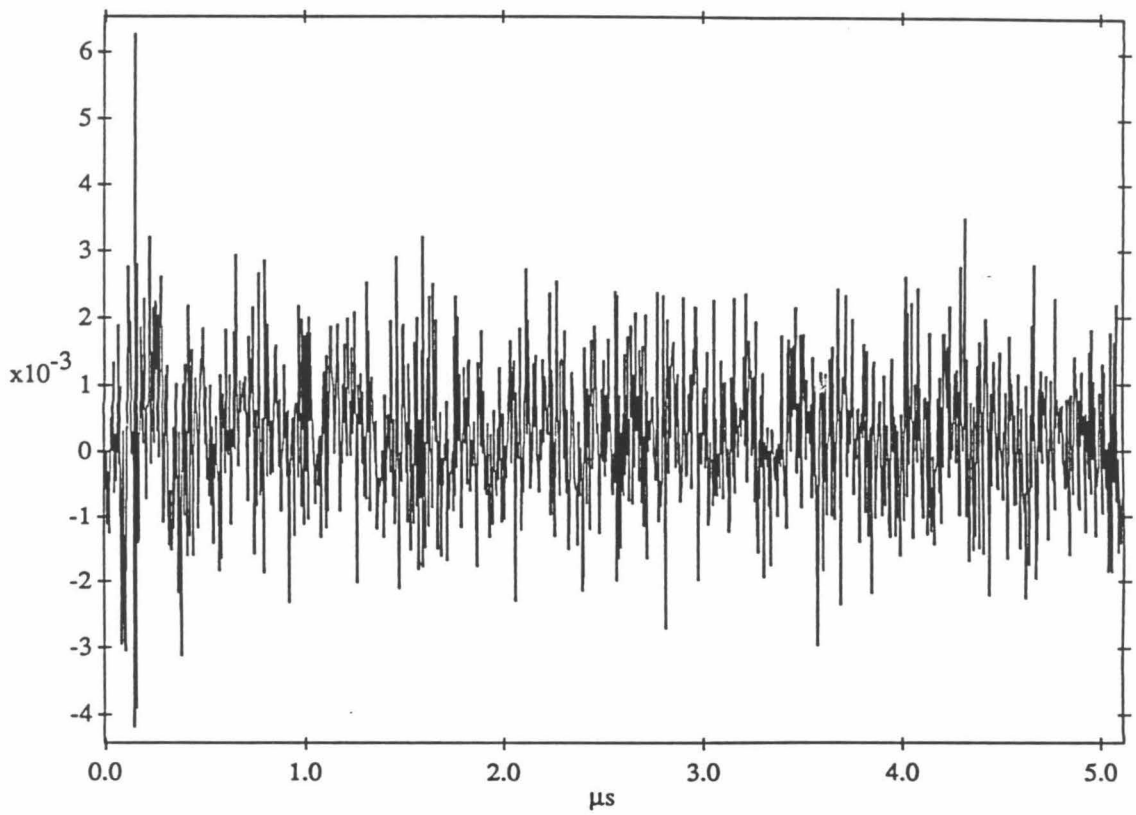
6
5
4
3
2
x10-3
1
0
-1
-2
-3
-4
0.0
1.0
2.0
3.0
4.0
5.0
μs

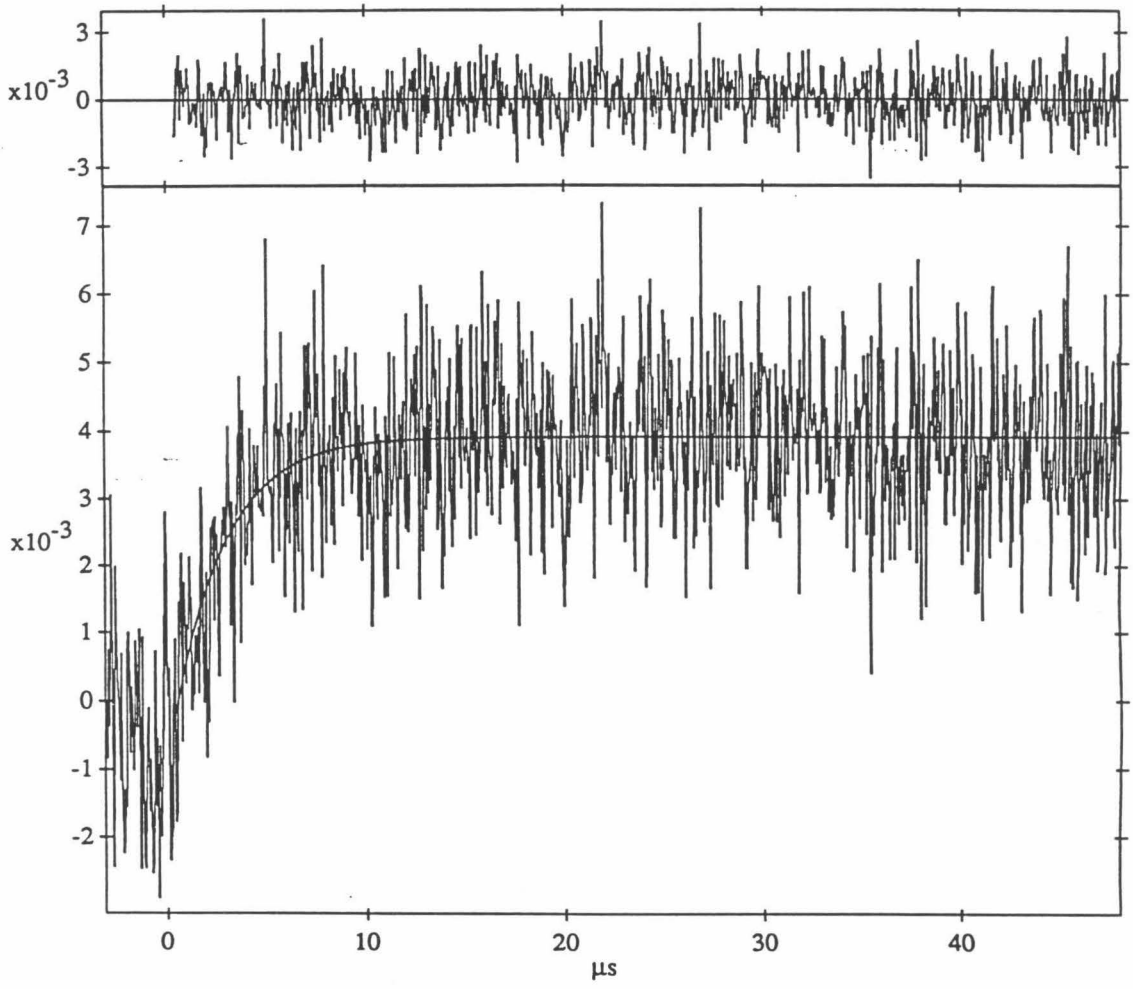
3
x10-3 0
-3
7
6
5
4
3
x10-3 2
1
0
-1
-2
0
10
20
30
40
μs

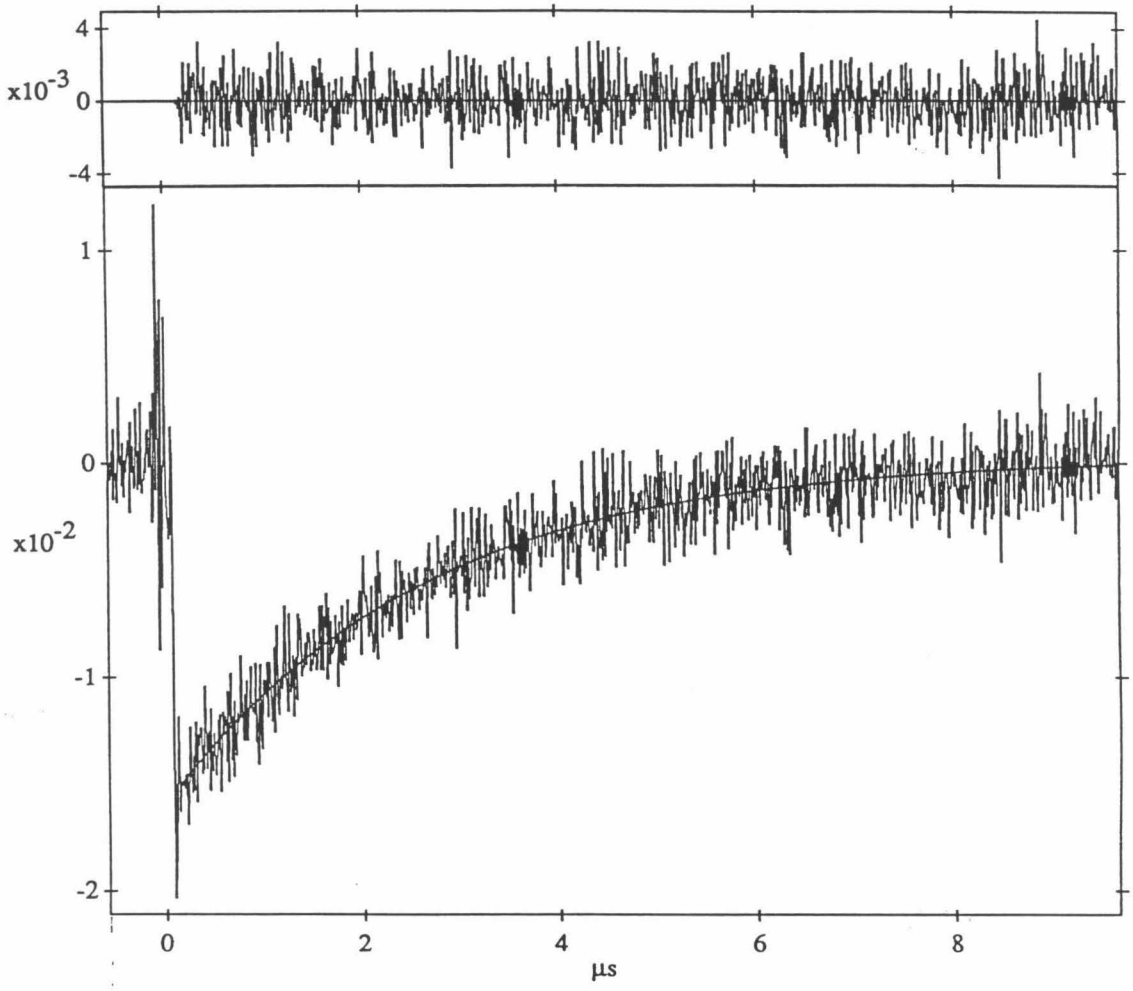
4
x10-3 0
-4
1
0
x10-2
-1
-2
0
2
4
6
8
µs

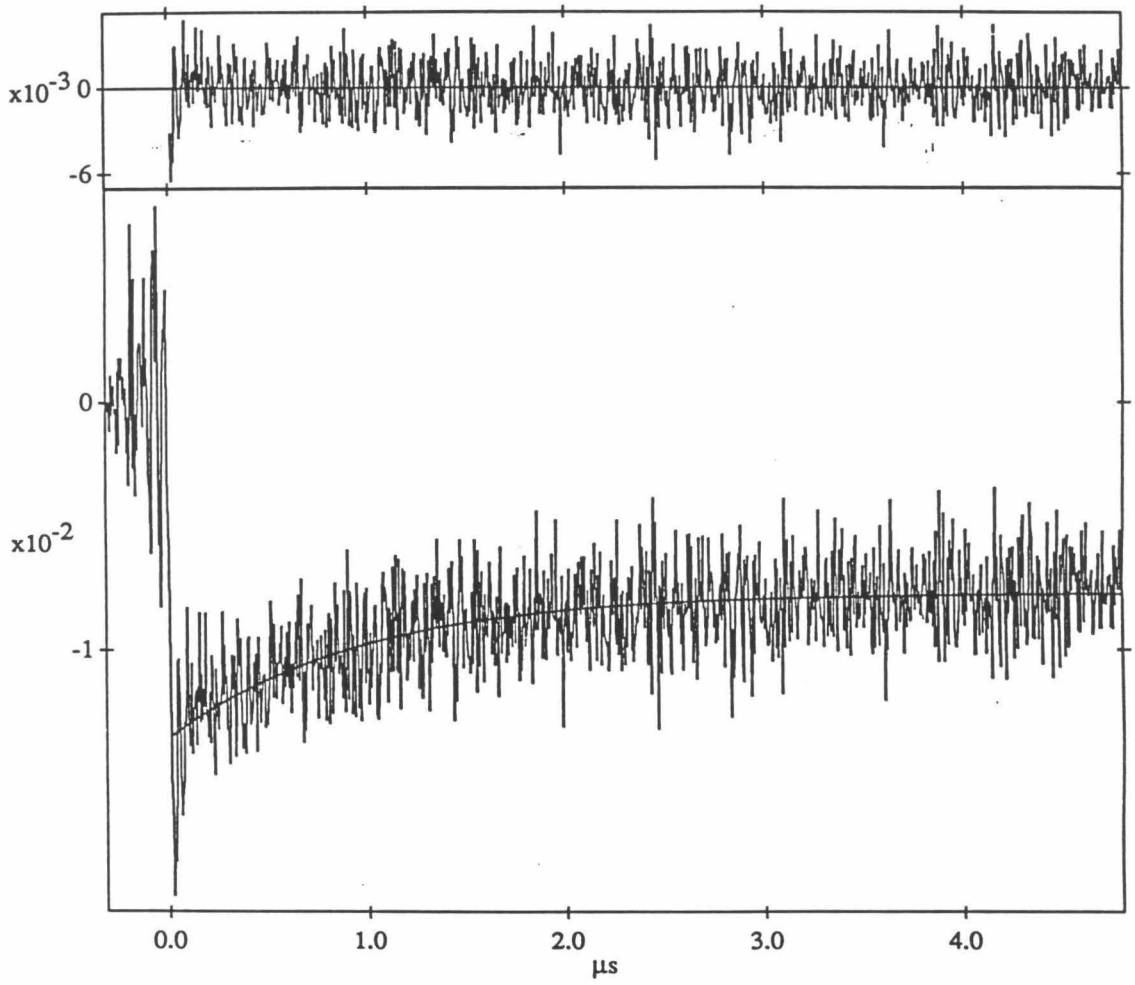
x10-3 0
-6
0
x10-2
-1
0.0
1.0
2.0
3.0
4.0
µs

Figure 2.8 Overlaid absorption spectra of the $Ru(bpy)_2Im$ label and M121E azurin at pH 4.5 and 8.0 showing the shift of the Cu LMCT up to wavelengths where the Ru label absorbs strongly.

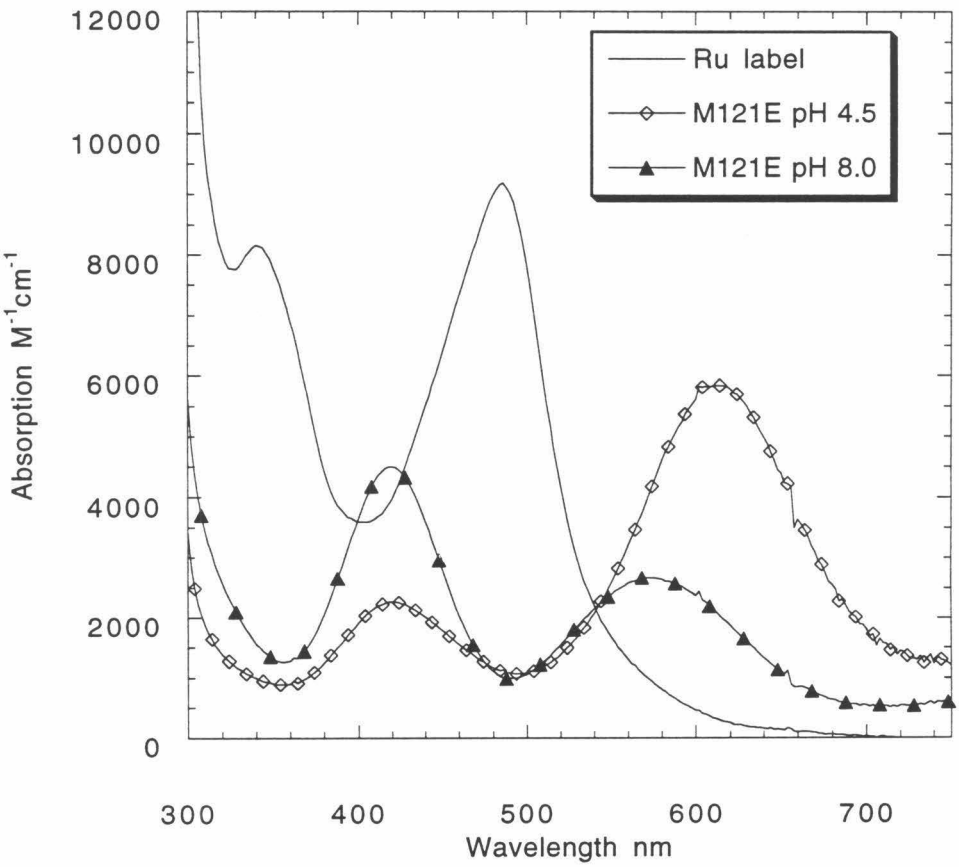
12000
10000
8000
6000
4000
2000
0
Absorption M-1cm-1
300
400
500
600
700
Wavelength nm
Ru label
M121E pH 4.5
M121E pH 8.0

Figure 2.9 Electron transfer rates for intramolecular electron transfer from ruthenium labels at positions 83 and 122 to the WT and M121E azurin Cu sites. ET rates to the M121E center could not be determined with the photoinduced methodology at pH 8.0; see text for interpretation.

ELECTRON TRANSFER RATES

Acceptor site		Wild Type pH 7.0	M121E pH 4.3	M121E pH 8.1
H83	FQ	$1.2(1) \times 10^6\ s^{-1}$ (a)	$3.9(2) \times 10^5\ s^{-1}$	$5.2(6) \times 10^5\ s^{-1}$
	PI		$4.4(5) \times 10^5\ s^{-1}$	
122H	FQ	$7.1(4) \times 10^6\ s^{-1}$ (b)	$1.9(2) \times 10^6\ s^{-1}$	$1.3(1) \times 10^6\ s^{-1}$
	PI		$1.9(4) \times 10^6\ s^{-1}$	
E° (vs. NHE)		326 mV (a)	350 mV (c)	184 mV (c)
-ΔG° (est.)		756 mV	712 mV	898 mV

FQ = rates determined by the flash/quench technique
PI = rates determined by the photoinduced technique

a. (Di Bilio et al. 1997)
b. (Langen et al. 1995)
c. (Karlsson et al. 1997)

References

Allen, J. P., Feher, G., Yeates, T. O., Koniya, H. and Rees, D. (1987). "Structure of the reaction center from *Rhodobacter sphaeroides* R-26 - the protein subunits." Proc. Natl. Acad. Sci. USA **84**: 6162-6166.

Boxer, S. G. (1990). "Mechanisms of long-distance electron transfer in proteins: lessons from photosynthetic reaction centers." Annu. Rev. Biopys. BIophys. Chem. **19**: 267-299.

Chang, I.-J., Gray, H. B. and Winkler, J. R. (1991). "High-driving force electron transfer in metalloproteins: Intramolecular oxidation of ferrocytochrome *c* by $Ru(2,2'\text{-bpy})_2(im)(His\text{-}33)^{3+}$." J. Am. Chem. Soc. **113**: 7056-7057.

Chang, T. K., Iverson, S. A., Rodrigues, C. G., Kiser, C. N., Lew, A. Y. C., Germanas, J. P. and Richards, J. H. (1991). "Gene synthesis, expression, and mutagenesis of the blue copper proteins azurin and plastocyanin." Proc. Natl. Acad. Sci. USA **88**: 1325-1329.

Connors, K. A. (1990). Chemical kinetics: the study of reactions rates in solution. New York, VCH Publishers, Inc.

Deisenhofer, J., Epp, O., Miki, K., Huber, R. and Michel, H. (1984). "X-ray structure-analysis of a membrane-protein complex - electron-density map at 3Å resolution and a model of the chromophores of the photosynthetic reaction center from *Rhodopseudomonas viridis*." J. Mol. Biol. **180**: 385-398.

Di Bilio, A. J., Hill, M. G., Bonander, N., Karlsson, B. G., Villahermosa, R. M., Malmström, B. G., Winkler, J. R. and Gray, H. B. (1997). "Reorganization energy of blue copper: effects of temperature and driving force on the rates of electron transfer in ruthenium- and osmium-modified azurins." J. Am. Chem. Soc. **119**: 9921-9922.

Faham, S., Day, M. W., Connick, W. B., Crane, B. R., Di Bilio, A. J., Schaefer, W. P., Rees, D. C. and Gray, H. B. (1998). "Structures of ruthenium-modified *Pseudomonas aeruginosa* azurin and $[Ru(2,\ 2'\text{-bipyridine})_2(\text{imidazole})_2]SO_4 \cdot 10H_2O$." submitted.

Germanas, J. P., Di Bilio, A. J., Gray, H. B. and Richards, J. H. (1993). "Site saturation of the histidine-46 position in *Pseudomonas aeruginosa* azurin: Characterization of the His46Asp copper and cobalt proteins." Biochem. **32**: 7698-7702.

Johnson, E. C., Sullivan, B. P., Salmon, D. J., Adeyemi, S. A. and Meyer, T. J. (1978). "Synthesis and properties of the chloro-bridged dimer [(bpy)2RuCl]22+ and its transient 3+ mixed-valence ion." Inorg. Chem. **17**(8): 2211-2215.

Karlsson, B. G., Tsai, L.-C., Nar, H., Sanders-Loehr, J., Bonander, N., Langer, V. and Sjölin, L. (1997). "X-ray structure determination and characterization of the *Pseudomonas aeruginosa* azurin mutant Met121Glu." Biochem. **36**: 4089-4095.

Kiser, C. N. (1997). Unpublished observations.

Kunkel, T. A., Bebenek, K. and McClary, J. (1991). "Efficient site-directed mutagenesis using uracil-containing DNA." Methods Enzymol. **204**: 125-139.

Langen, R. (1995). Electron transfer in proteins: theory and experiments. Pasadena, California Institute of Technology.

Langen, R., Chang, I.-J., Germanas, J. P., Richards, J. H., Winkler, J. R. and Gray, H. B. (1995). "Electron tunneling in proteins: coupling through a β-strand." Science **268**: 1733-1735.

Nar, H., Huber, R., Messerschmidt, A., Filippou, A. C., Barth, M., Jaquinod, M., van de Kemp, M. and Canters, G. W. (1992). "Characterization and crystal structure of zinc azurin, a by-product of heterologous expression in *Escherichia coli* of *Pseudomonas aeruginosa* copper azurin." Eur. J. Biochem. **205**: 1123-1129.

Pascher, T., Karlsson, B. G., Nordling, M., Malmström, B. G. and Vännård, T. (1993). "Reduction potentials and their pH dependence in site-directed mutant forms of azurin from *Pseudomonas aeruginosa*." Eur. J. Biochem. **212**: 289-296.

Regan, J. J., Di Bilio, A. J., Langen, R., Skov, L. K., Winkler, J. R., Gray, H. B. and Onuchic, J. N. (1995). "Electron tunneling in azurin: the coupling across a β-sheet." Chem. & Biol. **2**: 489-496.

Sigfridsson, K., Sundahl, M., Bjerrum, M. J. and Hansson, Ö. (1996). "Intraprotein electron transfer in a rutheinum-modified Tyr83-His plastocyanin mutant: evidence for strong electronic coupling." JBIC **1**: 405-414.

Winkler, J. R. and Gray, H. B. (1992). "Electron transfer in ruthenium-modified proteins." Chem. Rev. **92**: 369-379.

Wuttke, D. S. (1994). Preparation, characterization, and intramolecular electron-transfer studies of ruthenium-modified cytochromes *c*. California Institute of Technology.

Yeates, T. O., Koniya, H., Rees, D., Allen, J. P. and Feher, G. (1987). "Structure of the reaction center from *Rhodobacter sphaeroides* R-26 - membrane-protein interactions." Proc. Natl. Acad. Sci. USA **84**(18): 6438-6442.

Chapter 3

Functional Changes in the M121E Mutant of Azurin

Marcus-type analysis of ET rates

The Marcus theory of electron transfer has proven to be remarkably successful in explaining the important factors that determine ET rates in a variety of situations, from ET between small inorganic complexes in solution to ET within large biological complexes like the photosynthetic reaction center (Marcus and Sutin 1985). The semiclassical formulation of the original rate equation is an appropriate level of analysis for most biological systems:

$$k_{ET} = \sqrt[2]{\frac{4\pi^3}{h^2\lambda k_B T}}\,(H_{AB})^2\ \exp\text{-}\frac{(\Delta G^\circ+\lambda)^2}{4\lambda k_B T}$$

In this formulation the solvent is treated classically and the electronic coupling is treated as a quantum phenomenon. Independent measurement of all of the factors affecting the electron transfer rate, T, ΔG°, H_{AB}, and λ, is difficult. However, inferences about less directly accessible variables such as H_{AB} or λ can be made by spectroscopic measurements or by examination of ET rates for a series of DA systems where either of the more manipulable variables, T or ΔG°, is systematically varied.

In this chapter I will discuss the electron transfer rates reported in the previous chapter within the context of the semiclassical Marcus equation in an effort to determine how the substitution of a glutamic acid residue for the normal methionine ligand affects the functioning of the blue copper site.

Driving force

The free energy change for any chemical reaction is the difference in the energy of the products and the reactants. For electron transfer reactions this can be broken into the work it takes to bring the donor and acceptor together and the difference between the reduction potentials of the acceptor and donor. Since we are concerned here only with intramolecular electron transfer reactions, we can neglect the work term. For the flash-quench experiment and the back electron transfer in the photoinduced experiment, the $Ru(bpy)_2ImHis^{3+}$ label is the electron acceptor. The reduction potential for the 3+/2+ couple for a $Ru(bpy)_2Im_2$ model complex has been measured to be 0.98 eV (Casimiro et al. 1993). The reduction potential of the complex bound to a protein changes very little. The

reduction potential of $Ru(bpy)_2Im$ bound to H33 of cyt *c* has been directly measured to be 1.07 eV (Mines et al. 1996). The reduction potential of the complex bound to H83 of azurin is 1.082 V (Di Bilio et al. 1997). For the forward reaction in our photoinduced electron transfer scheme, the electron donor is the excited state of $Ru(bpy)_2ImHis^{2+*}$. This complex is a good electron donor and its reduction potential, estimated from difference between the energy of the excited state emission of the Ru^{2+} complex and the reduction potential of $Ru(bpy)_2Im_2^{3+/2+}$, is calculated to be -1.03 eV (Mines et al. 1996). (See figure 1.)

The reduction potentials of azurin and mutant forms thereof can be measured by spectroelectrochemistry (Taniguchi et al. 1980). The reduction potentials of type 1 copper proteins are all higher than the 115-150 mV potential of most inorganic $Cu^{2+/1+}$ complexes (Canters and Gilardi 1993). This, and more particularly, the large variation in reduction potentials of blue Cu proteins with very similar spectroscopic properties (184 mV for stellacyanin to 780 mV for fungal laccase (Taniguchi et al. 1982)) has been the subject of much discussion in the bioinorganic literature (Gray and Malmström 1983; St. Clair et al. 1992; Pascher et al. 1993). In most blue copper proteins, the Cu ion is buried under the surface of the protein in a fairly rigid, hydrophobic site. The enthalpy of reduction for the blue copper proteins is favorable ($\Delta H°$ = -16.6 kcal/mol for WT *P. aeruginosa* azurin), probably because the reduced protein has an electrically neutral Cu site buried in the hydrophobic interior (Cu^{1+} neutralized by the cysteine thiolate). The reaction entropies for reduction of blue copper proteins, however, are all negative (unfavorable), indicating an increase in order around the reduced copper protein (Taniguchi et al. 1982).

The reduction potential of WT azurin has also been observed to have a moderate pH dependence. Between pH 8.0 and 5.0, the potential increases from 292 mV to 349 mV (St. Clair et al. 1992). Formerly, this increase had been attributed to structural rearrangements that accompany the protonation of H35. Crystal structures of the oxidized protein at pH 5.5 and 9.0 show that protonation of H35 leads to formation of a strong hydrogen bond to the P36 carbonyl oxygen causing a change in the conformation of the peptide bond between P36 and G37 (Nar et al. 1991). This peptide bond flip causes changes in the adjoining loop regions but only very small changes in copper center, thus there is no pH-dependence in the spectroscopic properties of the wild type protein. The 60 mV increase in the WT reduction potential at low pH is consistent with an additional

positive charge in the vicinity of the Cu site favoring the Cu^{1+} oxidation state. However, the H35K mutant shows very little change in reduction potential compared to wild type and the pH dependence of the potential remains nearly the same, effectively ruling out H35 protonation as the source of the pH dependence of the WT azurin reduction potential (Pascher et al. 1993).

Changes in the ligand residues of *P. aeruginosa* azurin have been made using site directed mutagenesis. Surprisingly, changes can be made in all four side-chain ligands while still retaining the ability to bind copper. Although the blue color of the site is abolished, the C112D mutant binds copper and its reduction is reversible. The site's reduction potential is estimated from redox titration with cytochrome c_{551} to be ~180 mV (Mizogouchi 1996).[1] Glycine substitutions have been made for both histidine ligands and the sites can be converted to spectroscopically normal type 1 centers by adding imidazole ligands. However reduction of H117G, H46G, and all of their substituted derivatives is irreversible. This inability to reoxidize the H-X-G mutants is not due to chemical modification of the protein since one can remove the Cu^{1+} from H46G and reconstitute the protein with Cu^{2+}. It may be due to an increased reduction potential because a three-coordinate site stabilizes the Cu^{1+} form relative to the Cu^{2+} form (van Pouderoyen et al. 1996). Reduction of a His46 mutant containing a covalently attached ligand (His46Asp) is reversible, although its potential is somewhat lower than WT, in line with the increased polarity at the Cu site (Germanas et al. 1993).

Proteins containing all 20 natural amino acids at position 121 have been isolated (Chang et al. 1991; Karlsson et al. 1991). Many show very little change from the WT reduction potential. The changes observed correlate with the polarity of the site. Deleting the entire last β-strand in the M121End mutant increases the solvent accessibility of the site and drops the reduction potential to 205 mV. When the uncharged but polar methionine is changed to a non-polar leucine residue, the reduction potential at pH 7.0 is increased by 138 mV to 448 mV (Pascher et al. 1993). The reduction potential of one of the M121 mutants, M121E, shows an interesting pH dependence. At low pH it is rather similar to WT (370 mV at pH 4.0) but decreases dramatically with increasing pH, going to

---

[1]Cys112Asp will transfer electrons into and out of the copper site via the hydrophobic patch ('self-exchange' rates with WT azurin have been measured by stopped-flow: $k_{22} \approx 20\ M^{-1}\ s^{-1}$, k_{11} for WT azurin = $10^5\ M^{-1}\ s^{-1}$) though ET to sites on the β-strands seems to be severely impaired.

184 mV at pH 8.0. This, along with the changes in the optical and EPR spectra seen with this mutant, have been taken as evidence of changes in Cu coordination. When the axial glutamic acid ligand is deprotonated, it is presumed to bind the Cu, altering the spectroscopy of the site and decreasing the reduction potential by favoring the Cu^{2+} state (Karlsson et al. 1997).

Taking the difference between their reduction potentials, one can calculate the driving force ($-\Delta G°$) for electron transfer from the reduced M121E Cu center to the oxidized Ru label: 0.71 eV at low pH, 0.90 eV at high pH. The driving force for ET from the WT center (at pH 7.0) is 0.76 eV. Despite these 50-140 mV changes in driving force, calculations predict very little change in the electron transfer rates. (See figure 2.) If there are no changes to other ET parameters, one would expect the rates from M121E to H83 to be essentially the same as those from the wild type center. For the more closely coupled acceptor at H122, one would expect to see a small decrease in the M121E rates because their driving forces are not quite as close to the measured λ (0.80 eV (Di Bilio et al. 1997)) as the WT driving force.

Our results are not consistent with these expectations. The M121E ET rates are much lower than predicted rates. Clearly the naive assumption that only the driving force changes is incorrect. This implies that either the electronic coupling or the reorganization energy is different in the M121E azurin mutant.

Electronic coupling

As discussed in the introduction, the original motivation for this project was to determine if the spectroscopic changes seen in the M121E mutant at high pH would translate into increased electronic coupling between the copper center and labels placed on the 121-126 β-strand. An X-ray structure of the M121E mutant in the low pH form shows a closer interaction between the Cu^{2+} ion and the O of the glutamic acid ligand: a Cu-O bond distance of 2.21 Å, as compared to 3.15 Å for the Cu-S interaction in the WT center (Karlsson et al. 1997). (See figure 3.) But at low pH the M121E site is a fairly typical type I blue site - both spectroscopically and in terms of its reduction potential. Thus, one might expect the electron transfer rates from the M121E center to be about the same as those from the WT center.

At high pH, the deprotonated glutamic acid side chain interacts more strongly with the Cu ion. Evidence for this increased interaction includes an

additional coordinating oxygen seen in the EXAFS (Strange et al. 1996), shifts to higher energies of the LMCT bands in the M121E Ni^{2+}, Co^{2+}, and Cu^{2+} derivatives (Di Bilio et al. 1992), and increased rhombicity in the EPR spectrum at high pH (Karlsson et al. 1997). This increased metal-ligand interaction upon deprotonation would be expected to increase the electronic coupling (H_{AB}) into the Cu site, leading to higher electron transfer rates at high pH.

The observed ET rates for the M121E mutant do not conform to these initial expectations about changes in electronic coupling. All of the rates are lower than expected and while the M121E/H83 ET rates increase slightly with increasing pH, the M121E/K122H ET rate decreases at high pH - in direct contradiction to expectation if the electronic coupling through the new glutamic acid ligand increases.

Recent work has shown that changes in ligand residues that have very small effects on the spectroscopy of a blue Cu site can have dramatic effects on the electron transfer properties of the mutant (Regan et al. 1998). Changes in the paramagnetic NMR shifts of ligand protons indicate that the H46D mutation induces an increase in the interaction of the Cu with the axial methionine, accompanied by a decrease in its interaction with the CysS (Vila et al. 1997). This is seen as a subtle change in the spectroscopy of the site; the H46D azurin has a ~600 nm band that is slightly blue shifted and has a lower extinction coefficient than the WT LMCT. However, this small decrease in coupling between the Cu and its cysteine ligand leads to a dramatic decrease in the ET rate from the mutant site (a 36 fold drop from 1.2×10^6 to 3.2×10^4 s^{-1}).

The low pH spectrum of M121E shows an analogous blue shift and decrease in extinction coefficient of the LMCT band (Karlsson et al. 1997) and the ET rates are also significantly lower than wild type but they are only 2-6 fold lower, as opposed to 36 fold lower in the H46D mutant. And, more importantly, the decrease in rate does not correlate with the extent of change in the site's LMCT band. The low pH rate to H83 decreases more than the high pH rate but the converse is true for ET to labels at H122. So, while the M121E substitution may have some effect on the electronic couplings in the Cu site, either by changing the coupling through the axial ligand into the β-strand, or indirectly through its effects on the Cu-Cys bond, this does not seem to supply an internally consistent explanation for the rate changes seen.

Reorganization energy

All the rates reported here were taken at 298 K, so the other variable in the Marcus equation is the reorganization energy. According to the Marcus cross relation, the reorganization energy of a reaction is the average of the reorganization energies of the two components:

$$\lambda_{12} = \frac{(\lambda_{11} + \lambda_{22})}{2}$$

These reorganization energies can be broken down further into inner and outer sphere components:

$$\lambda = \lambda_i + \lambda_o$$

The inner sphere reorganization component is the energy required to alter bond distances and bond angles that change with the change in oxidation state. The outer sphere reorganization is the energy required for reorientation of the solvent around the changed complexes.

In blue copper proteins, the electron transfer reorganization energies are kept low by the small changes in ligand coordination (low λ_i) and minimal solvent reorganization (small λ_o) because the metal centers are separated from bulk solvent, buried beneath the hydrophobic patch at the 'northern end of the molecule. X-ray structures of oxidized and reduced WT *Alcaligenes denitrificans* azurin show small increases (0.05 - 0.1 Å) in all Cu-ligand bond lengths upon reduction, commensurate with the increase in radius of the Cu^{1+} ion; the copper atom is not displaced from the HisHisCys plane (Shepard et al. 1990). X-ray data are not available for reduced *P. aeruginosa* azurin but EXAFS data show similarly small changes in bond distances - with the possible exception of an increase in the MetS-Cu distance in the oxidized protein (Murphy et al. 1993).[2] In addition, Loppnow and coworkers have studied the inner sphere reorganization energy of the WT azurin charge transfer interaction by analyzing the absolute cross section of the resonance Raman spectra (Webb et al. 1997). Using this technique they were able to estimate the relative contributions to the relaxation of the excited CT state of population decay (relaxation into lower lying CT and LF states of the

[2]This result is, however, somewhat ambiguous since the Cu-S interaction that is fairly clearly seen at 2.7 Å in the reduced protein is not needed to fit the X-ray scattering of the oxidized protein at high pH and a sulfur included at 3.45 Å only slightly improves the fit of the low pH data. This may be due to increased mobility of the MetS ligand in the oxidized protein or, more plausibly, to increased distance bringing it into a shell where C back scattering destructively interferes with the S back scattering signal.

protein), specific vibrational modes, and solvent-like dissipation of energy. Adding up the mode-specific reorganization energies (λ for each RR band), they obtain 0.26 eV for the reorganization energy due to specific vibrational displacements. From the homogeneous line widths they further estimate that the rest of the protein provides 0.12 eV of 'solvent-like' reorganization energy. Their estimate of 0.38 eV for the total inner sphere reorganization during charge transfer further supports a low value of λ_{inner} for the electron transfer reactions of WT azurin.

Recently, Di Bilio measured the reorganization energy of the azurin WT Cu center (Di Bilio et al. 1997). By analyzing the driving force and temperature dependences of ET rates for a series of azurins modified at H83 with Ru and Os compounds, he obtained a λ for the ET between the Cu center and the $Ru(bpy)_2Im$ label of 0.80 eV. Taking a reorganization energy of 0.78 eV for the $Ru(bpy)_2Im$ label (estimated from ET studies with labeled cyt *c*), the reorganization energy of the blue copper center is 0.82 eV. Farver and Pecht have estimated the reorganization energy of ET from the disulfide bond at the 'southern' end of azurin to the Cu center to be 1.03 eV (Farver and Pecht 1997). This does not give us an independent measure of the reorganization energy of the Cu site alone because reorganization energy of the disulfide bond is not known. However, given the substantial bond length change for the disulfide radical, the S-S reorganization energy would be expected to be substantial, so 0.82 eV for the Cu center is in reasonable agreement with their expectations.

While direct determination of reorganization energies requires either a driving force or temperature dependence study, estimates for the reorganization energies of the M121E site can be made by assuming that the electronic coupling remains constant and calculating the reorganization rates from the ratio of two electron transfer rates.

$$\frac{k_1}{k_2} = \sqrt[2]{\frac{\lambda_1}{\lambda_2}}\ \exp\text{-}\ \frac{-\lambda_2(\Delta G_1^\circ + \lambda_1)^2 + \lambda_1(\Delta G_2^\circ + \lambda_2)^2}{4k_B T \lambda_1 \lambda_2}$$

Calculations comparing WT ET data from the 122 and 83 sites with M121E data give consistent reaction reorganization energies for each pH, 1.08 eV at low pH and 1.27 eV at high pH. Using the reorganization energy for $Ru(bpy)_2Im$, λ_{11}

= 0.78 eV, and the Marcus cross relation, $\lambda_{12} = (\lambda_{11} + \lambda_{22})/2$, calculations predict reorganization energies of 1.38 eV at low pH and 1.76 eV at high pH for the M121E Cu site. The assumption that there is no change in electronic coupling through the cysteine S-Cu bond is naive so these calculated reorganization energies represent an upper limit for the changes in the M121E Cu site.

Increased reorganization energies make sense if one examines the structure of the Cu site. The reorganization energy of the WT Cu center is low (λ_{22} = 0.82 eV) because the Cu ion in either oxidation state is protected from the surrounding aqueous medium. The crystal structure of the WT center shows that the Met ligand blocks access of the solvent to the Cu ion but is only weakly coordinated (Cu-S distance 3.15 Å (Nar et al. 1991)). A crystal structure of the M121E mutant shows that, even in the protonated form,[3] the glutamic acid ligand is well coordinated (Cu-O bond distance 2.2 Å (Karlsson et al. 1997)). In addition the M121E site is more polar, even when the glutamic acid residue is protonated. This leads to a more variable interaction with the Cu ion in its two oxidation states and a higher reorganization energy for the electron transfer reaction. At high pH, the glutamic acid residue is deprotonated becoming not only polar but negatively charged. This negative charge would be predicted to increase both the degree of inner sphere reorganization and the reorganization of the solvent around the site during oxidation.

Corroboration for increased mobility of the Cu site in the M121E mutant comes from perturbed angular correlation (PAC) studies (Danielsen et al. 1995). Data from several cadmium-substituted M121 azurin mutants show that the mutant Cu sites are less rigid than the WT site. Several of the mutants (Ala, Leu, and Glu) required two different nuclear quadrapole interactions (NQI) to model the site effectively. With the Ala and Leu mutants, one NQI is three coordinate (Cys, His, His) like the WT center while the other could best be described as four coordinate with an additional water molecule in the site. The data from the M121E mutant could not be modeled starting from the WT structure. However, one of the NQI's is modeled well starting from the crystal structure of the M121E mutant where the Cu is seen to be coordinated by C112, H46, H117, and one of the E121 oxygens. The other NQI may represent the site with E121 coordinated in

[3]As inferred by characteristic resonance Raman stretching frequencies.

a bidentate fashion. A further indication of decreased rigidity in the M121 mutant sites is an increase in the linewidths of the PAC spectra.

Conclusions

In summary, despite clear spectroscopic indications of increased ligand-metal interaction in the high pH form of the M121E mutant of azurin, this does not translate into increased electronic coupling to donors placed on β-strand leading away from that ligand. Our efforts to increase electron transfer rates through that section of the protein by the electronic coupling between the donor (the azurin Cu atom) and the bridge (the intervening protein) were thwarted by the simultaneous alteration of the nuclear factors, in particular a dramatic increase in the reorganization energy of the mutant Cu site. This gives a possible explanation for the puzzle of the almost absolute conservation of the methionine ligand in blue copper proteins despite the near normal stability and spectroscopy of substitutions at that ligand position. Methionine is a fairly large, polarizable but not very polar group; these properties help it exclude water from the Cu site while interacting minimally with the Cu ion. This is important in helping to tune the reduction potential of the site and, more importantly, in minimizing the reorganization energy during electron transfers.[4]

---

[4]In addition, phenomenological observations indicate it might play a role in stabilizing the Cu ion in the site and in protecting it from direct oxidation by O_2. Several of the M121 mutants loose Cu during procedures used routinely with the WT protein - Mono S strips Cu^{2+} from the M121E mutant (CNK, unpublished observations) and several of the mutants lost Cu during the course of reduction potential measurements using spectroelectrochemistry (Pascher et al. 1993).

Figure 3.1 Reduction potentials of various $Ru(bpy)_3$ species (Roundhill 1994). From data summarized in (Mines et al. 1996), the analogous potentials for the 3+/2+/2+* triangle for $Ru(bpy)_2$ImHis33 cytochrome *c* would be: E_{00} = 2.1 V and E° for $Ru^{3+/2+}$ = 1.07 V, E° for $Ru^{2+/1+}$ = -1.03 V.

Reduction potentials of Ru(bpy) $_3$species

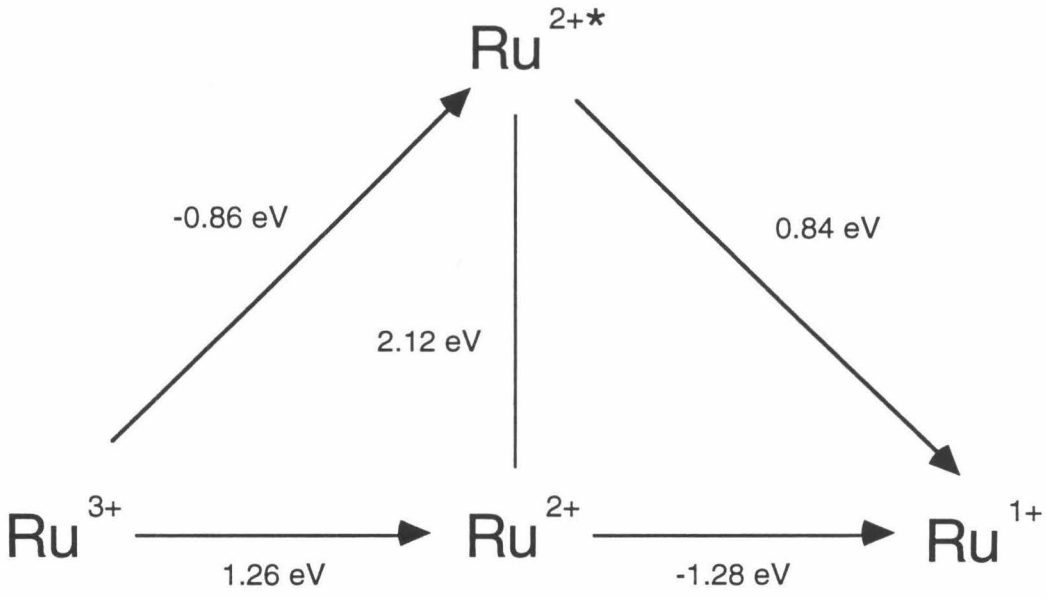

Figure 3.2 Calculated and observed electron transfer rates to ruthenium labels at positions 83 and 122 in azurin.

	H83		H122	
	calculated	observed	calculated	observed
WT		1.2×10^6 (a)		7.1×10^6 (b)
Low pH	1.1×10^6	4.1×10^5	6.6×10^6	1.9×10^6
High pH	1.1×10^6	5.0×10^5	6.5×10^6	1.3×10^6

(a) (Di Bilio et al. 1997)
(b) (Langen et al. 1995)

Figure 3.3 Oxidized copper site of the M121E mutant of *P. aeruginosa* azurin (Karlsson et al. 1997). The copper ion is ligated by four out of the five usual ligands, C112 (to the left and behind the Cu ion in this view), H117 (left front), H46 (right), and the carbonyl oxygen of G45 (below and to the right). The introduced glutamic acid side chain (top center) interacts with the Cu^{2+} ion via one of its oxygens. The resonance Raman spectrum of the crystal shows enhancements characteristic of the blue, low-pH form of the protein, indicating that this structure shows the position of the protonated glutamic acid. The heavy atoms are colored according to the standard CPK scheme: carbon: gray, nitrogen: blue, oxygen: red, sulfur: yellow. A similar view of the wild type center is shown in figure 1.6.

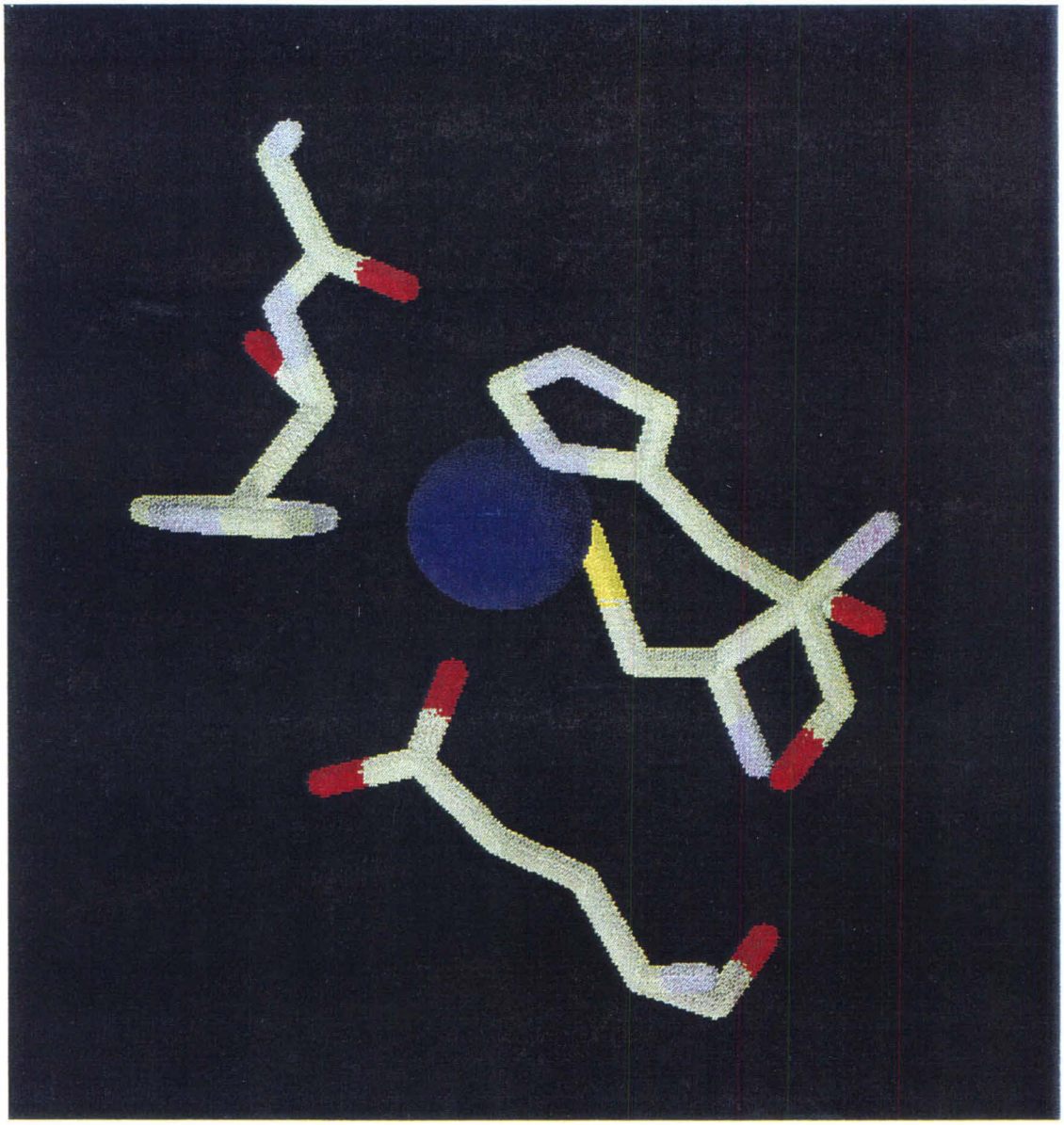

References

Canters, G. W. and Gilardi, G. (1993). "Engineering type 1 copper sites in proteins." FEBS Lett. **325**: 39-48.

Casimiro, D. R., Richards, J. H., Winkler, J. R. and Gray, H. B. (1993). "Electron transfer in ruthenium-modified cytochromes c. σ-Tunneling pathways through aromatic residues." J. Phys. Chem **97**: 13073-13077.

Chang, T. K., Iverson, S. A., Rodrigues, C. G., Kiser, C. N., Lew, A. Y. C., Germanas, J. P. and Richards, J. H. (1991). "Gene synthesis, expression, and mutagenesis of the blue copper proteins azurin and plastocyanin." Proc. Natl. Acad. Sci. USA **88**: 1325-1329.

Danielsen, E., Bauer, R., Hemmingsen, L., Andersen, M.-L., Bjerrum, M., Butz, T., Tröger, W., Canters, G. W., Hoitink, C. W. G., Karlsson, G., Hansson, Ö. and Messerschmidt, A. (1995). "Structure of metal site in azurin, Met121 mutants of azurin, and stellacyanin investigated by (111m)Cd perturbed angular correlation (PAC)." J. Biol. Chem. **270**(2): 573-580.

Di Bilio, A. J., Chang, T. K., Malomström, B. G., Gray, H. B., Karlsson, B. G., Nordling, M., Pascher, T. and Lundberg, L. G. (1992). "Electronic absorption spectra of M(II)(Met121X) azurins (M = Co, Ni, Cu; X = Leu, Gly, Asp, Glu): charge transfer energies and reduction potentials." Inorg. Chim. Acta **198-200**: 145-148.

Di Bilio, A. J., Hill, M. G., Bonander, N., Karlsson, B. G., Villahermosa, R. M., Malmström, B. G., Winkler, J. R. and Gray, H. B. (1997). "Reorganization energy of blue copper: effects of temperature and driving force on the rates of electron transfer in ruthenium- and osmium-modified azurins." J. Am. Chem. Soc. **119**: 9921-9922.

Farver, O. and Pecht, I. (1997). "The role of the medium in long-range electron transfer." JBIC **2**: 387-392.

Germanas, J. P., Di Bilio, A. J., Gray, H. B. and Richards, J. H. (1993). "Site saturation of the histidine-46 position in *Pseudomonas aeruginosa* azurin: Characterization of the His46Asp copper and cobalt proteins." Biochem. **32**: 7698-7702.

Gray, H. B. and Malmström, B. G. (1983). "On the relationship between protein-forced ligand fields and the properties of blue copper centers." Comments Inorg. Chem. **2**(5): 203-209.

Karlsson, B. G., Nordling, M., Pascher, T., Tsai, L.-C., Sjölin, L. and Lundberg, L. G. (1991). "Cassette mutagenesis of Met121 in azurin from *Pseudomonas aeruginosa*." Protien Eng. **4**(3): 343-349.

Karlsson, B. G., Tsai, L.-C., Nar, H., Sanders-Loehr, J., Bonander, N., Langer, V. and Sjölin, L. (1997). "X-ray structure determination and characterization of the *Pseudomonas aeruginosa* azurin mutant Met121Glu." Biochem. **36**: 4089-4095.

Langen, R., Chang, I.-J., Germanas, J. P., Richards, J. H., Winkler, J. R. and Gray, H. B. (1995). "Electron tunneling in proteins: coupling through a β-strand." Science **268**: 1733-1735.

Marcus, R. A. and Sutin, N. (1985). "Electron transfers in chemistry and biology." Biochim. Biophys. Acta **811**: 265-322.

Mines, G. A., Bjerrum, M. J., Hill, M. G., Casimiro, D. R., Chang, I.-J., Winkler, J. R. and Gray, H. B. (1996). "Rates of heme oxidation and reduction in Ru(His33)cytochrome c at very high driving forces." J. Am. Chem. Soc. **118**: 1961-1965.

Mizogouchi, T. J. (1996). Probing the role of the active-site cysteine of azurin by site-directed mutagenesis. California Institute of Technology.

Murphy, L. M., Strange, R. W., Karlsson, B. G., Lundberg, L. G., Pascher, T., Reinhammer, B. and Hasnian, S. S. (1993). "Structural characterization of azurin from *Pseudomonas aeruginosa* and some of its methionine-121 mutants." Biochem. **32**: 1965-1975.

Nar, H., Messerschmidt, A., Huber, R., van de Kamp, M. and Canters, G. W. (1991). "Crystal structure analysis of oxidized *Pseudomonas aeruginosa* azurin at pH 5.5 and pH 9.0. A pH-induced conformational transition involves a peptide bond flip." J. Mol. Biol. **221**: 765-772.

Pascher, T., Karlsson, B. G., Nordling, M., Malmström, B. G. and Vännård, T. (1993). "Reduction potentials and their pH dependence in site-directed mutant forms of azurin from *Pseudomonas aeruginosa*." Eur. J. Biochem. **212**: 289-296.

Regan, J. J., Di Bilio, A. J., Mizoguchi, T. J., Richards, J. H., Winkler, J. R. and Gray, H. B. (1998). "Electron tunneling in Ru-modified His46Asp azurin. Coupling through the Cu ligands." Inorg. Chim. Acta in press.

Roundhill, D. M. (1994). Photochemistry and Photophysics of Metal Complexes. New York, Plenum Press.

Shepard, W. E. B., Anderson, B. F., Lewandoski, D. A., Norris, G. E. and Baker, E. N. (1990). "Copper coordination geometry in azurin undergoes minimal change on reduction of copper(II) to copper (I)." J. Am. Chem. Soc. **112**: 7817-7819.

St. Clair, C. S., Ellis, W. R. and Gray, H. B. (1992). "Spectroelectrochemistry of blue copper proteins: pH and temperature dependencies of the reduction potentials of five azurins." Inorg. Chim. Acta **191**: 149-155.

Strange, R. W., Murphy, L. M., Karlsson, B. G., Reinhammar, B. and Hasnian, S. S. (1996). "Effect of pH and ligand binding on the structure of the Cu site of the Met121Glu mutant of azurin from *Pseudomonas aeruginosa*." Biochem. **35**: 16391-16398.

Taniguchi, V. T., Malmström, B. G., Anson, F. C. and Gray, H. B. (1982). "Temperature dependence of the reduction potential of blue copper in fungal laccase." Proc. Natl. Acad. Sci. **79**: 3387-3389.

Taniguchi, V. T., Sailasuta-Scott, N., Anson, F. C. and Gray, H. B. (1980). "Thermodynamics of metalloprotein electron transfer reactions." Pure Appl. Chem. **52**: 2265-2281.

van Pouderoyen, G., Andrew, C. R., Loehr, T. M., Sanders-Loehr, J., Mazumdar, S., Hill, H. A. O. and Canters, G. W. (1996). "Spectroscopic and mechanistic studies of type-1 and type-2 copper sites in *Pseudomonas aeruginosa* azurin as obtained by addition of external ligands to mutant His46Gly." Biochem. **35**: 1397-1407.

Vila, A. J., Ramirez, B. J., Di Bilio, A. J., Mizoguchi, T. J., Richards, J. H. and Gray, H. B. (1997). "Paramagnetic NMR spectroscopy of cobalt(II) and copper(II) derivatives of *Pseudomonas aeruginosa* His46Asp azurin." Inorg. Chem. **36**: 4567-4570.

Webb, M. A., Kwong, C. M. and Loppnow, G. R. (1997). "Excited-state charge-transfer dynamics of azurin, a blue copper protein, from resonance Raman intensities." J. Phys. Chem. B **101**: 5062-5069.

Chapter 4

Probing the CuA Center by Intramolecular Electron Transfer

Introduction

Although controversial when it was first proposed, Peter Mitchell's chemiosmotic theory is now accepted as the basic way organisms generate ATP (Mitchell 1961). The fundamental tenet of his mechanism is that while oxidizing substrates, organisms produce a proton gradient across a membrane. The influx of protons seeking to alleviate this gradient is then used by ATP synthetase to drive the production of ATP. One enzyme involved in the formation of the proton gradient is a terminal oxidase that binds molecular dioxygen and with the addition of four electrons and four protons, produces two water molecules. The energy released from the breaking of the oxygen-oxygen bonds is coupled to the pumping of four additional protons across the lipid bilayer in which the enzyme complex resides. There are several classes of terminal oxidases. One of the most common are the cytochrome *c* oxidases (CCO) which accept electrons from the soluble electron transport protein cytochrome *c* (Babcock and Wikström 1992).

Cytochrome *c* oxidases are multi-subunit enzymes (from 4-13 proteins) which contain 3 distinct metal cofactors. The primary site for electron entry into CCO is the CuA domain which resides in subunit II. This binuclear copper site accepts electrons from cytochrome *c* and then quickly equilibrates with the heme *a* site in subunit II. The function of the CuA and heme *a* sites are to facilitate electron transport into the oxygen binding site which resides well buried in the interior of the membrane. The oxygen is bound to a coupled heme a_3 and CuB. Flash-flow techniques have allowed the elucidation of several intermediate steps in the reduction of O_2 to water, as well as the rates at which they occur.

The structure of the CuA site of CCO was the subject of controversy for many years. Purification of this membrane protein by a variety of methods led to a wide range in values for the reported Cu content of the enzyme. It is difficult to observe the CuA center by absorption spectroscopy because the UV/Vis spectroscopy of CCO is dominated by the strong absorbances of the two heme-containing centers. A resolved absorption band at long wavelength (~830 nm) was assigned to the CuA center and two MCD bands at 480 and 530 nm were associated with the CuA center by a clever double resonance technique (Thomson et al. 1986). The MCD spectrum of CCO was taken in the presence and absence of microwave irradiation at the resonance frequency of the CCO EPR

signal. Bands associated with the CuA site were selectively suppressed by irradiation at the resonant frequency of the CuA site. The EPR signal intensity for the CuA site integrates to 1 Cu charge per subunit, in conflict with most of the atomic absorption data which indicated a total of 3 Cu atoms per molecule of CCO, 1 in the CuB site, leaving 2 for CuA center. Evidence that the CuA sites in CCO and nitrous oxide reductase (N_2OR) were similar helped solve this dilemma; nitrite reductase does not contain any heme cofactors and mutants have been isolated where the catalytically active Cu site of N_2OR, CuZ, does not form. Strong evidence for a binuclear Cu site was obtained from the EPR spectrum of this N_2OR variant which showed a seven line hyperfine splitting with intensities indicative of a mixed-valence, binuclear site.

With the publication of X-ray crystal structures for the *Paracoccus* (Iwata et al. 1995) and bovine (Tsukihara et al. 1995; Tsukihara et al. 1996) cytochrome *c* oxidases, the CCO CuA site has also been shown to be a binuclear copper site with a central parallelogram of two Cu atoms and two bridging cysteine sulfurs. In addition, each Cu has a histidine ligand and an addition terminal ligand, a methionine sulfur for one and a backbone carbonyl oxygen for the other. (See figure 1.) The discrepancy between the EPR and atomic absorption estimates of Cu content can be explained as a binuclear copper center in which a single charge is delocalized over both copper atoms, giving each of them a $+^1/_2$ formal charge. The evolutionary rational for the use a binuclear rather than mononuclear Cu site as an electron transporter has been the subject of much speculation (Ramirez et al. 1995; Bertini et al. 1996). One frequently mentioned possibility is the provision of separate entrances and exits for the electron which is particularly advantageous in a complex membrane-bound electron transporter. Another potential benefit is a longer range bridge for electron transport; a binuclear site in which the electron is delocalized would bridge those 6 Å with better coupling (less transmission loss over the distance) than is provided by coupling through normal protein medium. With the electron delocalized over a larger site, changes to the site geometry would also be expected to be smaller since the additional electron is shared over more atoms (smaller λ_{inner}). Recent EXAFS data on the mixed-valence and reduced CuA sites from *T. thermophilus* and *B. subtilis*, show very small changes in Cu-S bond lengths upon reduction. There is a small, symmetric expansion of the central Cu_2S_2 parallelogram that is similar to the

lowest energy A_{1g} modes observed by resonance Raman (Andrew et al. 1996; Blackburn et al. 1997).

Prior to the elucidation of the X-ray structure several groups had pursued the question of the composition and spectroscopy of the CuA site by making soluble fragments containing the CuA site from subunit II (Lappalainen et al. 1993; von Wachenfeldt et al. 1994; Slutter et al. 1996). In addition, CuA models were made by engineering proposed purple sites into other proteins. Lu and coworkers engineered a purple site into the β-barrel of azurin by addition of an additional Cys ligand and small rearrangements of the interligand loops (Hay et al. 1996). Addition of a mixture of Cu^{1+} and Cu^{2+} gives a strong purple color with the characteristic 480, 530, and 790 nm absorption bands. If one adds only Cu^{2+}, the protein spectrum shows an additional strong band at 600 nm characteristic of the blue copper centers. Reduction with ascorbate converts the protein entirely to the purple copper form. Canters and coworkers have made another purple center starting with the blue copper protein, amicyanin (Dennison et al. 1995). Saraste and coworkers, engineered a CuA site into the initial acceptor subunit of the functionally homologous cytochrome *bo* quinol oxidase (van der Oost et al. 1992). The C-terminal domains of subunit II of the quinol and cytochrome *c* oxidases have a high degree of homology and were predicted to form β-barrel structures. Saraste's engineered CyoA fragment has the spectroscopic signature predicted by the double resonance studies of CCO and the crystal structure of the protein shows a slightly distorted tetrahedron with the same ligand structure as was later seen in the CCO structures.

Experimental design

Claire Slutter, in this lab, had cloned and expressed the soluble portion of CCO subunit II from *Thermus thermophilus* (Slutter 1996). Extensive characterization of this fragment showed it contains a well delocalized CuA center very similar to other characterized CuA centers. I took this cloned fragment as the basis for studies of the electron transfer properties of the CuA site.

One of the central tenets of bioenergetics is that to maximize efficiency, the energy difference (the driving force) for each step should be as small as possible. For the electron transfer from the CuA site to the binuclear heme site, the energy difference has been measured to be a mere 50 mV. With this small a driving

force, and a metal to metal distance of ~19 Å, the rate of 1.8×10^4 s^{-1} is remarkable. Using the Marcus theory of electron transfer and the average distance dependence of ET (β = 1.0 $Å^{-1}$), this implies an exceedingly low reorganization energy for the reaction (150-500 mV (Ramirez et al. 1995)). I set out to test this proposal by measuring intramolecular electron transfer rates as a function of driving force in metal-modified mutants of the *T. thermophilus* CuA soluble fragment.

As was discussed in chapter 1, the rate of electron transfer varies with the driving force of the reaction. Figure 1.3 shows the classical Marcus driving force curve, the rate of electron transfer as a function of the driving force. The electron transfer rate is predicted to be maximal when the driving force ($-\Delta G°$) is equal to the reorganization energy for the reaction (λ_{12}). To measure the reorganization energy of the CuA site (λ_{11}), one needs electron transfer rates at a variety of driving forces and the reorganization energy of the labeling complex (λ_{22}, which can be estimated from the self-exchange rates of analogous inorganic complexes). I have made site-directed mutants of the CuA fragment to introduce modifiable histidines on the surface of the protein at sites predicted to be 12-15Å from the CuA site and I planned to covalently modify these histidines with Ru(tpy)(bpy)-, Ru(tpy)(phen)-, and Os(tpy)(bpy)- complexes. Electron transfer rates between the CuA and surface metal complexes would then be measured using the laser techniques described in chapter 2.

Material and methods

General

General molecular biology techniques were performed according to Maniatis or Current Protocols (Sambrook et al. 1989; Ausubel et al. 1995). PCR conditions and protein purification protocols are modifications of methods described in Slutter (Slutter 1996). Plasmid preparation and purification of PCR fragments was done using Qiagen plasmid prep kits and PCR cleanup/gel extraction kits (Qiagen, Chatsworth, CA). Taq polymerase was purchased from Boehringer Mannheim (Indianapolis, IN). Restriction enzymes were purchased from New England Biolabs (Beverly, MA) and Boehringer Mannheim and used with the supplied buffers according to manufacturer's instructions. Buffer exchange was done by ultrafiltration using Centricon10's or YM10 membranes (Amicon, Beverly, MA) or by gel filtration using PD10 pre-packed Sephadex G25

columns (Pharmacia, Uppsala, Sweden). Proteolytic digestions and mass spectrometry analysis was done at the California Institute of Technology's Protein/Peptide Micro Analytical Laboratory by Dr. Gary Hathaway.

Mutant construction

All genes used in this study were double mutants: H117Q plus the desired new surface histidine. (See figure 2 for design scheme.) For the mutants with histidines at positions 118-121, the mutagenesis was done with one cloning step, introducing the H117Q and X-to-H mutation with the same set of oligonucleotides. The rest of the mutations were made in two steps; the H117Q plasmid was constructed and then used as the template for the PCR mutagenesis to create the rest of the surface histidine mutations: 147H, 146H, 163-166H. The mutations leading away from M160, 163-166, were done with a single round of PCR using long oligonucleotides that extended to the mutation site from the BamHI restriction site marking the 3' end of the gene. The other, interior mutations were constructed using two-piece PCR employing a set of flanking primers, CuANdeI.s and CuABamHI.as, and sense and anti-sense primers covering the 146 or 147 mutation sites. The internal primers were designed so they started immediately 5' to a T residue (see figure 3 for sequences) (Reikofski and Tao 1992). Initially I had planned to do two temperature PCR (cycling between 96° and 72°C) so all the primers have melting temperatures around 82° C (calculated using 4° per GC pair, 2° per AT pair, and ignoring mismatches). However, two temperature PCR did not give adequate yields of PCR products despite the high annealing temperature of the primers. Also unsuccessful were attempts to use the mega-primer method which uses only a single internal mutagenic oligo (Reikofski and Tao 1992).

After construction of the desired series of mutants, I concluded that it would be better to be working with the "T9" truncation of the original construct. The original clone of the soluble portion of subunit II of *T. thermophilus* CCO contained the gene coding for amino acids 34 through 168 cloned into the pET9a expression vector (Novagen, Madison WI). N-terminal sequencing of the expressed protein from the original construct showed several nested N-terminal proteolytic cleavages including a considerable portion starting GVIPA. To address this N-terminal heterogeneity, and to remove H40 which might provide a competing labeling site, PCR mutagenesis was used to remove the first 10 amino acids of each mutant construct (new N-terminus MVIPA...). Production of

the correct truncated CuA domain (M. W. 13,942) was demonstrated by MALDI-MS. The sequence of the CuA gene and surrounding vector sequences of this plasmid (T9CuAH117Q) is given in Appendix C.

Primers were synthesized on the 0.4 μmole scale by the Beckman Institute oligonucleotide synthesis facility and resuspended to a final concentration of 25 pmoles/μliter in water before use. All PCR reactions contained (final concentrations): 60 mM Tris-HCl, 1.5 mM $(NH_4)_2SO_4$, 2 mM $MgCl_2$, pH 9.5 @ 22°C (Buffer J from the PCR Optimizer Kit, Invitrogen, San Diego, CA), 0.2 mM each dNTP, 2.5 pmole/μl sense and anti-sense primers, and 5 units Taq polymerase per 100 μl reaction. For reactions starting with purified plasmid templates, 0.25 to 0.5 μg was used in each 100 μl reaction; for the second round of two piece PCR mutagenesis, approximately half of each purified first-round reaction was used as template in the second round. Reaction mixtures overlaid with mineral oil were placed in a Perkin-Elmer DNA Thermal Cycler 480. Templates were denatured at 96°C for 5 minutes followed by thirty PCR cycles denaturing at 96°C for 30 seconds, annealing at 55°C for 30 seconds, and polymerizing at 72°C for 1 minute. Final polymerization was given 5 minutes at 72°C and the reactions were held at 4° C until further analysis or purification.

For the two piece PCR, in the first round the gene was amplified in two 100 μl reactions; the portion 5' to the mutation site was amplified using a sense primer that binds to the NdeI cloning site and an antisense primer covering the mutation site, and the 3' portion using a sense primer covering the mutation site and an anti-sense primer that anneals to the BamHI site following the CuA gene. The two PCR reactions were run on an agarose gel (1-2% agarose, 1X TAE) and the bands excised and purified using a Qiagen gel extraction kit according to the manufacturers instructions, eluting with 30 μl of 5 mM Tris, pH 8. Half (15 μl) of each was mixed together and used as the template for a second round of PCR using only the flanking primers, CuANdeI.s and CuABamHI.as. The resulting DNA was extracted from the PCR reaction mixture using a Qiagen PCR clean-up kit. The DNA, eluted in 30 μl of 5 mM Tris pH 8, was digested with NdeI and BamHI in NEB's BamHI buffer. These digests were purified (and the second round of PCR checked) by running on an agarose gel and extracting the band of appropriate size. A pET9a plasmid containing the β-lactamase gene was similarly digested and gel purified. Ligations in a total volume of 20 μl, containing 1X BMB ligase buffer, 0.4-2.0 μg digested pET vector DNA, 1/3 of each purified PCR

reaction (10 µl), 1 unit T4 DNA ligase (BMB), were incubated overnight at 16°C. 1 µl of the ligation mix was transformed into 20 µl of chemically competent BL21(DE3) cells (Novagen, Madison, WI).

Initial screening of transformed colonies was done by PCR, starting with 5 µl of a 50 µl cell suspension (in water). PCR was performed as above in a final reaction volume of 25 µl using the T7 promoter and terminator primers and 0.125 units of Taq polymerase per reaction. After 55 cycles, the results were assessed on a 1.2% agarose gel. Qiagen spin minipreps were done on colonies with inserts of the correct size, starting with 7 ml cultures of cells grown overnight in LB with 35 µg/ml kanamycin. The DNA was eluted in 20 µl 5 mM Tris, pH 8, and submitted to the Beckman Institute DNA Sequencing Facility for dye-terminated cycle sequencing with the T7 promoter and terminator primers. This mutagenesis procedure is extremely efficient; more than 90% of the colonies sequenced contained the desired mutation with no secondary mutations.

Protein expression and purification

Protein expression was carried out using the pET expression system from Novagen (Madison, WI). CuA expression is under the control of the T7 polymerase promoter in the pET9a expression vector. IPTG induction of the production of T7 polymerase under the control of the *lac* operon in the *E. coli* strain BL21(DE3) leads to overexpression of the cytoplasmic CuA soluble fragment. Typically small overnight starter cultures (50 ml LB with 50 µg/ml kanamycin) are grown from frozen glycerol stocks or from colonies of freshly transformed cells. These starter cultures are expanded into 1-2 l of LB (50 µg/ml kanamycin) in 4 l culture flasks. Cultures are grown with vigorous shaking at 37°C until the optical density (OD_{600}) of the culture is 0.6-1.0. IPTG is added to a final concentration of 0.4 mM and the cells shaken at 37°C for a further 8-12 hours. Cells are harvested by pelleting at 5,000 x g for 10 minutes. At this point, the cell pellet is usually frozen; freezing and thawing appears to increase the efficiency of cell disruption during the sonication step. The cell pellet is resuspended in 50 mM Tris-HCl pH 8.0, 25 ml per liter of cell culture. Triton X-100 is added to a final concentration of 0.1% and the cells are sonicated (4 30-second cycles at the microtip limit using a Branson Sonifier Cell Disrupter 200). Cell debris is removed by centrifugation, 20 minutes 18,000 x g. (Resuspension and sonication of the cell pellet sometimes leads to recovery of considerable additional CuA protein.)

CuA was initially purified by modifications of a method devised by Dr. Claire Slutter (personal communication). $CuSO_4$ is added to the decanted supernatant to a final concentration of 10 mM, turning the solution a dark purple. The solution is acidified by adding 1 M sodium acetate, pH 4.6, incubated for 30 minutes on ice, and centrifuged to remove the precipitated material. Acidification to pH 4.6 leads to considerable precipitation, mainly of contaminating proteins but carrying down variable amounts of CuA. Resuspension of the precipitate in 50 mM Tris pH 8.0 leads to the recovery of some of the precipitated CuA. Acidification of the original purple supernatant to pH 5.5 leads to precipitation of much smaller amounts of non-purple protein.

The pH of the supernatant is readjusted to approximately 7 using 5 M NaOH before loading it onto a HiTrap Chelating column (Pharmacia, Uppsala, Sweden) that has been charged with $CuSO_4$ and equilibrated in 100 mM potassium phosphate, 500 mM KCl, pH 7.0 (buffer A). The column is washed with 1-3 column volumes (5-15 ml) of buffer A, depending on how well the protein adheres to the chelating column. The protein is eluted with buffer A supplemented with 10 mM imidazole. The eluent is concentrated by ultrafiltration using a YM10 membrane (Amicon, Beverly, MA) and washed into either buffer A or 20 mM Tris. pH 8.0. The low binding affinity of the CuA mutants with a single surface histidine means that the HiTrap chelating column does not effectively purify CuA from most of the contaminating proteins but it does remove the Triton X100 from the sample and partially concentrates the sample.

Later in the project, the initial purification of CuA was modified. In this new procedure, $CuSO_4$ is added to the decanted supernatant to give a final concentration of 20 mM. The protein is washed into 20 mM Tris, pH 8.0, by repeated concentration and dilution with an Amicon ultrafiltration device and a YM10 membrane. Aliquots of the crude protein, enough to color the upper quarter of the column, are then injected onto a 5 ml HiTrap Q anion exchange column (Pharmacia, Uppsala, Sweden). The column is then washed with 3 column volumes of 20 mM Tris, pH 8.0. The protein is eluted either with a gradient of 10-20% 20 mM Tris, 200 mM NaCl, pH 8.0 or stepwise, using 20 mM Tris, 40 mM NaCl, pH 8.0. After processing several aliquots, contaminating proteins were removed from the column by washing in 2 M NaCl.

After either initial purification procedure, the protein is further purified by anion exchange FPLC. Protein equilibrated into 20 mM Tris pH 8.0 is loaded onto a MonoQ 10/10 column and eluted with a shallow gradient of 4-9% 20 mM Tris, 200 mM NaCl, pH 8.0, over 90 minutes. The major contaminants are retained on the column and eluted by washing briefly with 100% buffer B. Using very shallow gradients on the MonoQ FPLC, one can see two poorly resolved peaks with identical UV/Vis spectra. MALDI-TOF MS shows the first of the two peaks is the holo protein (M. W. 13,942); the second peak has a molecular weight of 13,985 which could be the holo protein with an additional acetyl group. After a single MonoQ column, CuA is generally used in the metal labeling reactions without further purification.

Metal modifications

Initial experiments indicated that the CuA metal center is not stable to incubation in imidazole. Incubation of the protein in 200 mM imidazole for 21 hours at room temperature in an open test tube (conditions similar to those used for adding imidazole to $Ru(bpy)_2H_2O$-His azurin) results in colorless protein that cannot be reconstituted by reduction followed by addition of $CuSO_4$. So we elected to try an alternate labeling system developed by Dr. Angelo Di Bilio (Di Bilio et al. 1998) which uses Ru(tpy)(bpy)- or Ru(tpy)(phen)- compounds to avoid the problem of having to fill the sixth Ru coordination site subsequent to protein labeling. The $Ru^{II}(tpy)(phen)H_2O$ and $Ru^{II}(tpy)(bpy)Cl$ used in this study were a gift from Dr. Di Bilio.

T9 H117Q/E119H CuA (50 mg in 10 mM HEPES, pH 7.7) is incubated with a 4-fold molar excess of $Ru^{II}(tpy)(phen)H_2O$ at 30° C for 7 days. During this time, protein precipitation is seen, perhaps eventually amounting to as much as 10-20% of the starting material. Unreacted $Ru^{II}(tpy)(phen)H_2O$ is removed by gel filtration (PD10 column) into IMAC buffer A, 20 mM HEPES, pH 7.7, 750 mM NaCl. Upon incubation at room temperature, non-specifically bound ruthenium often dissociates; this is removed by a second gel filtration step before the sample is loaded onto a Cu-charged IMAC chelating sepharose FPLC column (Pharmacia). The protein is eluted with a buffer consisting of 20 mM HEPES, pH 7.7, and 750 mM NH_4Cl. The first major peak has the UV/Vis spectrum expected for Ru(tpy)(phen)His119CuA. (See figure 4.) Its identity has been confirmed by MS analysis of purified fragments from a trypsin digest of the protein. The second peak has not been unambiguously identified but, like the third peak, has

a spectrum that is red shifted in comparison to the Ru(tpy)(phen)His119CuA spectrum. (See figure 5.) The third peak has a slightly red-shifted ruthenium peak consistent with labeling at a carboxylic acid residue; MS analysis of HPLC-purified trypsin digest products indicates that this peak is CuA labeled at position D54 with Ru(tpy)(phen). A small amount of unreacted CuA elutes from the IMAC column after these ruthenium-modified peaks.

Yields for the $Ru^{II}(tpy)(phen)H_2O$ labeling reaction are low (~2%). Additional labeling experiments using different buffer conditions (50 mM HEPES, pH 6.8, or 100 mM $NaCO_3$, pH 7.1), higher incubation temperatures (37° C), and up to a 10-fold molar excess of either $Ru^{II}(tpy)(phen)H_2O$ or $Ru^{II}(tpy)(bpy)Cl$ all gave similarly low yields of the desired labeled protein, 2-3.5%. At room temperature, the CuA soluble fragment is stable in 50% isopropanol; reaction of CuA with $Ru(tpy)(bpy)CO_3$ in 50% isopropanol did not show appreciable labeling after 5 days. However, enough $Ru^{II}(tpy)(phen)$H119 CuA was obtained to enable preliminary photoinduced ET data to be collected.

Results and discussion

Design of surface accessible histidines for labeling

As the starting point for covalent attachment of a second metal site in CuA, we would like to place histidine residues on the protein surface ~15 Å away from the CuA site. We do not currently have an X-ray or NMR structure for the *Thermus thermophilus* CuA fragment we work with. However, all CuA domains show a high degree of homology (Saraste 1990) so sequence alignment allows one to make inferences based on similarity to proteins of known structure (See figure 6). Crystallographic structures at 2.8 Å resolution are available for the complete cytochrome *c* oxidase complexes of *Paracoccus denitrificans* (Iwata et al. 1995)and bovine heart muscle (Tsukihara et al. 1995; Tsukihara et al. 1996). These two proteins show 50% and 45% similarity to the *T. thermophilus* CuA site.[1] In addition, there is a 2.3 Å resolution structure of the soluble domain of subunit II of *E. coli* quinol oxidase into which a purple copper center has been engineered (purple CyoA) (Wilmanns et al. 1995). The coordinates for the *P. denitrificans* structure, the structure having the highest overall sequence identity with our construct (28%), are not publicly available at this time. But the coordinates for the bovine CuA and CyoA sites are on deposit at the Protein Data Bank

[1]Using the BestFit program from the Genetics Computing Group package (Madison, WI).

(http://www.pdb.bnl.gov/) and have been used to estimate distances to the Cu site and surface accessibility of analogous residues in our *Thermus* soluble fragment.

While the overall fold of all CuA domains appears to be conserved, details of the loop regions are likely to be less well conserved than the strands. Therefore, I confined myself to histidine mutations on the β-strands leading into the Cu ligands. Figure 7 shows the CyoA fragment with the engineered CuA site with the residues on β-strands leading into the H172, C207, and M218 ligands highlighted (corresponding positions for the CuA fragment are H114, C149, and M160). The average distances from the Cu atoms to the δ-carbons of selected surface accessible CyoA residues are (CuA residue number in parentheses): K221(T164) 17.1 Å, D204(R146) 15.7 Å, I176(V118) 14.5 Å, P177(E119) 13.3, R178(G120) 20.7Å. The proline in CyoA causes a kink unlikely to be present in the analogous region in CuA so several residues in that region were mutated, V118H, E119H, G120H, T121H. The desired R146H and T164H mutations were flanked by additional histidine substitutions to allow for the possibility that the CuA strands are in a different register than the CyoA strands: I147H, R146H, T163H, T164H, and V165H. In initial expression studies, mutations to residues that are surface accessible in CyoA (E119H, G120H, T121H, R146H, and T164H) give proteins that express well and have the normal purple UV/Vis spectrum. The rest of the mutants did not express well and were not examined further. 'T9' truncations of the expressed purple mutants were made; an additional mutant H117Q/V166H was constructed at this time.

Metal modifications

Mass spectrometry analysis of HPLC-purified fragments from a tryptic digest of ruthenated CuA confirmed addition of Ru(tpy)(phen) to H119 in H117Q/E119H. However, despite exploration of a variety of incubation temperatures and buffer conditions, the yield of the desired product was uniformly low, ~2% of the initial protein. Since preliminary labeling experiments with $Ru(bpy)_2CO_3$ had given high yields (30-50%) of ruthenium modified protein, it is unlikely that H119 was buried within the protein interior and therefore inaccessible to metal modification. The steric bulk of the ligands in the $Ru(tpy)(phen)(H_2O)$ complex and the existence of only one free coordination site have severe consequences to the ligand substitution kinetics of the Ru labeling

reaction. Since osmium is more substitutionally inert than ruthenium, the Os(tpy)(bpy)- labeling reactions were not attempted.

Preliminary ET data

Photoinduced electron transfer experiments were performed as described for azurin in chapter 2. Figure 8 shows the absorption transients at 406 nm and 790 nm. At 406 nm, the Ru(tpy)(phen)(Im) isobestic, one can see the transient formation and disappearance of Ru(tpy)(phen)(His)$^{3+}$ (Di Bilio 1997). At 790 nm one can observe the regeneration of the oxidized (purple) CuA center during the back electron transfer reaction. The ET rates at the two wavelengths, 1.23×10^6 s^{-1} and 1.92×10^6 s^{-1} respectively, are in reasonable agreement. More extensive data collection at additional wavelengths would be needed to obtain a better value for the true electron transfer rate constant. This would be possible with the preparation of additional sample. However, the limitations on the amount of labeled protein obtained imply that it would be impractical to continue to pursue a driving force study using M(tpy)(N-N)- systems (M = Ru, Os; N-N = dipyridyl ligands such as bipyridine and phenanthroline).

Fortunately, I have recently shown that the instability of the CuA center in imidazole can be alleviated if the imidazole reaction is done under anaerobic conditions. This opens up opportunities to use alternative $Ru(N\text{-}N)_2Im$- labels with driving forces ranging from 0.56 to 1.02 eV (Mines et al. 1996). This should provide enough of a span of driving forces to indicate whether the reorganization energy of the binuclear CuA center is substantially smaller than that of other electron transport proteins such as azurin and cytochrome *c*.

Figure 4.1 The binuclear copper site of the CyoA model for CuA (Wilmanns et al. 1995). The central parallelogram of two Cu and two cysteine sulfur atoms is shown obliquely. The histidine ligands flank the site. The methionine sulfur is on the upper right and the backbone carbonyl sixth ligand is on the lower left.

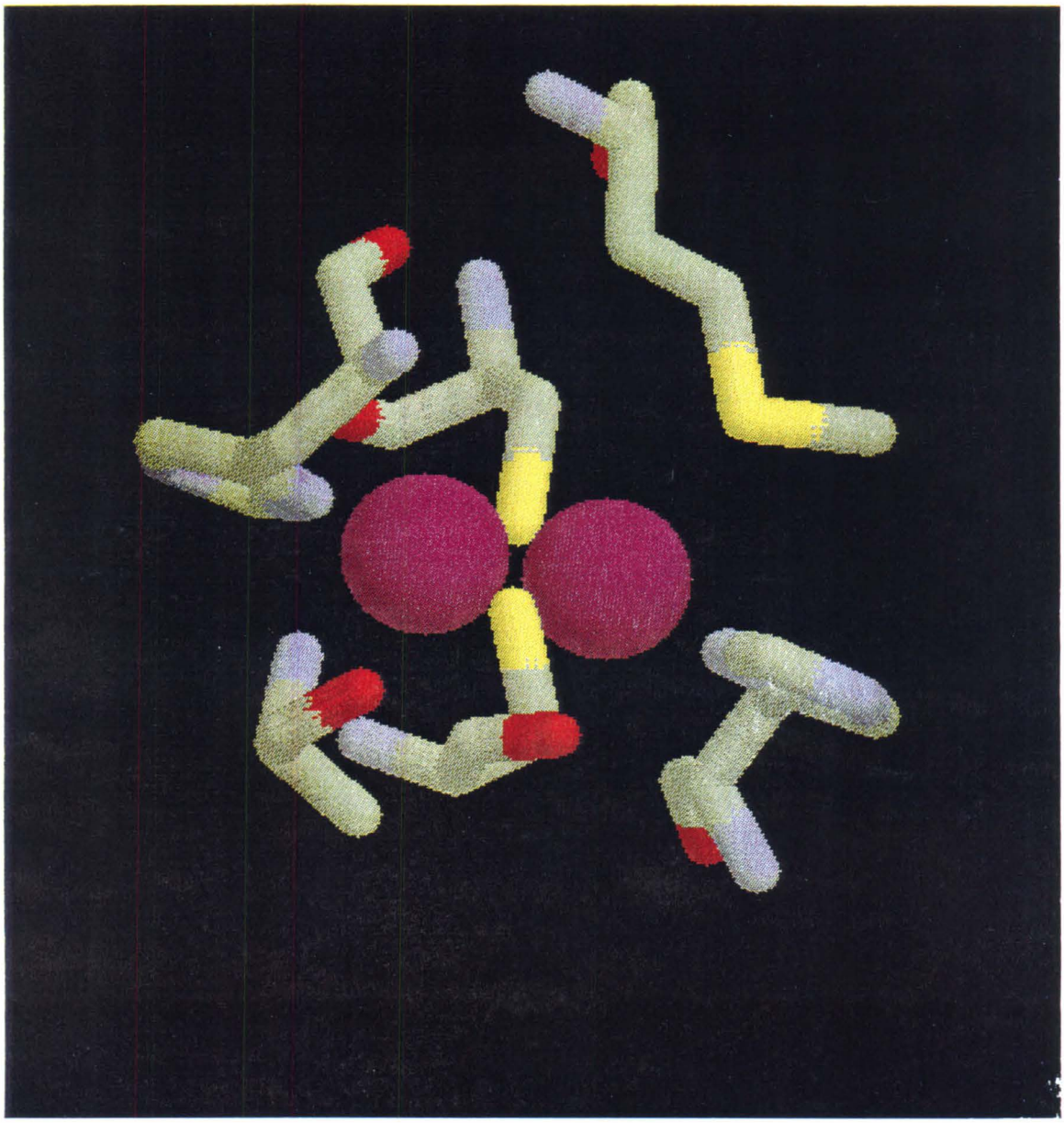

Figure 4.2 PCR strategy for construction of CuA mutants.

The base plasmid 117Q and the 117Q/118-121H series of mutants were constructed in a single cloning step by two piece PCR. The gene for the CuA soluble fragment was amplified using sense and anti-sense mutagenic primers paired with the appropriate flanking sense and anti-sense primers, CuANdeI.s and CuABamHI.as. The purified fragments from this first round of PCR then served as template for a second round of PCR with the flanking CuANdeI.s and CuABamHI.as primers. The resulting full length gene was restriction enzyme digested and cloned into pET9a as a NdeI/BamHI fragment.

The 117Q/146H and 117Q/147H mutants were done in a single cloning step by two piece PCR. The CuA gene containing the 117Q mutation was amplified using sense and anti-sense mutagenic primers paired with the appropriate flanking sense and anti-sense primers, CuANdeI.s and CuABamHI.as. The purified fragments from this first round of PCR then served as template for a second round of PCR with the flanking CuANdeI.s and CuABamHI.as primers. The resulting full length gene was restriction enzyme digested and cloned into pET9a as a NdeI/BamHI fragment.

The 117Q/163-166H series of mutants was constructed with one round of PCR using mutagenic primers that spanned the mutation and the BamHI site. The CuA gene containing the 117Q mutation was amplified using CuANdeI.s and the mutagenic anti-sense primers. The purified fragments were restriction enzyme digested and cloned into pET9a as NdeI/BamHI fragments.

Construction of the 'T9' truncated versions of these mutant CuA's was accomplished by cloning the PCR product produced by amplifying each of the mutants with the T9CuA.s and CuABamHI.as primers.

Construction of the CuA 117Q base plasmid

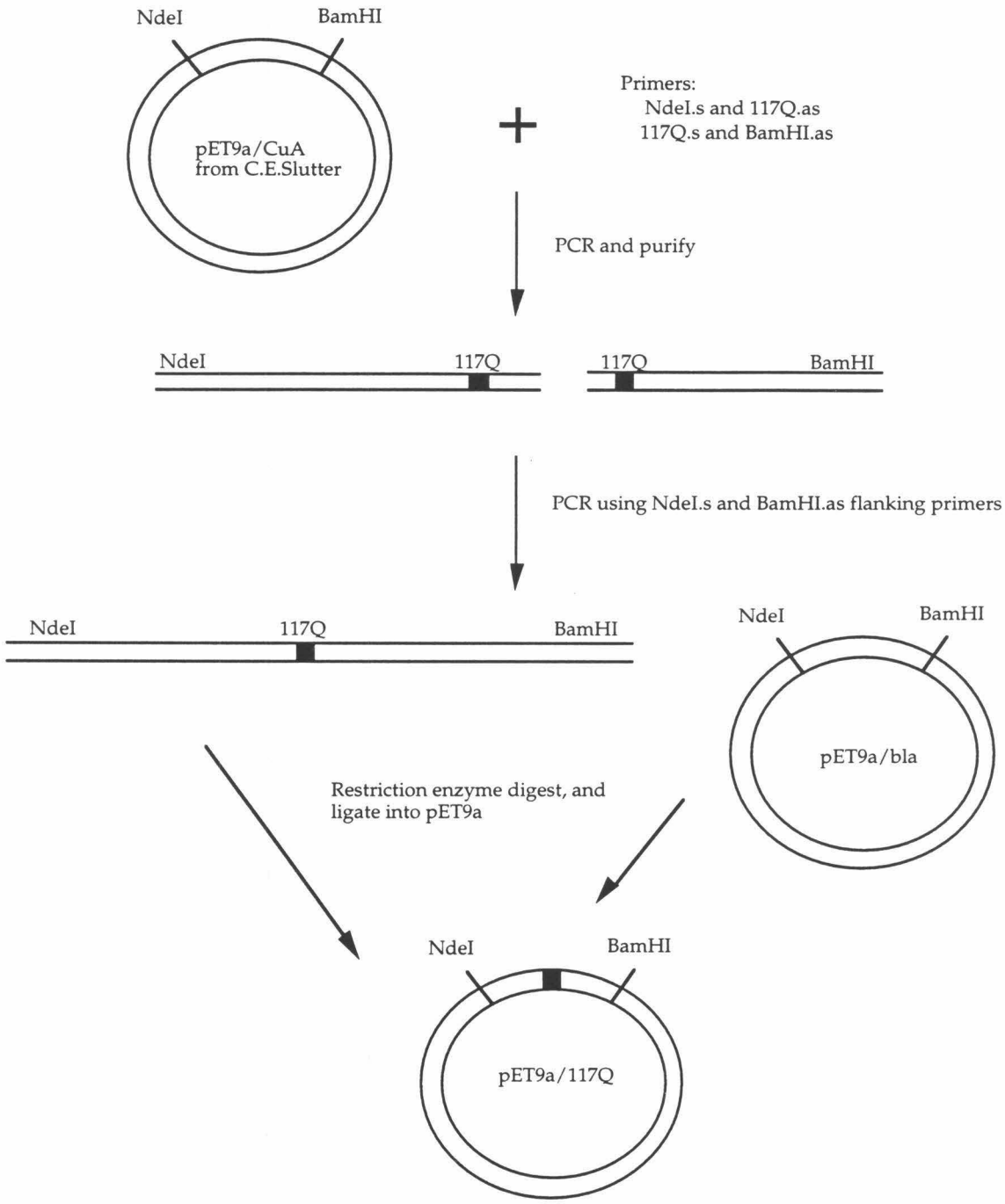

Construction of the CuA 117Q/146H and 117Q/147H plasmids

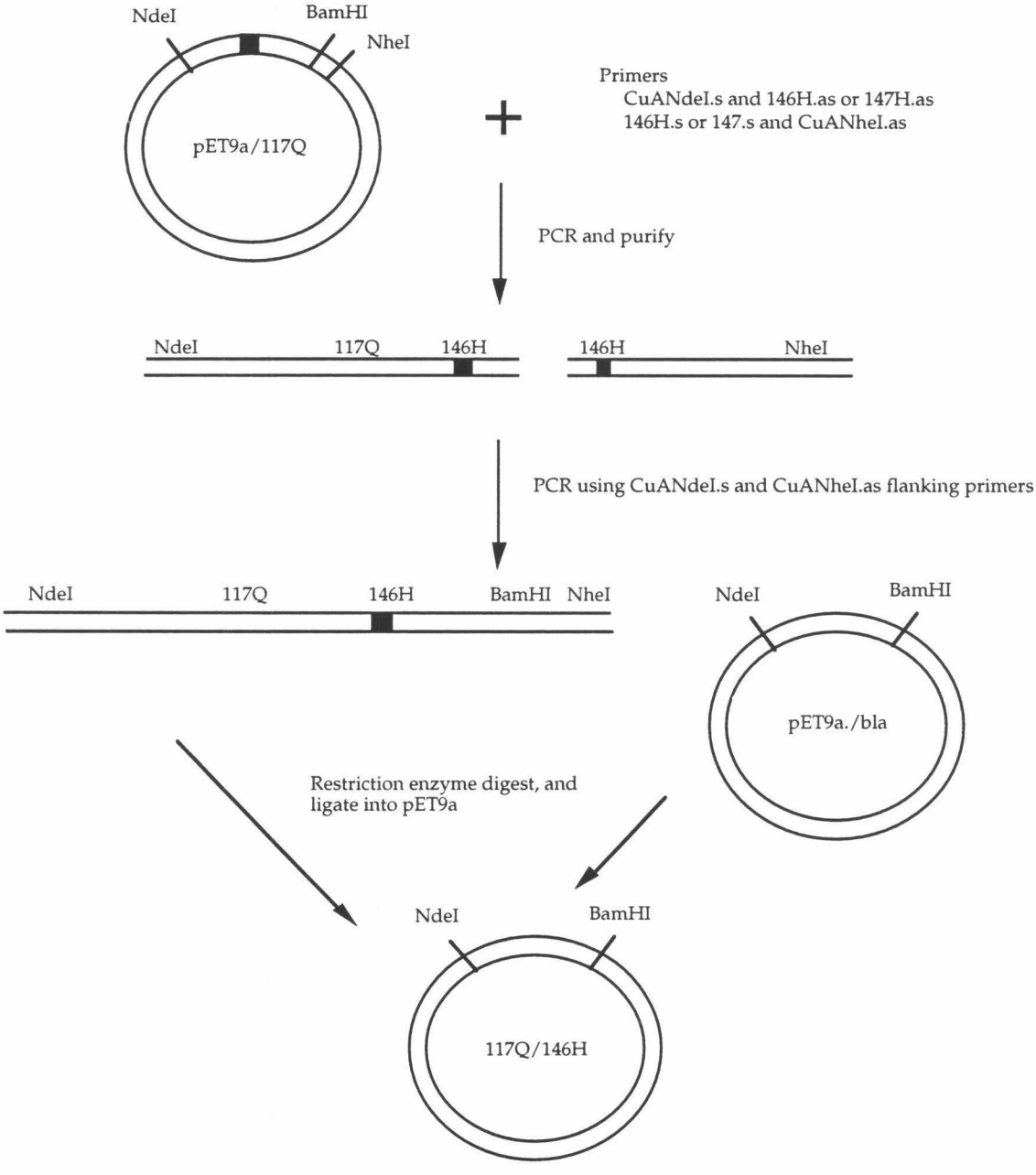

Construction of the CuA 117Q /163-5H plasmids

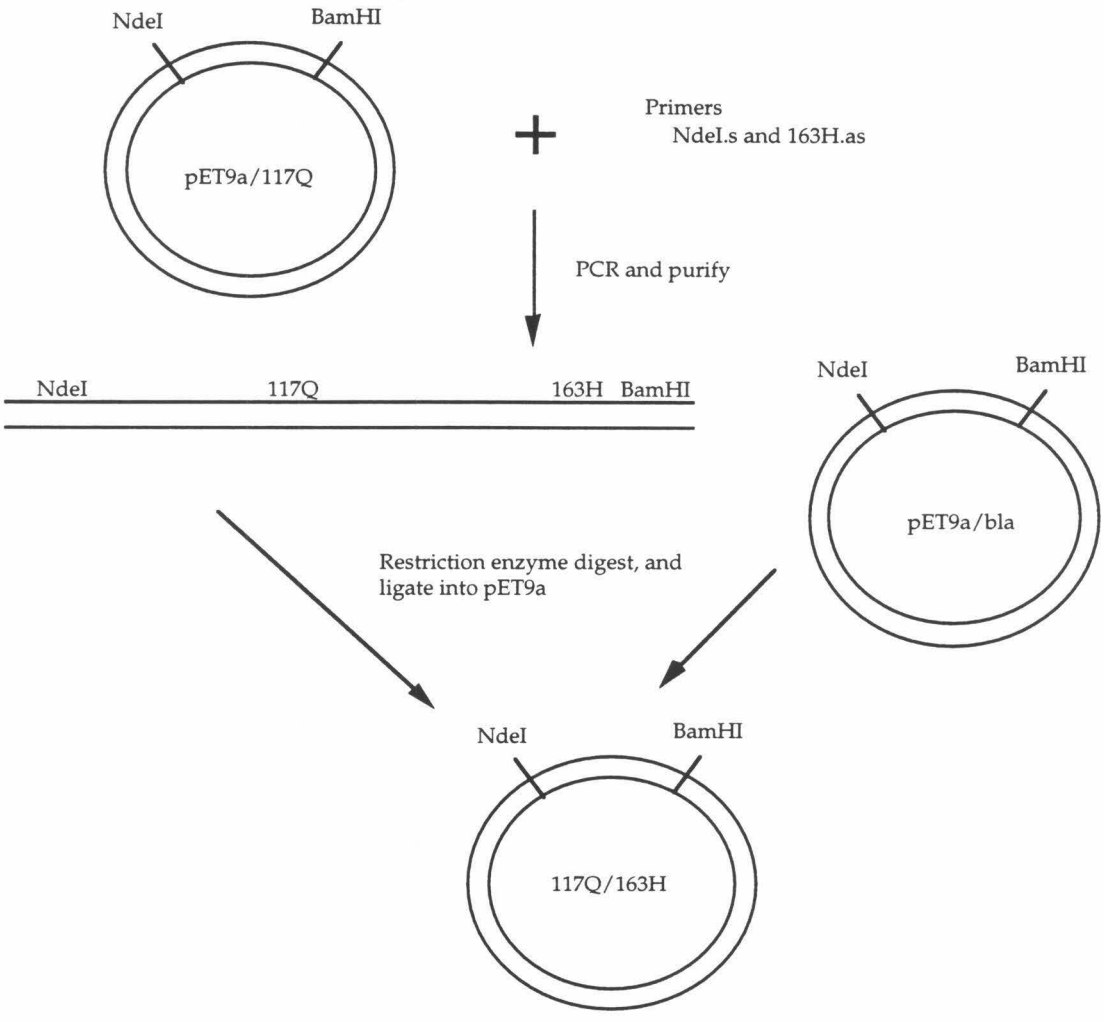

Truncated versions of the histidine mutants that expressed well were made by the same strategy as above using the T9CuA.s and CuABamHI.as primers.

Figure 4.3 Primers for site-directed mutagenesis of the CuA soluble fragment.

Flanking primers with restriction sites underlined

CuANdeI.s CTT TAA GAA GGA GAT ATA CAT ATG GCC TAC A

T9CuA.s GCC ACC CAC ACC CAT ATG GTC ATT CCC GC

CuANheI.as GC GTG CTG CTA GCG CTA TAT GCG TTG A

CuABamHI.as TTA GCA GCC GGA TCC TCA CTC CTT CAC

His substitution primers mutated codons in boldface

H117QCuA.s C CAC GGC TTT **CAG** GTG GAG GGC ACC AA

H117QCuA.as GGT GCC CTC CAC **CTG** AAA GCC GTG GAT

CuAV118H.s C CAC GGC TTT **CAG CAC** GAG GGC ACC AAC AT

CuAV118H.as GTT GGT GCC CTC **GTG CTG** AAA GCC GTG GAT

CuAE119H.s C CAC GGC TTT **CAG** GTG **CAC** GGC ACC AAC AT

CuAE119H.as GTT GGT GCC **GTG** CAC **CTG** AAA GCC GTG GAT

CuAG120H.s C CAC GGC TTT **CAG** GTG GAG **CAC** ACC AAC AT

CuAG120H.as GAT GTT GGT **GTG** CTC CAC **CTG** AAA GCC GTG

CuAT121H.s C CAC GGC TTT **CAG** GTG GAG GGC **CAC** AAC AT

CuAT121H.as GAT GTT **GTG** GCC CTC CAC **CTG** AAA GCC G

CuAI147H.s G GAG TAC CGC **CAC** ATC TGC AAC CAG TAC

CuAI147H.as GTA CTG GTT GCA GAT **GTG** GCG GTA CTC C

CuAR148H.s G GAG TAC **CAC** ATC ATC TGC AAC CAG TAC

CuAR148H.as GTA CTG GTT GCA GAT GAT **GTG** GTA CTC C

CuAT163H.as TTA GCA GCC GGA TCC TCA CTC CTT CAC CAC GAT CGT **GTG** GAA C

CuAI164H.as TTA GCA GCC GGA TCC TCA CTC CTT CAC CAC GAT **GTG** GCC G

CuAV165H.as TTA GCA GCC GGA TCC TCA CTC CTT CAC CAC **GTG** CGT G

CuAV166H.as TTA GCA GCC GGA TCC TCA CTC CTT CAC **GTG** GAT C

Figure 4.4 (a) Absorption spectra of T9 H117Q/E119H CuA and the Ru^{II}(tpy)(phen)Im model. The solid line is the predicted spectrum of a 1:1 complex of the two. (b) Comparison of the predicted T9 H117Q/E119HRu^{II}(tpy)(phen) CuA spectrum and the spectrum of the first peak from the IMAC column purification.

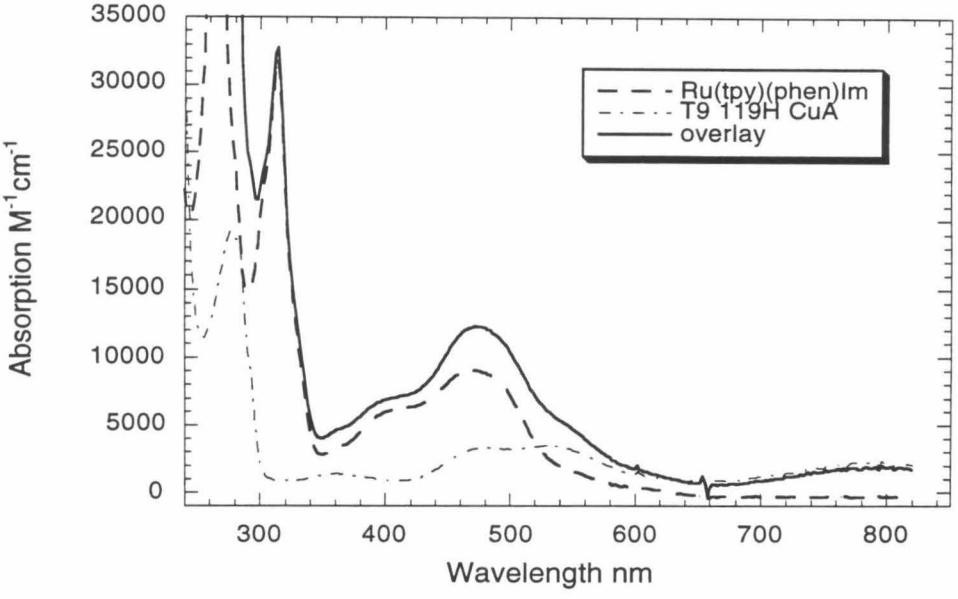
35000
30000
25000
20000
15000
10000
5000
0
Absorption M-1cm-1
300
400
500
600
700
800
Wavelength nm
Ru(tpy)(phen)Im
T9 119H CuA
overlay

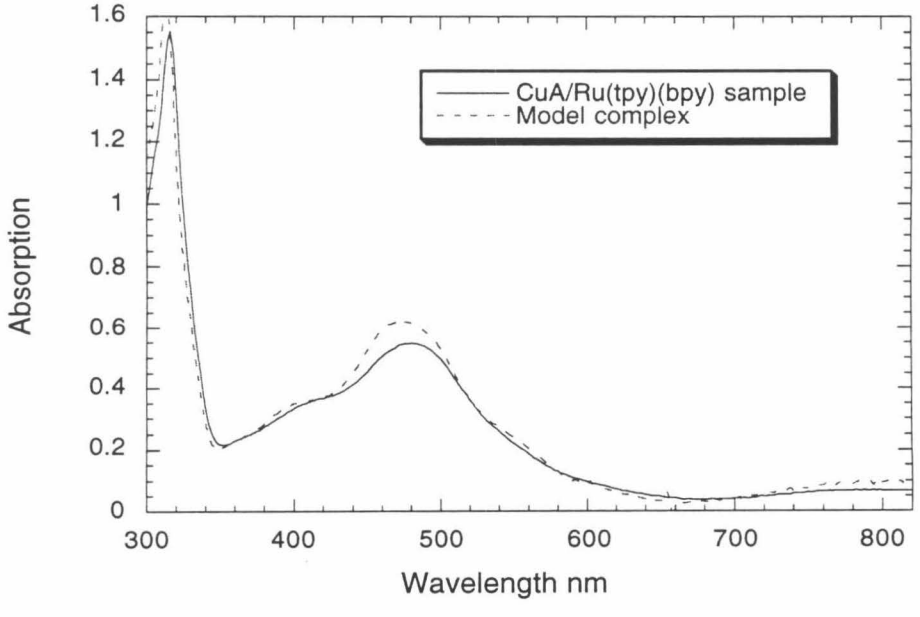
1.6
1.4
1.2
1
0.8
0.6
0.4
0.2
0
Absorption
300
400
500
600
700
800
Wavelength nm
CuA/Ru(tpy)(bpy) sample
Model complex

Figure 4.5 Spectra of fractions from the IMAC purification of T9 H117Q/E119HRu^{II}(tpy)(phen) CuA. The first peak is the desired product. The third peak is CuA labeled at D54.

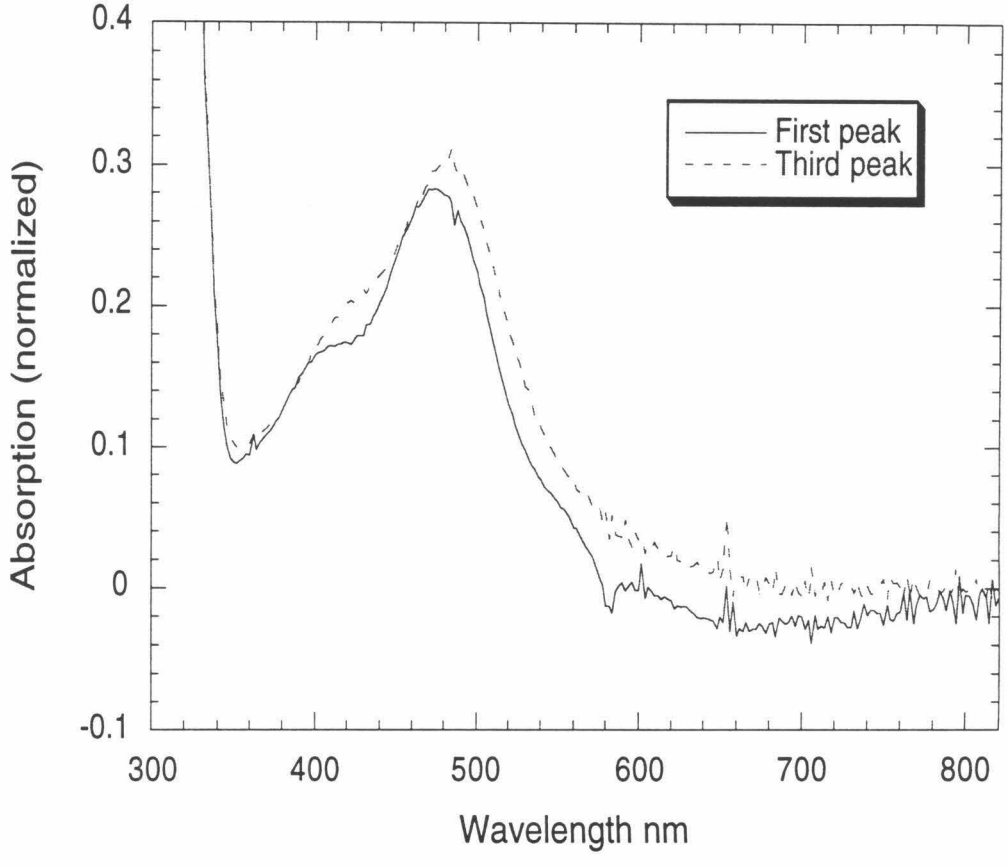
0.4
0.3
0.2
0.1
0
-0.1
Absorption (normalized)
300
400
500
600
700
800
Wavelength nm
First peak
Third peak

Figure 4.6 Alignment of the protein sequences of the CuA domains discussed in the text: bovine, *Paracoccus denitrificans, Thermus thermophilus,* and subunit II of the *E. coli* quinol oxidase. Protein sequences from Entrez at the National Center for Biotechnology Information (http://www.ncbi.nlm.nih.gov/Entrez/). Alignment was done using the Pileup program from the Genetics Computer Group, Madison, Wisconsin.

```
Bovine                                                      MAYPMQLGFQ
Para.  MMAIATKRRG VAAVMSLGVA TMTAVPALAQ DVLGDLPVIG KPVNGGMNFQ
Therm.
CyoA                      MR LRKYNKSLGW LSLFAGTVLL SGCNSALLDP

Bovine DATSPIMEEL LHFHDHTLMI .....VFLIS SLVLYIISLM LTTKLTHTST
Para.  PASSPLAHDQ QWLDHFVLYI ITAVTIFVCL LLLICIVRFN RRANPVPARF
Therm.       MVDE HKAHKAILAY EKGWLAFSLA MLFVFIALIA YTLATHTAGV
CyoA   KGQIGLEQRS LILTAFGLML IVVIPAILMA VGFAWKYRAS NKDAKYSPNW

Bovine MDAQEVETIW TILPAIILIL IALPSLRILY MMDE....I. NNPSLTVKTM
Para.  THNTPIEVIW TLVPVLILVA IGAFSLPILF RSQE....MP NDPDLVIKAI
Therm. IPAGKLERV. .......... .....DPTTV RQEG....PW ADPAQAVVQT
CyoA   SHSNKVEAVV WTVPILIIIF LAVLTWKTTH ALEPSKPLAH DEKPITIEVV

Bovine GHQWYWSYEY TDYEDLSFDS YMIPTSELKP GELR....LL EVDNRVVLPM
Para.  GHQWYWSYEY PN.DGVAFDA LMLEKEALAD AGYSEDEYLL ATDNPVVVPV
Therm. GPNQYTVYVL AF..AFGYQP .......... .......... ...NPIEVPQ
CyoA   SMDWKWFFIY PEQG...... .......... .........I ATVNEIAFPA

Bovine EMTIRMLVSS EDVLHSWAVP SLGLKTDAIP GRLNQTTLMS SRPGLYYGQC
Para.  GKKVLVQVTA TDVIHAWTIP AFAVKQDAVP GRIAQLWFSV DQEGVYFGQC
Therm. GAEIVFKITS PDVIHGFHVE GTNINVEVLP GEVSTVRYTF KRPGEYRIIC
CyoA   NTPVYFKVTS NSVMNSFFIP RLGSQIYAMA GMQTRLHLIA NEPGTYDGIS

Bovine SEICGSNHSF M..PIVLELV PLKYFEKWSA SML
Para.  SELCGINHAY M..PIVVKAV SQEKYEAWLA GAKEEFAADA SDYLPASPVK
Therm. NQYCGLGHQN MFGTIVVKE
CyoA   ASYSGPGFSG MKFKAIATPD RAA.FDQWVA KAKQSPNTMS DMAAFEKLAA

Bovine
Para.  LASAE
Therm.
CyoA   PSEYNQVEYF SNVKPDLFAD VINKFMAHGK SMDMTQPEGE
```

Figure 4.7 Space-filling model of the CyoA CuA model system, *E. coli* quinol oxidase into which a CuA site has been engineered. The introduced CuA ligand residues are shown in purple. The position corresponding to the naturally occurring surface histidine in *T. thermophilus* CuA, H117, is shown in violet. The positions corresponding to the mutations made in this study, E119H, R146H, and T164H, are shown in cyan, blue, and yellow respectively.

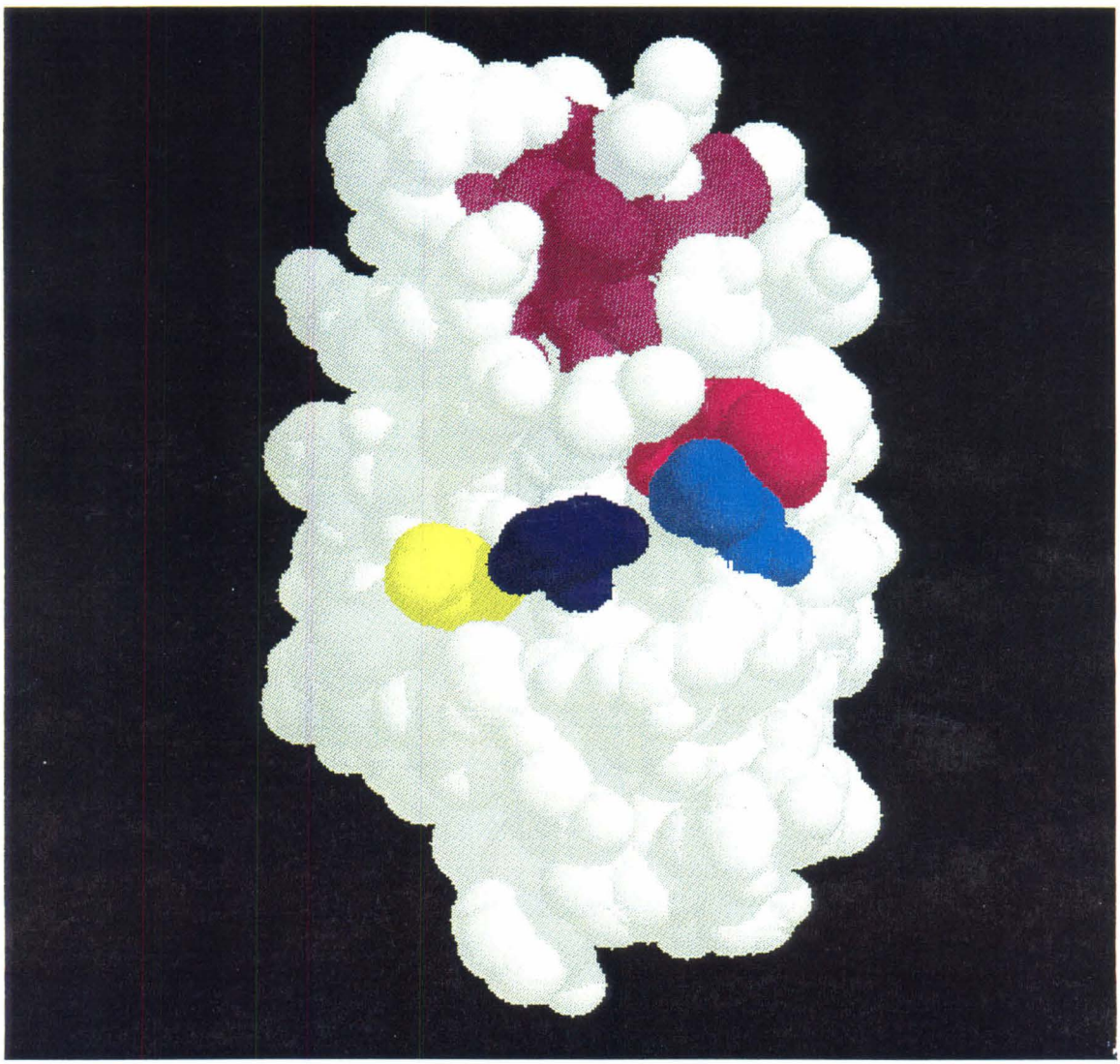

Figure 4.8 Absorption transients of T9 H117Q/E119HRu(tpy)(phen)CuA at 406 nm (a) and 790 nm (b). Single exponential fits to the data give ET rates of 1.23×10^6 s^{-1} and 1.92×10^6 s^{-1} respectively.

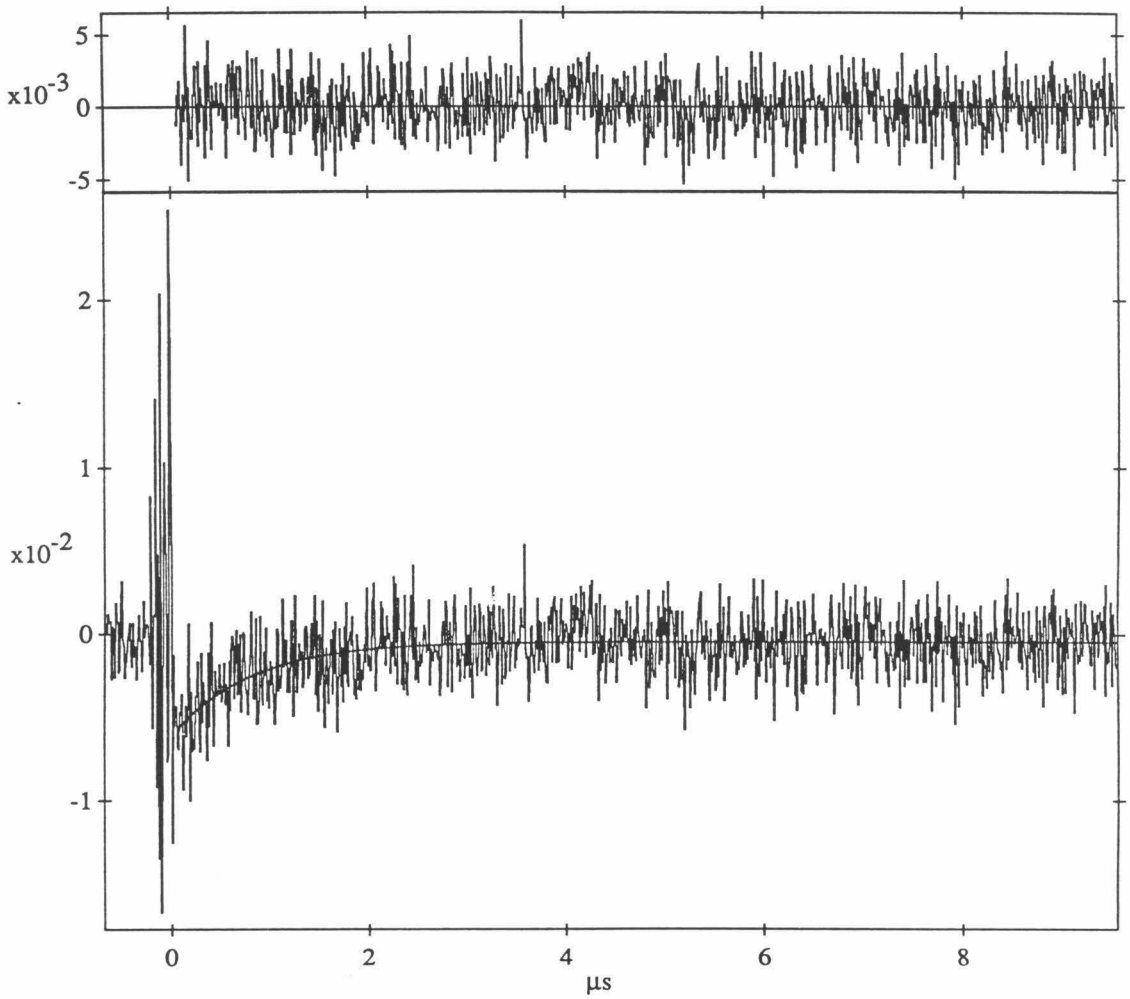
5
x10-3
0
-5
2
1
x10-2
0
-1
0
2
4
6
8
µs

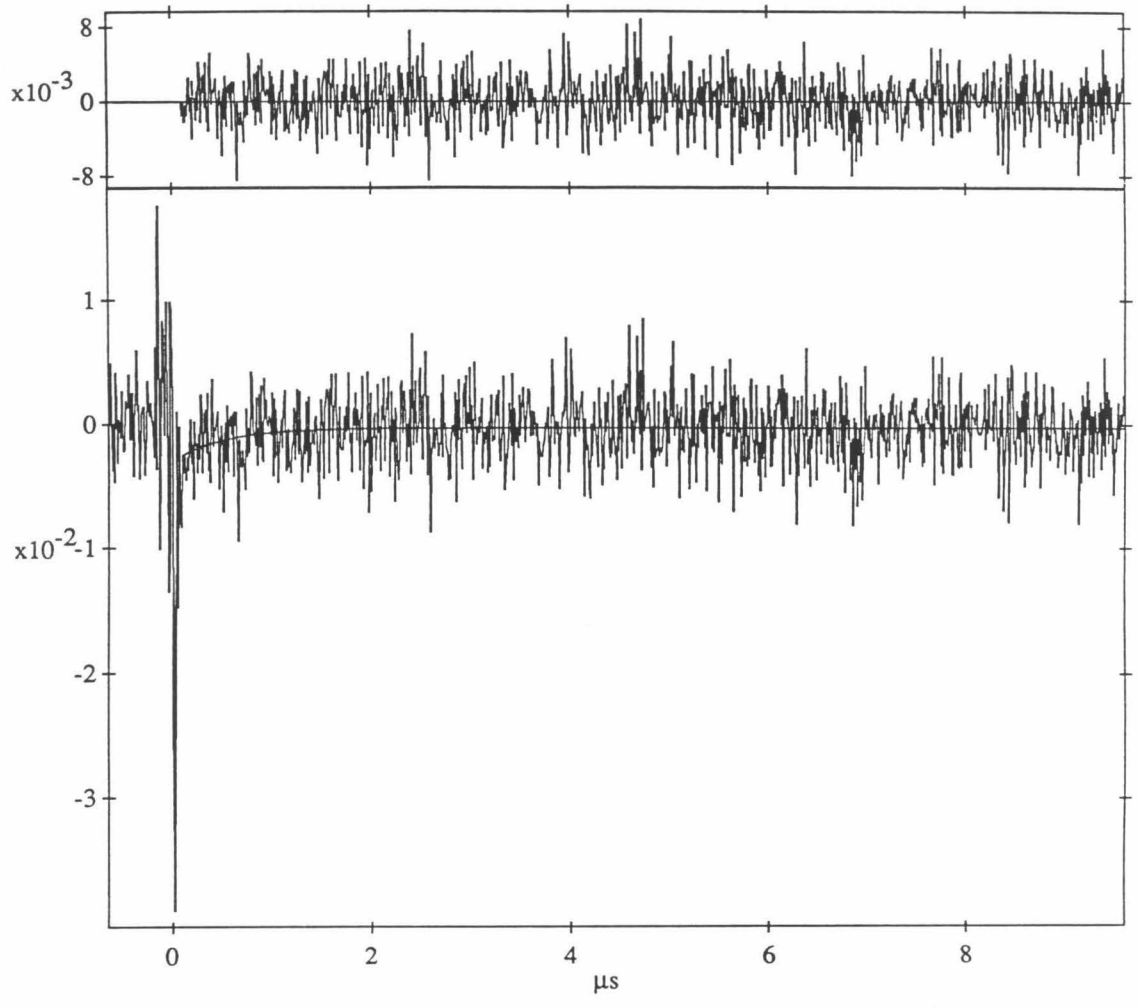
8
x10-3 0
-8
1
0
x10-2 -1
-2
-3
0
2
4
6
8
µs

References

Andrew, C. R., Fraczkiewicz, R., Czernuszewicz, R. S., Lappalainen, P., Saraste, M. and Sanders-Loehr, J. (1996). "Identification and description of copper-thiolate vibrations in the dinuclear CuA site of cytochrome *c* oxidase." J. Am. Chem. Soc. **118**: 10436-10445.

Ausubel, F., Brent, R., Kingston, R. E., Moore, D. D., Seidman, J. G., Smith, J. A. and Struhl, K., Ed. (1995). Short Protocols in Molecular Biology. New York, Wiley.

Babcock, G. T. and Wikström, M. (1992). "Oxygen activation and the conservation of energy in cell respiration." Nature **356**: 301-309.

Bertini, I., Bren, K. L., Clemente, A., Fee, J. A., Gray, H. B., Luchinat, C., Malmstrom, B. G., Richards, J. H., Sanders, D. and Slutter, C. E. (1996). "The CuA center of a soluble domain from *Thermus* cytochrome *ba(3)*- an NMR investigation of the paramagnetic protein." J. Am. Chem. Soc. **118**(46): 11658-11659.

Blackburn, N. J., de Vries, S., Barr, M. E., Houser, R. P., Tolman, W. B., Sanders, D. and Fee, J. A. (1997). "X-ray absorption studies on the mixed-valence and fully reduced forms of the soluble CuA domains of cytochrome *c* oxidase." J. Am. Chem. Soc. **119**: 6135-6143.

Dennison, C., Vijgenboom, E., de Vries, S., van der Oost, J. and Canters, G. W. (1995). "Introduction of a CuA site into the blue copper protein amicyanin from *Thiobacillus versutus*." FEBS Lett. **365**: 92-94.

Di Bilio, A. J. (1997). Personal communication.

Di Bilio, A. J., Dennison, C., Gray, H. B., Ramirez, B. E., Sykes, A. G. and Winkler, J. R. (1998). "Electron transfer in ruthenium-modified plastocyanin." submitted.

Hay, M., Richards, J. H. and Lu, Y. (1996). "Construction and characterization of an azurin analog for the purple copper site in cytochrome *c* oxidase." Proc. Natl. Acac. Sci. USA **93**: 461-464.

Iwata, S., Ostermeier, C., Ludwig, B. and Michel, H. (1995). "Structure at 2.8 Å resolution of cytochrome *c* oxidase from *Paracoccus denitrificans*." Nature **376**: 660-669.

Lappalainen, P., Aasa, R., Malmström, B. G. and Saraste, M. (1993). "Soluble CuA-binding domain from the Paracoccus cytochrome *c* oxidase." J. Biol. Chem. **268**: 26416-26421.

Mines, G. A., Bjerrum, M. J., Hill, M. G., Casimiro, D. R., Chang, I.-J., Winkler, J. R. and Gray, H. B. (1996). "Rates of heme oxidation and reduction in Ru(His33)cytochrome c at very high driving forces." J. Am. Chem. Soc. **118**: 1961-1965.

Mitchell, P. (1961). "Coupling of phosphorylation to electron and hydrogen transfer by a chemi-osmotic type of mechanism." Nature **191**: 144-148.

Ramirez, B., Malmström, B. G., Winkler, J. R. and Gray, H. B. (1995). "The currents of life: The terminal electron-transfer complex of respiration." Proc. Natl. Acad. Sci. USA **92**: 11949-11951.

Reikofski, J. and Tao, B. Y. (1992). "Polymerase chain-reaction (PCR) techniques for site-directed mutagenesis." Biotech. Adv. **10**(4): 535-547.

Sambrook, J., Fritsch, E. F. and Maniatis, T. (1989). Molecular Cloning A Laboratory Manual. New York, Cold Spring Harbor Press.

Saraste, M. (1990). "Structural feature of cytochrome oxidase." Quart. Rev. Biophys. **23**(4): 331-366.

Slutter, C. E. (1996). Overexpression and Characterization of the Copper A Domain from Cytochrome *ba3* or *Thermus thermophilus*. Division of Chemistry and Chemical Engineering. Pasadena, California Institute of Technology.

Slutter, C. E., Sanders, D., Wittung, P., Malmstrom, B. G., Aasa, R., Richards, J. H., Gray, H. G. and Fee, J. A. (1996). "Water-soluble, recombinant CuA domain of the cytochrome *ba3* subunit II from *Thermus thermophilus*." Biochem. **35**(11): 3387-3395.

Thomson, A. J., Greenwood, C., Peterson, J. and Varrett, C. P. (1986). "Determination of the optical properties of CuA(II) in bovine cytochrome *c* oxidase using magnetic circular dichroism as an optical detector of paramagnetic resonance." J. Inorg. Biochem. **28**: 195-205.

Tsukihara, T., Aoyama, H., Yamashita, E., Tomizaki, T., Yamaguchi, H., Shinzawa-Itoh, K., Nakashima, R., Yaono, R. and Yoshikawa, S. (1995). "Structures of metal sites of oxidized bovine heart cytochrome *c* oxidase at 2.8 Å." Science **269**: 1069-1074.

Tsukihara, T., Aoyama, H., Yamashita, E., Tomizaki, T., Yamaguchi, H., Shinzawa-Itoh, K., Nakashima, R., Yaono, R. and Yoshikawa, S. (1996). "The whole structure of the 13-subunit oxidized cytochrome *c* oxidase at 2.8 Å." Science **272**: 1136-1144.

van der Oost, J., Lappalainen, P., Mushacchio, A., Warne, A., Lemieux, L., Rumbly, J., Gennis, R. B., Aasa, R., Pascher, T., Malmström, B. G. and Saraste, M. (1992). "Restoration of a lost metal-binding site: construction of two different copper sites into a subunit of the *E coli* cytochrome *o* quinol oxidase complex." EMBO **11**(9): 3209-3217.

von Wachenfeldt, C., de Vries, S. and van der Oost, J. (1994). "The CuA site of the *caa3*-type oxidase of *Bacillus subtilis* is a mixed-valence binuclear copper center." FEBS Lett. **340**: 109-113.

Wilmanns, M., Lappalainen, P., Kelly, M., Sauer-Eriksson, E. and Saraste, M. (1995). "Crystal structure of the membrane-exposed domain from a respiratory quinol oxidase complex with an engineered dinuclear copper center." Proc. Natl. Acad. Sci. USA **92**: 11955-11959.

Appendix A

Site-saturation Mutagenesis of M121 of *Pseudomonas aeruginosa* Azurin

Proc. Natl. Acad. Sci. USA
Vol. 88, pp. 1325–1329, February 1991
Biochemistry

Gene synthesis, expression, and mutagenesis of the blue copper proteins azurin and plastocyanin

(copper center/synthetic gene)

THOMAS K. CHANG*, SHEILA A. IVERSON†, CLYDE G. RODRIGUES*, CYNTHIA N. KISER‡, AGNES Y. C. LEW*, JURIS P. GERMANAS*, AND JOHN H. RICHARDS*

Divisions of *Chemistry and Chemical Engineering and ‡Biology, California Institute of Technology, Pasadena, CA 91125; and †Department of Molecular Biology, Research Institute of Scripps Clinic, La Jolla, CA 92037

Communicated by Harry B. Gray, October 31, 1990

ABSTRACT **Genes for the blue copper proteins *Populus nigra* var. *italica* plastocyanin and *Pseudomonas aeruginosa* azurin have been constructed by a stepwise procedure. The leader sequence for azurin has been placed before the genes directing plastocyanin and azurin transport to the periplasmic space when the genes are expressed in *Escherichia coli*. Site-saturation mutagenesis has been used to alter two copper-binding residues of azurin (Met-121 and His-46) and Met-92 of plastocyanin. While the plastocyanin mutants do not appear to bind copper, the azurin variants all bind copper and show characteristic type I blue copper centers. In particular, the electronic spectra reflect the dominance of the charge transfer interaction between copper and the thiolate of Cys-112, being relatively insensitive to changes in Met-121 or His-46. In contrast, removal of Met-121 appreciably alters the EPR spectra of the mutants, although, to a first order, the spectra of all mutants are themselves similar, suggesting a more distorted geometry around copper in the mutants than in the wild type.**

The family of blue copper proteins includes plastocyanins (1) from green plants and some algae and azurin (2) from bacteria. These proteins perform essential roles as electron carriers (3, 4) in such important processes as photosynthesis and bacterial respiration. They provide a unique ligand environment (5–8) to their single type I copper atom that endows them with a rich blue color as well as an unusually high potential for the Cu(II)–Cu(I) couple (9). Furthermore, the ligation geometries are essentially identical for both Cu(II) and Cu(I) forms near neutral pH, giving these proteins the ability to transfer electrons very rapidly (10, 11). Lastly, the three-dimensional structures for a representative azurin at 1.8 Å (12) and plastocyanin at 1.6 Å (13) have been determined. For these reasons, the blue copper proteins provide attractive candidates for mutagenic structure–function studies (14) aimed at gaining insights into such diverse aspects of their behaviors as electronic spectra, paramagnetic properties, redox potentials, rates of electron transfer, transmission of electrons through the interior of the protein for subsequent transfer to redox partners, and surface sites involved in such protein–protein interactions. The close relationship in both structure and function of the plastocyanins and azurins provides an additional attraction for the concurrent study of these questions against these similar, but nevertheless significantly different, protein backgrounds.

We have approached this problem by the total synthesis of genes for poplar (*Populus nigra* var. *italica*) leaf plastocyanin (because of its highly refined three-dimensional structure; ref. 13) and *Pseudomonas aeruginosa* azurin (15). The synthetic genes were introduced adjacent to synthetic leader sequences for plastocyanin and azurin and the resulting constructs were expressed in *Escherichia coli*. When grown in the presence of 1 mM Cu(II), the properly processed and folded native proteins can be isolated from the periplasm. Because of the presence in the synthetic genes of relatively closely spaced sites for restriction endonuclease digestion, cassette mutagenesis (16) allows facile creation of specific mutants or families of mutants obtained by procedures such as site saturation (17). Using these approaches, we have created mutants at two of the copper ligation sites of azurin (His-46 and Met-121) and at one site of plastocyanin (Met-92).

The publication costs of this article were defrayed in part by page charge payment. This article must therefore be hereby marked "*advertisement*" in accordance with 18 U.S.C. §1734 solely to indicate this fact.

MATERIALS AND METHODS

Materials. Most restriction enzymes were purchased from Boehringer Mannheim or New England Biolabs. Polynucleotide kinase was purchased from New England Biolabs. DNA ligase was purchased from either BRL or Boehringer Mannheim. Ampicillin was purchased from Sigma; isopropyl β-D-thiogalactopyranoside, Tris, and other buffer reagents came from Boehringer Mannheim. FMC provided the high purity, low melting point agarose (GTG grade) used in preparative gels. Plasmid pBR322 was purchased from BRL, while pUC18 and chromatographic material came from Pharmacia. The Vectastain Elite kit for Western blotting was purchased from Vector Laboratories. Rabbit anti-plastocyanin or anti-azurin antibody was obtained from Berkeley Antibody (Richmond, CA).

E. coli strain LS1, an HB101 derivative, was used in the construction of both genes. Cells harboring the plasmids with the partially constructed gene were grown in L broth (10 g of tryptone per liter/5 g of yeast extract per liter/5 g of NaCl per liter). *E. coli* strain TG1 (18), a JM101 derivative, was used during the expression experiments. This strain was grown in a richer medium such as modified XB (25 g of tryptone per liter/7.5 g of yeast extract per liter/20 mM $MgSO_4$/50 mM sodium phosphate, pH 7.5) containing 1 mM $CuSO_4$.

Oligonucleotides were synthesized by phosphoramidite chemistry (19) on an Applied Biosystems automated DNA synthesizer (model 380A or 380B). They were then purified by electrophoresis on polyacrylamide gels followed by passage through NACS PREPAC columns from BRL. Alternatively, the dimethoxytrityl group could be left attached to the 5′-terminal nucleotide at the end of the synthesis and the oligonucleotides purified through OPC cartridges obtained from Applied Biosystems.

Gene Synthesis. Our approach involves synthesis of the gene in a stepwise fashion. The construction of the gene by this method proceeds from the ends toward the middle. Segments of the gene are sequentially cloned into an appropriate vector that allows amplification of the growing gene at intermediate stages of synthesis. After a segment has been inserted and the plasmid amplified, the resulting intermediate, containing two unique restriction sites within the segment last inserted, is opened at these sites, which then act as recipients for the next segment of the gene. Importantly, although all bases that

define one of the particular sites used for opening must, of course, be present in that intermediate, the site(s) need not be reconstituted for incorporation of the next cassette; only those bases necessary to provide compatible overhangs or located upstream of the upstream site and downstream of the downstream site need to be retained in the final gene. Thus, any particular restriction endonuclease may in principle be used multiple times in a given synthesis.

Though a very conservative approach for the synthesis of genes that encode plastocyanin (297 base pairs) or azurin (384 base pairs), this general strategy has considerable flexibility and should prove particularly suited to the synthesis of larger genes that might be difficult to prepare by the consecutive annealing of segments followed by cloning. The approach also permits editing at intermediate stages. This strategy is shown in Fig. 1, which outlines the steps used in synthesis of the structural genes for plastocyanin and azurin. We used pBR322 as the vector for this synthesis and constructed the gene between the *Eco*RI and *Ava* I sites after removal of the Tet^R gene that occupies this region of pBR322. This removes a large number of unique restriction sites that can subsequently be utilized in gene synthesis and leaves the β-lactamase gene intact as a selectable marker. Fig. 2 shows the base sequences and restriction sites for the two synthetic genes. In a similar way, a ribosome binding site and plastocyanin (20, 21) or azurin (22, 23) leader sequences were prepared and introduced just in front of the structural genes and then ligated into the polylinker site of pUC18 for expression that is controlled by a *lac* promoter induced by isopropyl β-D-thiogalactopyranoside.

Expression. A pUC18 vector (24) into which the appropriate genetic information had been inserted (promoter, ribosome binding site, spacer, leader sequence, and structural gene) was used to transform *E. coli* (TG1), and the cells were grown at 37°C in medium (25 g of bactotryptone, 7.5 g of yeast extract, and 5 g of NaCl per liter) containing 1 mM $CuSO_4$ and 50 μg of ampicillin per ml. After reaching logarithmic phase (OD_{600}, 0.5–1.0), the cells were induced with isopropyl β-D-thiogalactopyranoside (0.5 mM) and allowed to grow an additional 3–5 hr.

Protein Isolation. For Western blot analysis, a small sample of cells (≈2 ml) was centrifuged in a microcentrifuge and suspended in 100 μl of buffer (10% glycine/5% 2-mercaptoethanol/3% SDS/62.5 mM Tris·HCl, pH 7.6/1 mM EDTA/0.05% bromophenol blue). The solution was heated at 95°C for 10 min. The resulting solution was vigorously mixed in a Vortex to reduce viscosity and a 5-μl aliquot was loaded onto a SDS/15% polyacrylamide gel with a 4% stack. After electrophoresis, protein from the gel was transferred to a nitrocellulose membrane using a Bio-Rad Trans-Blot cell equipped with a surface electrode. The protein (azurin or plastocyanin) was visualized by using rabbit antibody raised against the appropriate protein together with the Vectastain Western blotting kit.

Osmotic extrusion was used for isolation of protein. Cells were harvested in a Sorvall superspeed centrifuge and the resulting pellet was resuspended in a hyperosmotic solution (20% sucrose/30 mM Tris·HCl, pH 8). After sitting on ice for 10 min, the solution was centrifuged to a pellet and gently resuspended in a cold solution of 0.5 mM $MgCl_2$. (In the case of plastocyanin, this solution also contains 1 mM $CuSO_4$; see below.) Periplasmic proteins were extruded and the cell debris was removed by further centrifugation.

Protein Purification. *Azurin.* To the solution obtained after osmotic extrusion was added 1/10th vol of 0.5 M ammonium acetate buffer (pH 4.1). This causes some contaminating proteins to precipitate. The supernatant was filtered through a 0.22-μm filter and the pH was adjusted to 4.1 before being loaded onto a column (5 × 5 cm) of CM-Sepharose previously equilibrated with ammonium acetate (pH 4.1). The column was washed with the same buffer, and the rich blue azurin was then eluted with ammonium acetate (pH 5.1). The fractions containing azurin were concentrated by ultrafiltration (Amicon YM3) and dialyzed against ammonium acetate buffer (pH 4.1). The solution was applied to an FPLC Mono S cation-exchange column and the azurin eluted with a pH gradient of 4.1–9, and further purified using a Sepharose 12 gel-filtration column at pH 7.0.

Plastocyanin. For purification of plastocyanin, the osmotic extrusion buffer contained 0.5 mM $MgCl_2$, 1.0 mM $CuSO_4$, and 1 mM [bis(2-hydroxyethyl)amino]tris(hydroxymethyl)-methane (Bistris) (pH 7.5). Plastocyanin was purified by anion-exchange chromatography [Q-Sepharose, 20 mM Bistris (pH 6.5)], eluted in buffer containing 0.5 M NaCl followed by two consecutive FPLC gel filtrations [Sepharose 12, 16/50; run 1, 20 mM Bistris (pH 6.5); run 2, 60 mM Tris (pH 8.0)] and FPLC anion-exchange [Mono Q, 10/10; 20 mM Tris (pH 8.0) eluted with a 0–0.5 M NaCl gradient]. All buffers also contained 5 mM $K_3Fe(CN)_6$ to maintain the Cu(II) form of the protein.

Mutagenesis. Mutants were prepared by cassette mutagenesis, in which the DNA sequences were inserted between appropriate restriction sites. For preparation of families of mutants, as for example at Met-121 in azurin, the approach of site saturation was used with mixed oligonucleotide cassettes NN(G/C) (21) to generate all 20 amino acid substitutions at a site at one time.

Spectral Analysis. CD spectra were recorded on a Jasco J-600 spectrophotometer. EPR spectra were recorded on a Varian E-Line Century series X-band spectrometer at 77 K and 9.077 GHz.

RESULTS AND DISCUSSION

Before the successful approaches for expression outlined above, many other attempts to produce blue copper proteins were tried. Biosynthesis of full-length apoplastocyanin itself directly into the cytoplasm of *E. coli* seemed to cause death of the cells. However, fusion proteins such as protein A–apoplastocyanin could be isolated in good yields. Cleavage of this fusion protein by factor Xa (25–27), enterokinase (28–30), or formic acid (31) (with appropriately unique amino acid target sequences inserted between protein A and plastocyanin), although fraught with various technical difficulties, did

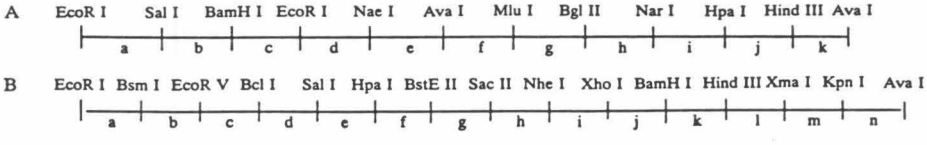

FIG. 1. General strategies used in the construction of plastocyanin (*A*) and azurin (*B*) genes. In each step of gene synthesis, the plasmid was cleaved at two adjacent restriction sites, and the next piece was ligated into that opening. This approach allows for isolation and amplification of a partially constructed gene for editing. (*A*) Step 1, a–c and k; step 2, d and e; step 3, f, g, i, and j; step 4, h. The *Eco*RI and *Ava* I sites of pBR322 between which this gene was constructed were destroyed during ligation, making the *Eco*RI and *Ava* I sites within the plastocyanin gene unique on the entire plasmid. (*B*) Step 1, l–n; step 2, a and k; step 3, b–e; step 4, f and j; step 5, g–i.

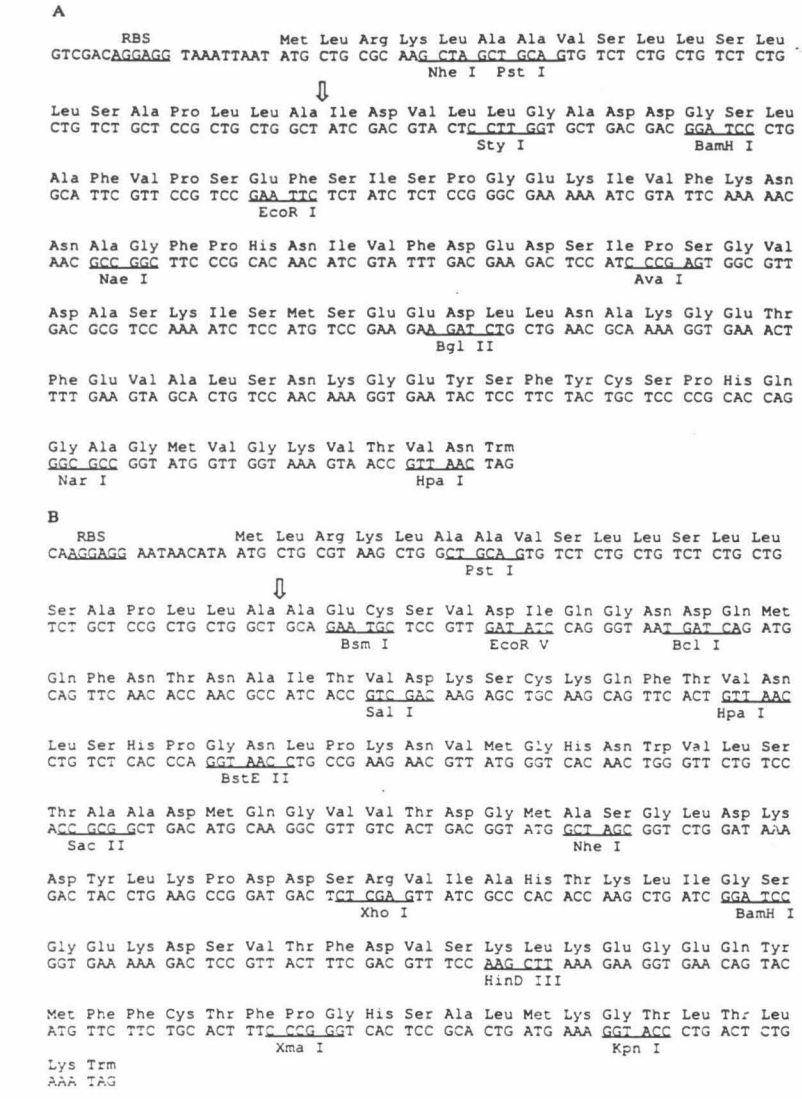

FIG. 2. Base sequences and restriction sites for plastocyanin (*A*) and azurin (*B*), including the ribosomal binding sites (RBS) and the azurin signal sequence from *P. aeruginosa*. Arrow indicates the junction between the signal sequence and the structural gene of plastocyanin or azurin that is correctly cleaved by *E. coli* signal peptidase upon cell membrane translocation. Each of the restriction sites is unique when these genes are located between the *Eco*RI and *Ava* I sites of pBR322.

produce apoplastocyanin whose efficient refolding in the presence of Cu(II) has yet to be achieved.

Far more successful expression was achieved when the blue copper proteins were transported to the periplasm as constructs involving the leader sequence for *P. aeruginosa* azurin (23, 32) or white campion plastocyanin (20, 21) followed by a structural gene. In these experiments, vectors incorporating the azurin leader followed by either the plastocyanin or azurin gene under control of the isopropyl β-D-thiogalactopyranoside-inducible *lac* promoter and grown in medium containing 1 mM Cu(II) led to the blue copper protein, properly processed and folded, being present in the periplasm. Use of a construct involving the entire plastocyanin leader (from white campion) followed by the structural gene for poplar plastocyanin also produced properly processed and folded plastocyanin, although in considerably lower yields than were obtained with a vector containing the azurin leader/plastocyanin sequence. The correct removal of the plastocyanin sequence during processing to generate mature plastocyanin upon translocation to the *E. coli* periplasm is an intriguing result as the complete plastocyanin leader (66 amino acids) is in fact two concatenated signal sequences; the first governs transport of plastocyanin into the chloroplast stroma while the second controls the subsequent translocation into the thylakoid lumen. The junction between these two sequences is unknown (21). Moreover, growth in the presence of 1 mM Cu(II) gave considerably higher yields of blue copper proteins than growths without Cu(II), presumably because of the greater resistance to proteolysis of the holoproteins (33). Our constructs contained a synthetic ribosome binding site designed from a consensus sequence (34–36); higher yields will likely be possible with more efficient ribosome binding sites as, for example, from that of the native azurin gene (23).

Azurin and plastocyanin were characterized by amino acid analyses, N-terminal sequencing, determination of the mass

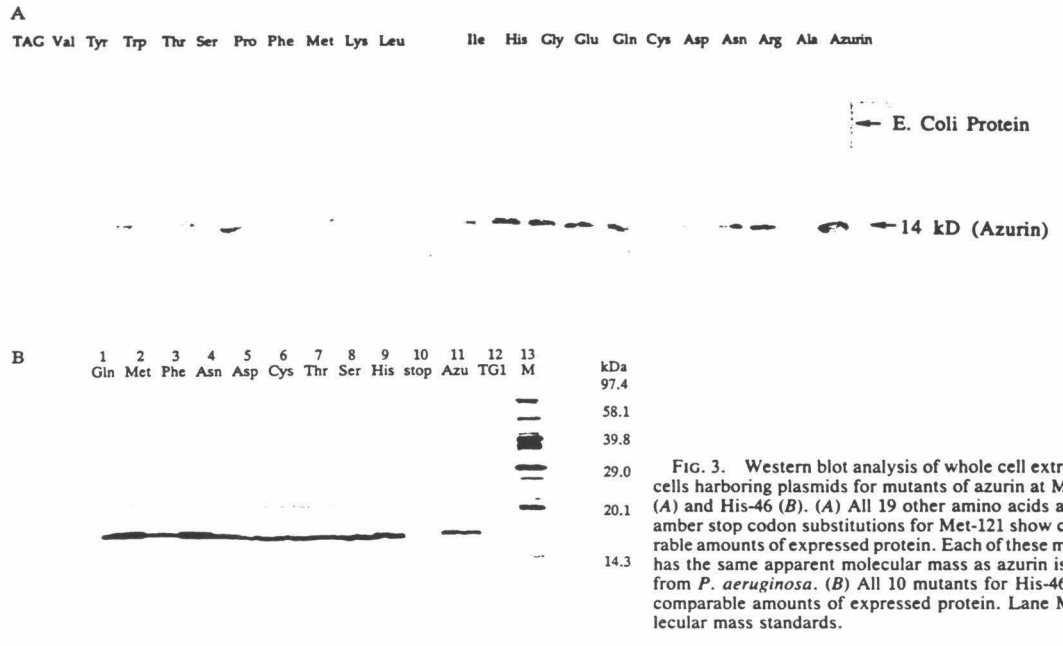

FIG. 3. Western blot analysis of whole cell extracts of cells harboring plasmids for mutants of azurin at Met-121 (*A*) and His-46 (*B*). (*A*) All 19 other amino acids and the amber stop codon substitutions for Met-121 show comparable amounts of expressed protein. Each of these mutants has the same apparent molecular mass as azurin isolated from *P. aeruginosa*. (*B*) All 10 mutants for His-46 show comparable amounts of expressed protein. Lane M, molecular mass standards.

of the molecular ion by time-of-flight mass spectrometry, UV-visible spectra, and CD. In all cases, the proteins from *E. coli* were indistinguishable from analogous proteins from native sources.

Mutagenesis. *General.* At least three aspects of the function of blue copper proteins hold interest and should be amenable to analysis by mutagenic approaches: (*i*) the copper center, including the nature of ligands and their geometry; (*ii*) intramolecular electron transmission; (*iii*) docking sites involved in interactions between proteins and transfer of electrons along the redox chain.

Most of our work has so far focused on the first question with preliminary attention to two of the four copper ligands (Met-121 and His-46 in azurin). (The other two ligands in azurin are His-117 and Cys-112.) By site saturation (17), we have prepared genes for all 19 possible mutants at Met-121 and His-46. Expression of the Met-121 mutants has shown that protein for 20 of these can be demonstrated in the periplasm by Western blot analysis (Fig. 3). Of these, seven Met-121 mutants have been isolated as copper-containing proteins and characterized in a preliminary way. Of particular interest is the observation that all manifest the characteristic rich blue color originating most likely in the interaction between the copper and the thiolate of Cys-112. Nevertheless, replacement of Met-121 does result in clear changes in the electronic spectra as summarized in Table 1. Another mutant at this site, Met-121 → Leu, increases the redox potential by 70 mV and shifts the peak at 625 nm by 5 nm (37). Of the 19 mutants at His-46, one has been purified (His-46 → Asp). It is also a deep blue protein with the spectral characteristics outlined in Table 1. CD spectra of the azurin mutants show all of the previously identified peaks, although at slightly altered frequencies. These results, along with the UV-visible data, indicate that the essential integrity of the copper site has been retained in these mutants.

Table 1. Spectroscopic characteristics of azurin mutants based on UV-visible and CD observations

	Major peak, nm	Minor peak, nm
Wild type	625	445
Met-121 → Val	630	459
Met-121 → Ile	626	459
Met-121 → Asn	622	447
Met-121 → Asp	622	445
Met-121 → His	612	449
His-46 → Asp	616	458

The absorbance maxima of the two peaks within the visible region for the six mutants shown are all shifted by relatively small amounts due to both the absence of methionine and probably slightly perturbed geometries of the copper site.

Frozen solution EPR spectra for the wild-type azurin and three Met-121 mutants were recorded and the g and A values were determined (Table 2). Preliminary examination of the data suggests that the spectra of the mutants are more rhombic than the spectrum of the wild-type protein.

Fascinatingly, a great latitude in ligands, almost universally conserved throughout the blue copper family, can be accommodated in these mutants of azurin, while preserving the ability to bind copper and apparently normal, stable protein folding. [Some exceptional proteins with ligands other than the four commonly observed probably exist in nature—for example, stellacyanin (38), amicyanin (39), and rusticyanin (40).] The ability to generate analogues of these ligand environments at will should prove particularly useful.

Other examples of substituting either a conserved or a semiconserved residue of azurin have recently been reported. Both His-35 → Lys and Glu-91 → Gln have unchanged spectroscopic and redox properties, while in Phe-114 → Ala the optical band is downshifted by 7 nm and the

Table 2. Spin hamiltonian parameters for wild-type azurin [50 mM ammonium acetate (pH 7)] and Met-121 mutants [pH9]

	$g_{\parallel}$	$A_{\parallel}$, $\times 10^4$ cm^{-1}	$g_{\perp}$
Wild type	2.271	61	2.054
Met-121 → Asn	2.249	36	2.056
Met-121 → Ile	2.246	35	2.060
Met-121 → Val	2.243	34	2.064

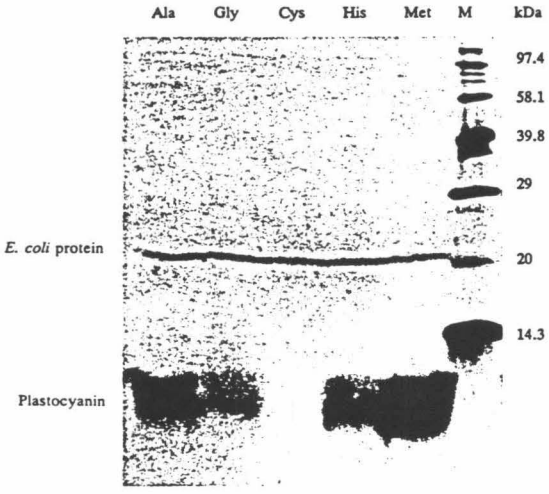

FIG. 4. Western blot analysis of plastocyanin and four mutants at Met-92. Three of the mutants (His, Gly, and Ala) show a band at the same molecular mass as the native plastocyanin. No protein can be visualized for the Met-92 → Cys mutant. Lane M, molecular mass standards.

reduction potential is lowered by 20–24 mV (41). Another mutation at a conserved residue within the hydrophobic patch, Met-44 → Lys, causes only a minimal effect on the spectroscopic properties but significantly affects the electron self-exchange rate (42).

Plastocyanin. The ability to create a particular mutation against both the azurin and plastocyanin backgrounds provides one of the rationales for the concurrent study of both families of proteins. To this end, we have prepared mutants at Met-92 of plastocyanin. (This is the ligand in plastocyanin analogous to Met-121 in azurin.) Site saturation generated all 19 mutant genes. Of these mutants, Met-92 → Cys, Met-92 → His, Met-92 → Ala, and Met-92 → Gly have been studied. On producing these mutants, *E. coli* has a frustrating tendency to lyse (behavior not observed with analogous mutants of azurin). This problem can be circumvented if the cells are aerated but not agitated during expression. Western blot analysis (Fig. 4) shows protein for the mutants Met-92 → His, Met-92 → Ala, and Met-92 → Gly present in the periplasm; no protein for the Met-92 → Cys has been observed. In no case has it so far been possible to isolate a blue copper-containing protein with any of these mutants. This may be due to a kinetic difficulty these proteins have in acquiring the copper or because the thermodynamic affinity for a copper ligand has been sharply reduced. Thus, although azurin and plastocyanin share very similar overall three-dimensional structures and almost identical copper sites, analogous mutations in these two systems seem to behave differently.

We gratefully acknowledge early encouragement for this work by I. Pecht and the continuing enthusiasm of H. B. Gray and Angel J. Di Bilio for determining the EPR spectra. This work was supported by National Institutes of Health Grant GM16424, National Science Foundation Grant CHE-8814222, and National Institutes of Health Grant DK19038. This is contribution 8218 from Division of Chemistry of the California Institute of Technology.

1. Boulter, D., Haslett, B. G., Peacock, D., Ramshaw, J. A. M. & Scawen, M. D. (1977) in *International Review of Biochemistry, Plant Biochemistry II*, ed. Northcote, D. H. (University Park Press, Baltimore), Vol. 13, pp. 1–40.
2. Ryden, L. & Lungren, J. (1976) *Nature (London)* **261**, 344–346.
3. Farver, O. & Pecht, I. (1984) in *Copper Proteins and Copper Enzymes*, ed. Lontie, R. (CRC, Boca Raton, FL), Vol. 1, pp. 183–214.
4. Adman, E. T. (1985) in *Topics in Molecular and Structural Biology, Metalloproteins*, ed. Harrison, P. M. (Verlag Chemie, Weinheim, F.R.G.), Vol. 6, pp. 1–42.
5. McMillin, D. R. & Morris, M. C. (1981) *Proc. Natl. Acad. Sci. USA* **78**, 6567–6570.
6. McMillin, D. R. (1985) *J. Chem. Educ.* **62**, 997–1001.
7. Penfield, K. W., Gay, R. R., Himmelwright, R. S., Eickman, N. C., Norris, V. A., Freeman, H. C. & Solomon, E. I. (1981) *J. Am. Chem. Soc.* **103**, 4382–4388.
8. Penfield, K. W., Gerwirth, A. A. & Solomon, E. I. (1985) *J. Am. Chem. Soc.* **107**, 4519–4529.
9. Gray, H. B. & Solomon, E. I. (1981) in *Metal Ions in Biology*, ed. Spiro, T. G. (Wiley, New York), Vol. 3. pp. 1–39.
10. Kostic, N. M., Margalit, R., Che, C.-M. & Gray, H. B. (1983) *J. Am. Chem. Soc.* **105**, 7765–7767.
11. Marcus, R. A. & Sutin, N. (1985) *Biochim. Biophys. Acta* **811**, 265–322.
12. Guss, J. M., Harrowell, P. R., Murata, M., Norris, V. A. & Freeman, H. C. (1986) *J. Mol. Biol.* **192**, 361–387.
13. Baker, E. N. (1988) *J. Mol. Biol.* **203**, 1071–1095.
14. Dalbadie-McFarland, G., Cohen, L. W., Riggs, A. D., Morin, A. D., Itakura, K. & Richards, J. H. (1982) *Proc. Natl. Acad. Sci. USA* **79**, 6409–6413.
15. Adman, E. T. & Jensen, L. H. (1981) *Isr. J. Chem.* **21**, 8–12.
16. Richards, J. H. (1986) *Nature (London)* **323**, 187.
17. Schultz, S. C. & Richards, J. H. (1986) *Proc. Natl. Acad. Sci. USA* **83**, 1588–1592.
18. Gibson, T. J. (1984) Ph.D. thesis (Cambridge Univ., U.K.).
19. Beaucage, S. L. & Carruthers, M. H. (1986) *Tetrahedron Lett.* **22**, 1859–1862.
20. Smeekens, S., de Groot, M., van Binsbergen, J. & Weisbeek, P. (1985) *Nature (London)* **317**, 456–458.
21. Smeekens, S., Bauerle, C., Hageman, J., Keegstra, K. & Weisbeek, P. (1986) *Cell* **46**, 365–375.
22. Canters, G. W. (1987) *FEBS Lett.* **212**, 168–172.
23. Arvidsson, R. H. A., Nordling, M. & Lundberg, L. G. (1989) *Eur. J. Biochem.* **179**, 195–200.
24. Vieira, J. & Messing, J. (1982) *Gene* **19**, 259–268.
25. Titani, K., Hermodson, M. A., Fujikawa, K., Ericsson, L. H., Walsh, K. A., Neurath, H. & Davie, E. W. (1972) *Biochemistry* **11**, 4899–4903.
26. Fujikawa, K., Legaz, M. E. & Davie, E. W. (1972) *Biochemistry* **11**, 4892–4898.
27. Nagai, K. & Thøgersen, H. C. (1984) *Nature (London)* **309**, 810–812.
28. Anderson, L. E., Walsh, K. A. & Neurath, H. (1977) *Biochemistry* **16**, 3354–3360.
29. Baratti, J., Maroux, S., Louvard, D. & Desnuelle, P. (1973) *Biochim. Biophys. Acta* **315**, 147–161.
30. Maroux, S., Baratti, J. & Desnuelle (1971) *J. Biol. Chem.* **246**, 5031–5039.
31. Nilsson, B., Holmgren, E., Josephson, S., Gatenbeck, S., Philipson, L. & Uhlen, M. (1985) *Nucleic Acids Res.* **13**, 1151–1162.
32. Karlsson, B. G., Pascher, T., Nordling, M., Arvidsson, R. H. A. & Lundberg, L. G. (1989) *FEBS Lett.* **246**, 211–217.
33. Merchant, S. & Bogorad, L. (1986) *J. Biol. Chem.* **261**, 15850–15853.
34. Gold, L. M. & Stormo, G. D. (1987) in *Escherichia coli and Salmonella typhimurium*, ed. Neidhardt, F. C. (Am. Soc. Microbiol., Washington), pp. 1302–1307.
35. Gren, E. J. (1984) *Biochimie* **66**, 1–29.
36. Stormo, G. D. (1986) in *Maximizing Gene Expression*, ed. Reznikoff, W. & Gold, L. (Butterworth, Boston), pp. 195–224.
37. Karlsson, B. G., Aasa, R., Malmström, B. G. & Lundberg, L. G. (1989) *FEBS Lett.* **253**, 99–102.
38. Engeseth, H. R., Hermodson, M. A. & McMillin, D. R. (1984) *FEBS Lett.* **171**, 257–261.
39. Tobari, J. & Harada, Y. (1981) *Biochem. Biophys. Res. Commun.* **101**, 502–508.
40. Ingledew, W. J. & Cobley, J. C. (1980) *Biochim. Biophys. Acta* **590**, 14–23.
41. Pascher, T., Bergström, J., Malmström, B. G., Vänngård, T. & Lundberg, L. G. (1989) *FEBS Lett.* **258**, 266–268.
42. van de Kamp, M., Floris, R., Hali, F. C. & Canters, G. W. (1990) *J. Am. Chem. Soc.* **112**, 907–908.

Selected M121 mutants in the pET9a expression system.

The site-saturation mutagenesis of the azurin Cu ligand M121 described in the previous paper was carried out using cassette mutagenesis on the synthetic azurin gene cloned into pUC18. Subsequent to this work, a better expression system for azurin was developed in this lab (Germanas et al. 1993). Rather than transfer all the previously constructed M121 mutants into the pET expression system, representative mutants at M121 have been constructed directly from the wild type azurin cloned into pET9a using PCR mutagenesis.

The sense-strand primer spans the upstream Nde I restriction enzyme site. (See figure 1.) The anti-sense primer starts downstream of the azurin gene and contains two mutations, one to give the desired amino acid at position 121 and one to restore the Bgl II restriction enzyme site that is lost upon ligation to the compatible Bam HI overhang from the pET9a vector. Bam HI cannot be used to clone azurin into pET9a because our synthetic gene contains an internal Bam HI site.

The PCR reactions contained BMB buffer, dNTP's (0.2 mM each), 5 units Taq polymerase, 0.35 µg template DNA, and 250 pmoles of each primer in a total volume of 100 µl. Reaction mixtures overlaid with mineral oil were placed in a Perkin-Elmer DNA Thermal Cycler 480. Templates were denatured at 96°C for 5 minutes followed by 30 PCR cycles denaturing at 96°C for 30 seconds, annealing at 55°C for 30 seconds, and polymerizing at 72°C for 1 minute. Final polymerization was given 5 minutes at 72°C. The PCR products were extracted from the reaction mix using 15 µl Qiaex II resin according to the manufacturer's instructions (Qiaex II Gel Extraction Kit, Qiagen, Chatsworth, CA). The DNA was eluted with 20 µl water and digested with Nde I and Bgl II in BMB buffer H (50 mM Tris HCl, 10 mM $MgCl_2$, 100 mM NaCl, 1 mM dithioerythritol - final concentrations). The vector, pET9a/bla (pET9a containing the β-lactamase gene, a kind gift from Dr. Claire Slutter), was digested with Nde I and Bam HI in New England Biolabs (Beverly, MA) Bam HI buffer. Digests were purified on a 1.2% low melting point agarose gel; the bands were cut out and the agarose removed by overnight digestion with 1 unit of Gelase (Epicenter Technologies, Madison WI) followed by ethanol precipitation and resuspension in 20 µl water. Ligations contained 1x NEB ligation buffer, 50 units ligase (New England Biolabs Beverly, MA), an estimated 1.5 µg pET9a vector DNA, and the PCR products. After 21

hours at 16°C, 1 µl of each ligation was transformed into 20 µl of competent BL21(DE3) cells (Novagen, Madison, WI).

Initial screening of transformed colonies was done by PCR, starting with 5 µl of cells suspended in 50 µl water. PCR was performed as above in a final reaction volume of 25 µl using the T7 promoter and terminator primers and 0.125 units of Taq polymerase per reaction. After 55 cycles, the results were assessed on a 1.2% agarose gel. Qiagen Plasmid Maxipreps were done on colonies with inserts of the correct size, starting with 100 ml cultures of cells grown overnight in LB with 35 µg/ml kanamycin. After isopropanol precipitation, the DNA was resuspended in 100 µl water (average yields: 100 µl at 4.2 µg/µl). The identities of the mutants were confirmed by dye-terminated cycle sequencing with the T7 promoter and terminator primers at the Beckman Institute DNA Sequencing Facility.

Germanas, J. P., Di Bilio, A. J., Gray, H. B. and Richards, J. H. (1993). "Site saturation of the histidine-46 position in *Pseudomonas aeruginosa* azurin: Characterization of the His46Asp copper and cobalt proteins." Biochem. **32**: 7698-7702.

Figure A.1
Oligonucleotides for selected M121 mutants in pET9a. Restriction enzyme recognition sites are underlined; mutations at position 121 are in boldface.

Azfront.s
CTT TAA GAA GGA GAT ATA CAT ATG CTG CG

M121G.as
GCA GCC AGA TCT CTA TTT CAG AGT CAG GGT ACC TTT **ACC** CAG T

M121K.as
GCA GCC AGA TCT CTA TTT CAG AGT CAG GGT ACC TTT **TTT** CAG T

M121D.as
GCA GCC AGA TCT CTA TTT CAG AGT CAG GGT ACC TTT **ATC** CAG T

M121L.as
GCA GCC AGA TCT CTA TTT CAG AGT CAG GGT ACC TTT **CAG** CAG T

Appendix B

Map and Gene Sequence of pET/ASA

Figure B.1 Azurin gene with some potentially useful (though not necessarily unique) restriction enzyme sites annotated. The junction between the signal sequence and the mature protein is shown. The metal ligands are indicated in the protein sequence by boldface type.

```
Nde I           Pst I                        <- Signal sequence
ATGCTGCGTAAGCTGGCTGCAGTGTCTCTGCTGTCTCTGCTGTCTGCTCCGCTGCTGGCT
M  L  R  K  L  A  A  V  S  L  L  S  L  L  S  A  P  L  L  A

Mature protein ->          Bcl I
GCTGAATGCTCCGTTGATATCCAGGGTAATGATCAGATGCAGTTCAACACCAACGCCATC
A  E  C  S  V  D  I  Q  G  N  D  Q  M  Q  F  N  T  N  A  I

   Sal I                      Hpa I            BstE II
ACCGTCGACAAGAGCTGCAAGCAGTTCACTGTTAACCTGTCTCACCCAGGTAACCTGCCG
T  V  D  K  S  C  K  Q  F  T  V  N  L  S  H  P  G  N  L  P

                                    Sac II
AAGAACGTTATGGGTCACAACTGGGTTCTGTCCACCGCGGCTGACATGCAAGGCGTTGTC
K  N  V  M  G  H  N  W  V  L  S  T  A  A  D  M  Q  G  V  V

            Nhe I                                        Xho I
ACTGACGGTATGGCTAGCGGTCTGGATAAAGACTACCTGAAGCCGGATGACTCTCGAGTT
T  D  G  M  A  S  G  L  D  K  D  Y  L  K  P  D  D  S  R  V

                      BamH I
ATCGCCCACACCAAGCTGATCGGATCCGGTGAAAAAGACTCCGTTACTTTCGACGTTTCC
I  A  H  T  K  L  I  G  S  G  E  K  D  S  V  T  F  D  V  S

Hind III                                        Xma I
AAGCTTAAAGAAGGTGAACAGTACATGTTCTTCTGCACTTTCCCGGGTCACTCCGCACTG
K  L  K  E  G  E  Q  Y  M  F  F  C  T  F  P  G  H  S  A  L

       KpnI
ATGAAAGGTACCCTGACTCTGAAATAG
M  K  G  T  L  T  L  K  End
```

Figure B.2 Map of the plasmid pET9A/ASA: the azurin gene, with signal sequence, cloned downstream of the T7 polymerase promotor in the expression vector pET9a. The origin of replication and kanamycin resistance gene are also shown. Recognition sites for restriction enzymes cutting only once in the plasmid are shown along the outside of the plasmid.

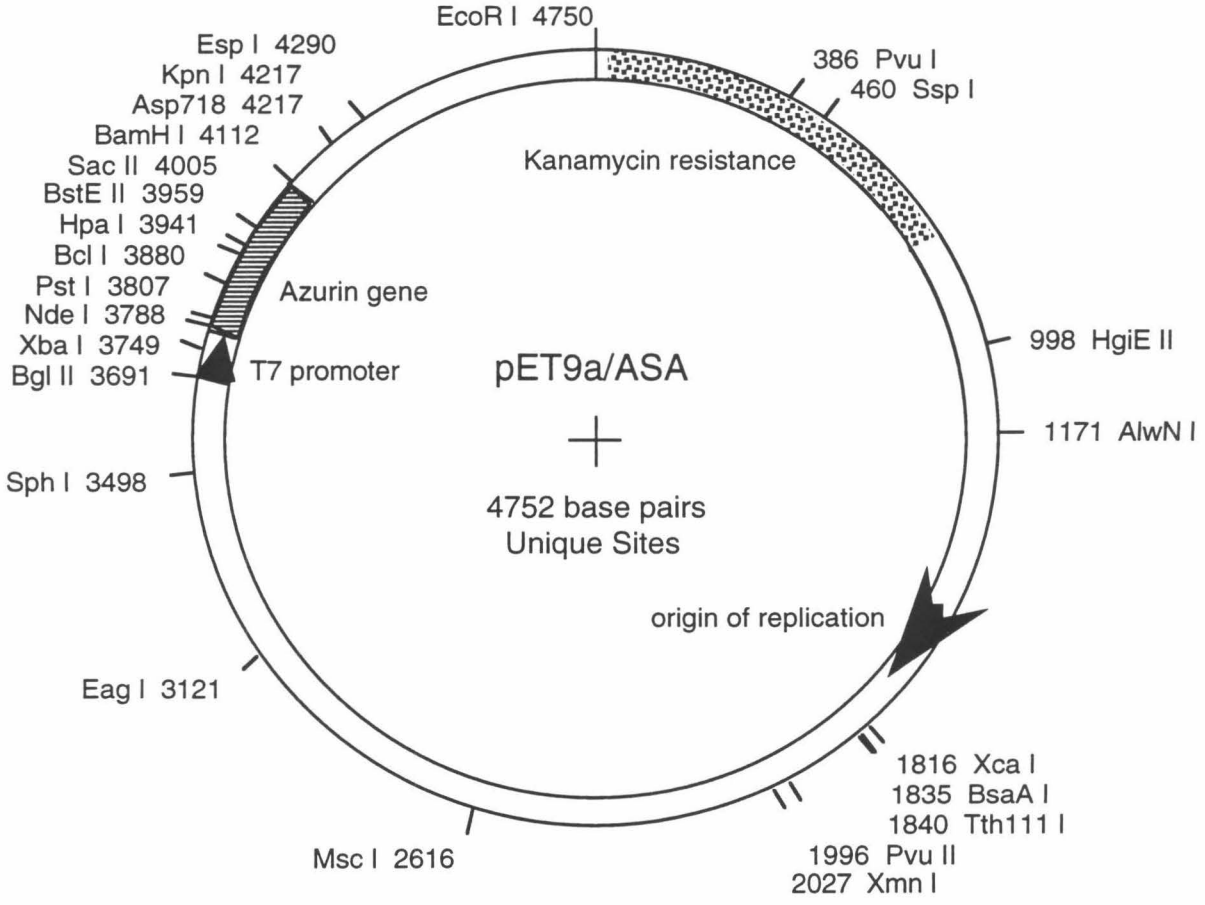
EcoR I 4750
Esp I 4290
Kpn I 4217
Asp718 4217
BamH I 4112
Sac II 4005
BstE II 3959
Hpa I 3941
Bcl I 3880
Pst I 3807
Nde I 3788
Xba I 3749
Bgl II 3691
386 Pvu I
460 Ssp I
Kanamycin resistance
Azurin gene
T7 promoter
pET9a/ASA
4752 base pairs
Unique Sites
998 HgiE II
1171 AlwN I
Sph I 3498
origin of replication
Eag I 3121
1816 Xca I
1835 BsaA I
1840 Tth111 I
Msc I 2616
1996 Pvu II
2027 Xmn I

Appendix C

Map and Gene Sequence of pET/T9CuA

Figure C.1 DNA and protein sequences for the 'T9' soluble CuA domain from *Thermus thermophilus*. The valine following the initiating methionine is residue 44 in the sequence of the intact cytochrome *c* subunit II. The metal ligands, H117, C149, Q151, C153, H157, and M160, are in boldface. In the plasmids with surface histidines introduced by site-directed mutagenesis, the non-ligand, surface histidine H117 (underlined) was mutated to a glutamine residue. These plasmids differ from the original CuA fragment described by Slutter (Slutter 1996) by the introduction of a silent mutation at V132 (GTC -> GTT).

Slutter, C. E. (1996). Overexpression and Characterization of the Copper A Domain from Cytochrome *ba3* or *Thermus thermophilus*. Division of Chemistry and Chemical Engineering. Pasadena, California Institute of Technology.

ATGGTCATTCCCGCCGGAAAGCTTGAGCGCGTGGACCCCACCACGGTAAGGCAGGAAGGC
M V I P A G K L E R V D P T T V R Q E G

CCCTGGGCCGACCCGGCCCAAGCGGTGGTGCAGACCGGCCCCAACCAGTACACGGTCTAC
P W A D P A Q A V V Q T G P N Q Y T V Y

GTCCTGGCCTTCGCCTTCGGCTACCAGCCGAACCCCATTGAGGTGCCCCAAGGGGCGGAG
V L A F A F G Y Q P N P I E V P Q G A E

ATCGTCTTCAAGATCACGAGCCCGGACGTGATCCACGGCTTTCACGTGGAGGGCACCAAC
I V F K I T S P D V I **H** G F H V E G T N

ATCAACGTGGAGGTGCTCCCGGGCGAGGTTTCCACCGTGCGCTACACCTTCAAAAGGCCC
I N V E V L P G E V S T V R Y T F K R P

GGGGAGTACCGCATCATCTGCAACCAGTACTGCGGCCTAGGCCACCAGAACATGTTCGGC
G E Y R I I **C** N **Q** Y **C** G L G **H** Q N **M** F G

ACGATCGTGGTGAAGGAGTGA
T I V V K E Stop

Figure C.2 Map of the plasmid pET9a/T9CuA: the 'T9' soluble CuA fragment from *Thermus thermophilus* cloned downstream of the T7 polymerase promoter in the expression vector pTE9a. The origin of replication and the kanamycin resistance gene are also shown. Recognition sites for restriction enzymes cutting only once in the plasmid are shown along the outside of the plasmid.

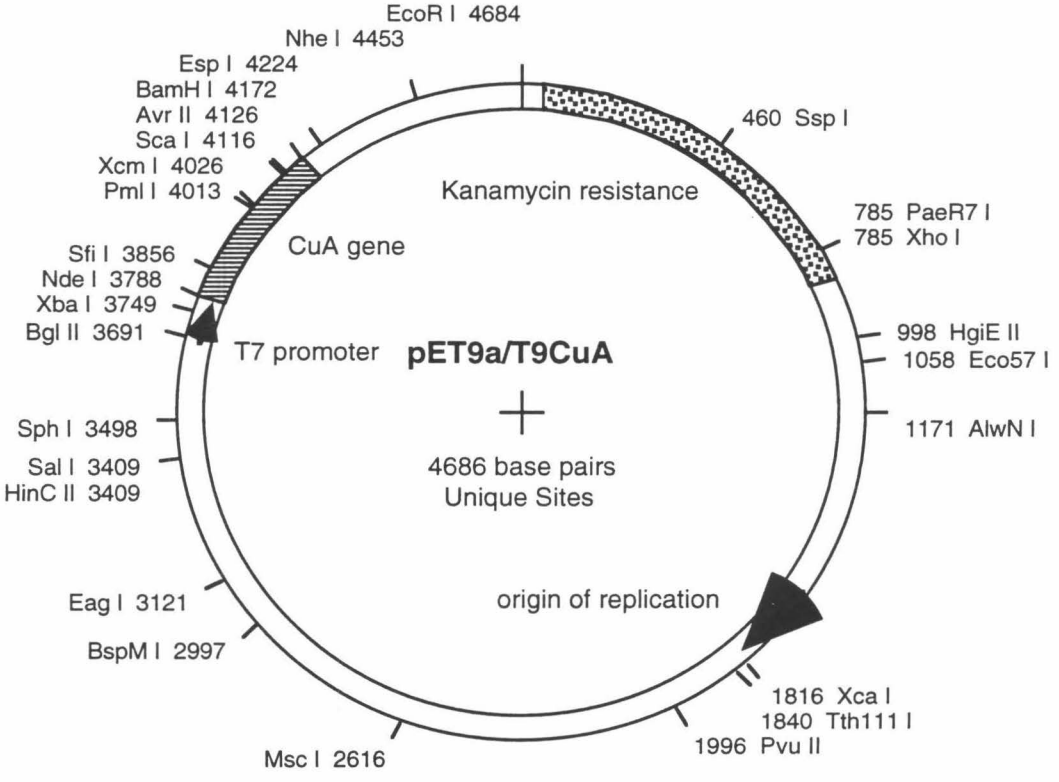
EcoR I 4684
Nhe I 4453
Esp I 4224
BamH I 4172
Avr II 4126
Sca I 4116
Xcm I 4026
Pml I 4013
Sfi I 3856
Nde I 3788
Xba I 3749
Bgl II 3691
Sph I 3498
Sal I 3409
HinC II 3409
Eag I 3121
BspM I 2997
Msc I 2616
460 Ssp I
785 PaeR7 I
785 Xho I
998 HgiE II
1058 Eco57 I
1171 AlwN I
1816 Xca I
1840 Tth111 I
1996 Pvu II
Kanamycin resistance
CuA gene
T7 promoter
pET9a/T9CuA
4686 base pairs
Unique Sites
origin of replication